Austenitization of Ultra High Strength Steel by Direct Contact Heating for Hot Forming Die Quenching

by

Natalie Field

A thesis
presented to the University of Waterloo
in fulfillment of the
thesis requirement for the degree of
Master of Applied Science
in
Mechanical and Mechatronics Engineering

Waterloo, Ontario, Canada, 2017

Author's Declaration

I hereby declare that I am the sole author of this thesis. This is a true copy of the thesis, including any required final revisions, as accepted by my examiners.

I understand that my thesis may be made electronically available to the public.

Abstract

Hot forming die quenching (HFDQ) is a heat treatment process used in automotive manufacturing to produce ultra-high strength steels. It involves heating steel sheets to a temperature above 1153 K and holding them for a period of time to ensure that the microstructure has fully transformed to austenite. Rapid quenching is subsequently performed to insure the austenite-martensite transformation of the steel crystallographic structure. The improved strength of these steels allows automotive manufacturers to use thinner sheets for structural members, resulting in reduced net vehicle weight and improved fuel efficiency without compromising safety performance.

Austentization is mainly done using roller hearth furnaces, but the high energy requirements, slow heating time, and large production space has motivated investigation of direct contact heating as an alternative strategy. Previous work using a small scale prototype produced austenitized steel coupons in less than 25 seconds, and accomplished tailored microstructures within a coupon by use of different thermal effusivities in the die striking surface. Even though the striking surface is isothermal, the differing thermal properties of the steel and ceramic provide nonuniform heating over the blank and incomplete austenitization, leading to bainitic regions in the formed part. This method may be easier to control compared to other tailoring procedures, which focus on slower and nonuniform cooling during the quenching stage.

This thesis builds upon the previous work and describes the design and fabrication of an electrically-fired, half scale industrial sized direct contact heating die with tailoring capabilities. The die was installed alongside a flat quenching die, with a transfer system between them, all encompassed within a 900 ton press. An FEM simulation was used to design the direct contact heating die. The model also included a constitutive metallurgical submodel, derived from Gleeble dilatometry measurements, that was used to predict heating and austenitization kinetics of the blank. Model predictions were confirmed using thermocouple measurements recorded during HFDQ, and metallurgical and microstructural analysis of formed blanks. The austenitization model allows for future optimization in the striking surface design as well as the performance of heat treated ultrahigh strength steels.

Acknowledgements

I would like to thank my supervisors, Dr. Kyle Daun and Dr. Adrian Gerlich for their guidance, encouragement, patience, and support through my degree. In particular, I would like to thank Dr. Kyle Daun for his optimism and numerous brainstorming sessions that helped me troubleshoot challenging experimental design and computer modelling tasks.

I would also like to thank my industrial sponsor, F&P Manufacturing Inc., for their technical expertise and financial support, as well as ArcelorMittal for providing Usibor® 1500P testing material.

I am grateful to Professor Michael Worswick, who generously allowed me to work in his lab space for my experiments and to Eckhard Budziarek, Jim Merli, Jason Benninger, Ryan George, Neil Griffet, Andy Barber, the machine shop staff, and the talented and patient Tom Gawel for their expertise and efforts.

I would like to thank my current and previous lab mates, Roger Tsang, Tim Sipkens, Sam Grauer, Josh Rasera, Kamal Jhajj, Nigel Singh, and honorary lab mate Jeff Hou for their friendship and support.

I would like to thank my friends and family for their encouragement and love throughout everything as well as Michael, whose patience, kindness, generosity, and support through many long days of work helped me accomplish this goal.

Table of Contents

List of Figures

List of Tables

List of Nomenclatures

Symbol	**Units**	**Definition**
T_{die}	K	Temperature of die
T_∞	K	Bolster surface temperature
T_{surf}	K	Surface temperature of heating die
T_{surr}	K	Temperature of heating die surroundings
Bi		Biot number
$\overline{Nu_L}$		Nusselt number
Ra_L		Rayleigh number
U	$W/(m^2 \cdot K)$	Overall heat transfer coefficient between monolith and bottom insulation
$\overline{h}$	$W/(m^2 \cdot K)$	Convection coefficient
m	kg	Mass of die
c_p	$kJ/(kg \cdot K)$	Specific heat of RA 330®
t	s	Time
P	W	Power
k	$W/(m \cdot K)$	Thermal conductivity
k_f	$W/(m \cdot K)$	Thermal conductivity of air
σ	$W/(m^2 \cdot K^4)$	Stefan-Boltzmann constant
$q''_{\rho c_p k}$	W/m^2	Heat flux between blank and striking surface
q_{rad}	W	Radiation from heating die surface
A_{surf}	m^2	Bottom die surface area

L_c	m	Characteristic length of monolith
L	m	Thickness of bottom insulation
L_{open}	m	Separation distance between lower and upper heating die surface
$F_{surf\text{-}surr}$		View factor between heating die surface and surroundings
ε		Emissivity of heating die surface
g	m/s^2	Gravitational acceleration
β	K^{-1}	Volume expansion coefficient
α_{td}	m^2/s	Thermal diffusivity
ν	m^2/s	Kinematic viscosity
ρ	kg/m^3	Density
I	A	Current
R	Ω	Electrical resistance
V	V	Voltage
α		Phase fraction of austenite
K		Temperature dependent function
n		Avrami exponent
R	$kJ/(mol \cdot K)$	Universal gas constant
E_A	kJ/mol	Activation energy
A	K^{-1}	Pre-exponential constant
d	μm	Average diagonal of indenter square
F	mN	Applied force of indenter

Chapter 1

Introduction

1.1 Motivation

The Canadian automotive industry, boasting the position of eighth largest in the world, is a critical contributor to the Canadian economy. In order to maintain its globally-competitive edge, the Canadian government provides monetary incentives, such as the Automotive Innovation Fund, for automotive manufacturers to engage in large scale research and development projects to build innovative, greener, and more fuel efficient vehicles [1]; this helps automotive companies to comply with new legislations such as the 2016 to 2025 regulation requiring the reduction of automotive fleet carbon emissions levels from 155grams/km to 101grams/km [2]. Hot-forming-die-quenching (HFDQ), also known as hot stamping or press hardening, is a manufacturing process that has gained the attention of the automotive industry for its capability to produce lighter and stronger steel components such as A pillars, B pillars, engine struts, and roof rails. The process uses manganese boron steel alloy sheets cut into specified 2-D geometries, known as ‘blanks’. These blanks are heated to approximately 1223 K, and then transferred to a quenching/forming die for rapid cooling and forming into the final component shape. Figure 1 shows a schematic of the HFDQ process, the heating transforms the microstructure of the steel to austenite and the rapid quenching stage induces the formation of martensite, which is a much stronger crystalline structure.

The formed ultra-high strength steel (UHSS) components require less material without compromising component strength, which translate to reduced fuel consumptions of 0.15 - 0.7 L/100km per 100kg of mass reduction [3]. The hot forming manufacturing process exploits the high ductility and low flow-stress during forming of hot UHSS blanks to produce parts having complex component geometries in a single stroke.

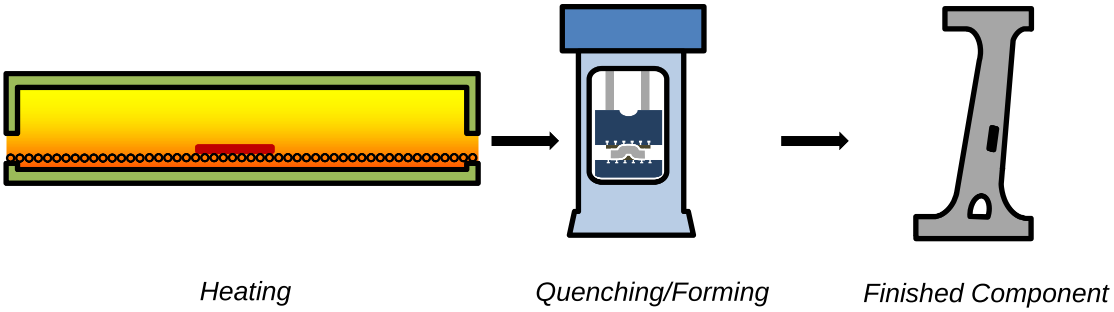

Figure 1: HFDQ process using traditional roller hearth furnace for heating

A number of steels are capable of producing the desired martensitic microstructure after heat treating, but the most commonly used steel grade in HFDQ is Usibor® 1500P [4]. It is a 22MnB5 steel with an Al-Si coating that prevents oxidation during furnace heating.

While roller hearth furnaces are the traditional heating stage used for HFDQ, they have several drawbacks in terms of high energy consumption, large floor-space, and incompatibility with the Al-Si coating of the blanks that results in ruined rollers and inefficient execution of the manufacturing process. Consequently, the goal of this work is to develop a semi industrial-sized direct contact heating die (often referred to as heating die) as an alternative to roller hearth furnaces. The heating die is a novel process designed to work in tandem with quenching/forming dies, all encompassed within a common hydraulic press. In this proposed process, the blanks are inserted into the heating die maintained at approximately 1273 K. Through conduction the blank is heated to 1223 K at a fraction of the time required for roller hearth furnaces. After heating, the blank is automatically-transferred to the quenching/forming die. Given that the heating die and forming die are on a common press, the transfer of the blank is simpler than the transfer in HFDQ processes using roller hearth furnaces, and this has the potential of being a faster and more efficient transfer process. The heating die requires significantly less space and energy to operate than roller hearth furnaces, and coupled with its reduced required heating time, translates to a considerably more efficient manufacturing process with reduced capital per produced component.

Lastly, the application of the heating die to produce parts having tailored microstructures is investigated. Current research has shown interest in producing components with crystallographic gradients that correspond to regions of high strength (martensite) and low strength (since the as-received steel contains microconstiuents such as bainite, ferrite, and pearlite) so that preferential crumple zones can be integrated into certain structural components for improved crash safety.

1.2 Industrial Context

The work in this thesis was carried out in collaboration with F&P Manufacturing Inc. (F&P), a tier-one automotive manufacturing supplier location in Tottenham, Ontario, and the Canadian subsidiary of F-Tech Inc. F&P presently uses cold stamping, welding, and hydroforming to fabricate parts and is expanding its capabilities to include hot forming. In 2012 F&P partnered with the University of Waterloo to develop a research project focused on producing an alternative to roller hearth furnaces for HFDQ. A lab-scale prototype was developed by Joshua Rasera, Peter Plaisier, Brad Froese, and Cameron Rush in 2013 that satisfied two key functional requirements of the heating stage for HFDQ: austenization of the 22MnB5 steel; and formation of the Al-Si-Fe layer. Further testing and refinement of the prototype was conducted by Joshua Rasera from 2013-2015, as part of his Master's thesis research. The final goal of this collaboration is to develop a new heating technology that will be installed in F&Ps facility to give the company a competitive edge with HFDQ process technology that operates at a lower cost than that of other competitors.

1.3 Literature Review

This section discusses the history of HFDQ along with operational parameters and drawbacks of roller hearth furnaces. The most prominently-used material in HFDQ, 22MnB5, as well as techniques developed to replace roller hearth furnaces, is examined and discussed. Finally the proposed technology, direct contact heating, is detailed in terms of its operating principles, drawbacks, advantages, and previous work.

1.3.1 Hot Forming Die Quenching

The hot forming process was invented and patented by a Swedish Company, Plannja, in 1977 for saw and lawn mower blade manufacturing [4], and adopted into the automotive industry in 1984 by SAAB. Hot forming was used to produce components in the Saab 900 that had a stronger martensitic crystalline structure that could also be made out of thinner cross sections, translating into a lighter, more fuel-efficient vehicles. This process aligned well with meeting recent government CO_2 emission standards since a reduction in 10% of the vehicle had been reported to result in a 6-8% improvement in fuel economy [5]. Since its inception, the popularity of HFDQ has grown and the number of manufactured components have increased dramatically, with an expected production of over 450 million parts per year in 2013 [6], with manganese boron steel (22MnB5) as the most common implementation in the process. The components produced for automotive application can be seen in Figure 2.

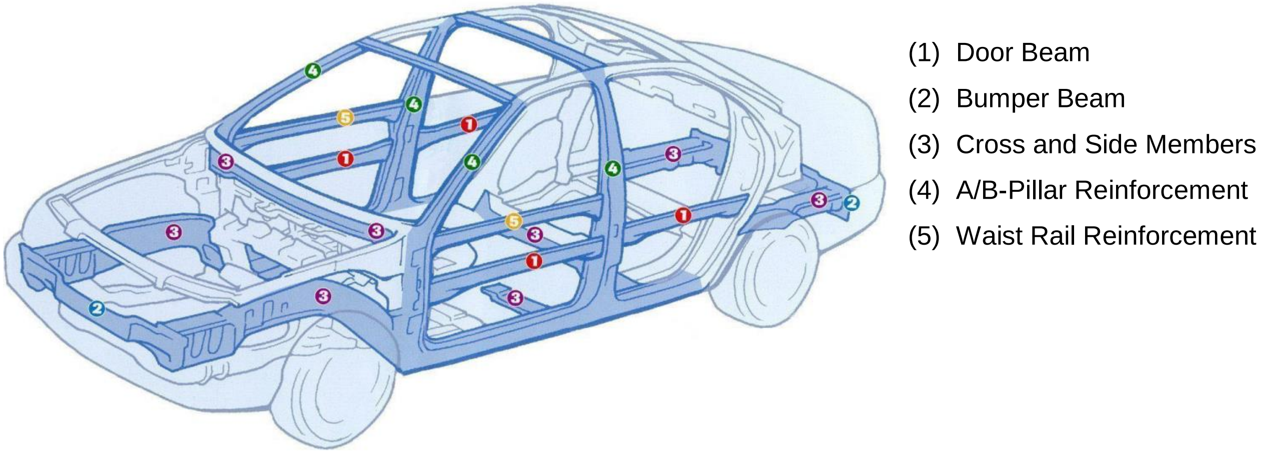

Figure 2: Automotive structural components manufactured by HFDQ [7]

Hot-forming-die-quenching consists of three stages: (*i*) transformation of the steel into austenite, a single phase solid solution of carbon stable at high temperatures; (*ii*) transfer of the steel to the forming die; (*iii*) subsequent forming and quenching of the steel part to produce a martensitic component. The heating stage austenitizes the part, increases ductility of the steel and reduces the necessary force required for forming in comparison to cold working [8]. The heating stage also allows the formation of an Al-Si-Fe layer, and prevents the formation of oxide scales [4]. Two variations of hot forming currently in use are direct and indirect, which are shown schematically in Figure 3. In the direct process, steel sheets are heated, typically in a furnace, which are then transferred to a forming/quenching die to produce the final component. In contrast, indirect hot forming starts with steel components that have nearly been formed in the desired shape, which are then heated, transferred to a forming die, and quenched and pressed into the final shape. The emphasis of this work is on the direct process.

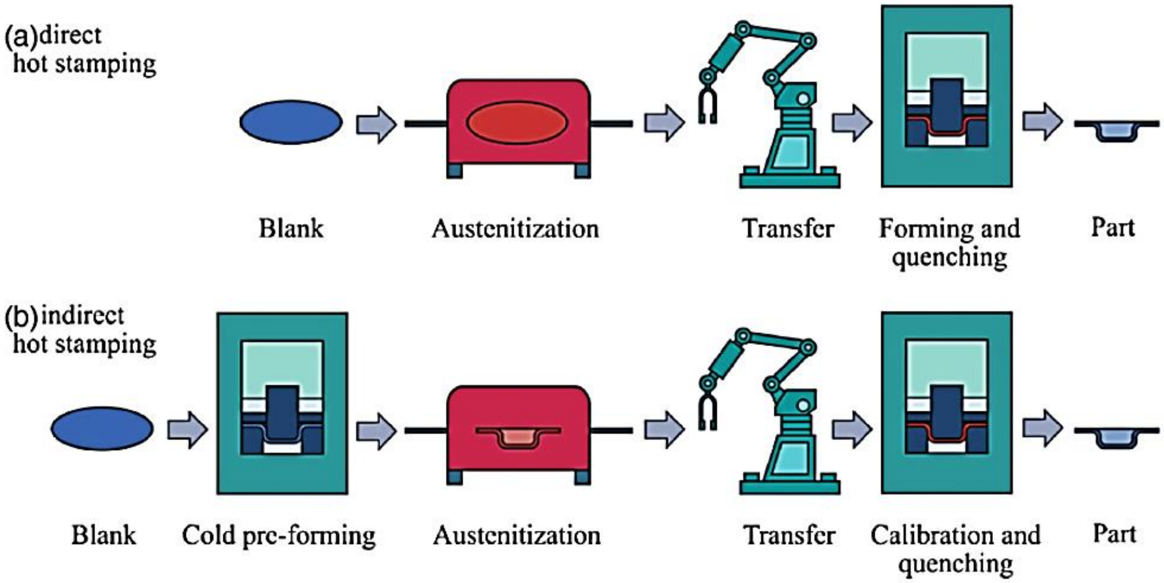

Figure 3: Basic hot stamping process chains: a) direct hot stamping, b) in-direct hot stamping [4]

HFDQ of 22MnB5 results in uniform mechanical properties and reduces, if not eliminates, spring-back in the part [9]. In comparison, inconsistent properties can result from cold working as the material experiences non-uniform strain hardening. In this case heat treatment can be applied to restore any compromised material strength, however this is slow and costly.

Research into making hot stamping more effective and efficient have mostly focused on alterations to the stamping phase, such as changes to the tooling material [10], die closing time [11], and energy used for press operation [12], whilst innovative research on the heating side has been lacking.

1.3.2 Usibor ® 1500P

Usibor® 1500P is the most prevalent UHSS used in HFDQ, produced by ArcelorMittal. It is a 22MnB5 steel with an Al-Si alloy coating. The nominal chemical composition of the material is shown in Table 1. For a heating rate of 5 K /s, the temperature at which austenite formation begins, or the Ac1 temperature, which is typically taken to be around 993 K, whilst the temperature that 22MnB5 reaches complete austenization, the Ac3 temperature, is typically taken as 1153 K [13].

Table 1: Chemical composition of 22MnB5 steel used in experiments (wt %)

C	Mn	Cr	B	Ti	Al	Si	P	S	N
0.22	1.16	0.19	0.0026	0.033	0.041	0.19	0.011	0.002	0.0055

The Ac1 and Ac3 temperatures for 22MnB5 steel are shown in Figure 4 along a line demonstrating the HFDQ heating process. Martensite formation is dependent on the austenite crystalline structure rapidly quenching. If the material is not quenched quickly enough other phases will form and become the final crystalline structure of the material. In HFDQ to guarantee a martensitic microstructure, the quenching rate must be sufficient to avoid the bainite “nose” which represents the formation of bainite in the material. Figure 4 shows that the boron present in the material causes a shift in the bainite “nose” of the time-temperature transformation (TTT) diagram to the right allowing for the necessary quenching rate to be reduced. The Al-Si coating protects the steel substrate from decarburizing and oxidizing during heating in the furnace. It melts at 848K and transforms into a permanent Al-Si-Fe layer by reacting with iron that diffuses into the coating from the steel substrate [14]. The Al-Si-Fe layer also provides additional long-term corrosion protection for the steel.

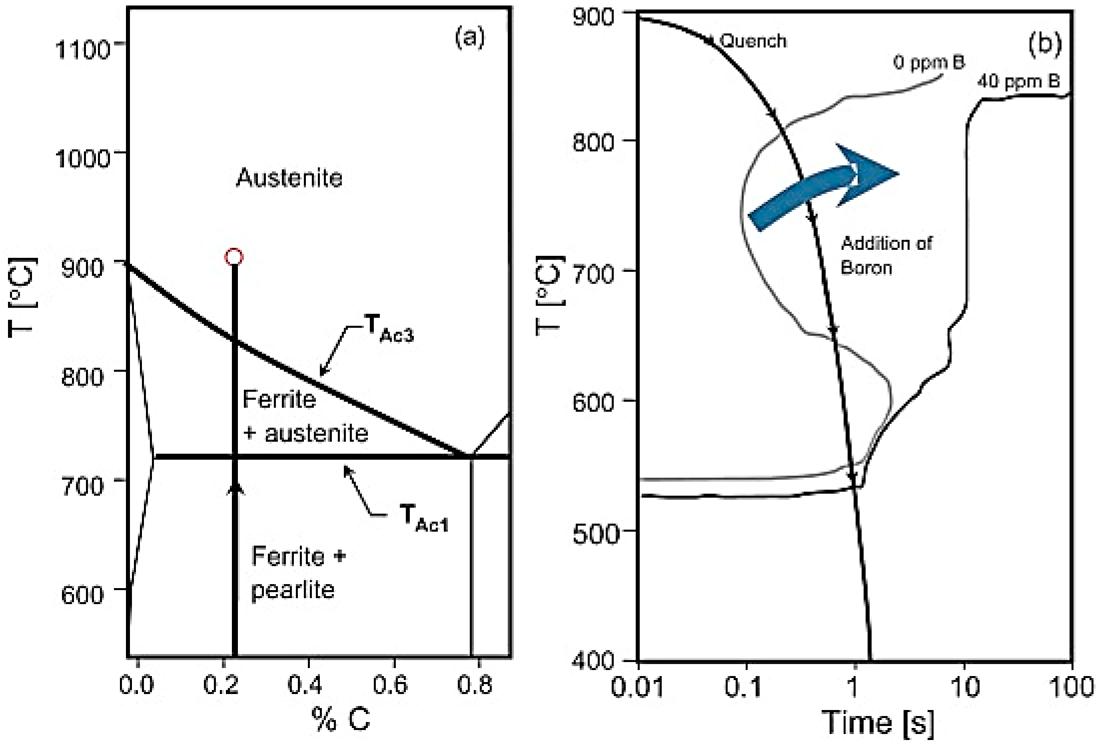

Figure 4: (a) Iron-carbon phase diagram showing austenite forming process for 22MnB5 steel and (b) hypothetical time temperature transformation (TTT) curve showing effects of boron addition in low carbon steel [14]

1.3.3 Roller Hearth Furnaces

The purpose of heating in HFDQ is to transform the as-received composition of ferrite and pearlite into the ductile austenite phase so that the blank can be formed into the desired shape and the material can be transformed into a much stronger crystalline structure, martensite, during the forming/quenching phase. The temperatures necessary for the blanks to be heated to and the quenching rate required are dictated by the Ac3 temperature and TTT diagram of the material 22MnB5, shown in Figure 4.

Traditionally the heating step in HFDQ is done using roller hearth furnaces. This technology consists of an insulated heating chamber, heating source, rollers suitable for high temperatures, and an assortment of sensors, servos, and controllers. The sizes of roller hearths vary according to mill productivity, blank geometry, required heating time, and other buffer time requirements [15], with the average furnace length used in industry being around 30-40 meters [4]. With an operating temperature range of 1223-1473 K and the size of these furnaces, the energy consumed during operation is significant. The roller hearth design requires that the length of the furnace coupled with the roller speed ensures that the blank fully austenitizes, and for the case of coated blanks, that the coating fully transforms. The coating on the blanks, made up of Al-Si, has caused operational issues for the rollers as a build-up of the coating accumulates on the rollers over time and permeates into the material, causing it to crack and shatter [12], [16]. Replacement of the rollers is a significant issue for manufacturers as it remains largely unresolved, despite efforts by researchers to develop new coatings [16]. These drawbacks, coupled with the pressure for the automotive industry to produce stronger and more energy efficient components, have pushed manufacturers into investigating alternate heating processes. Publications that have investigated improvements on the heating process have suggested induction heating, electrical resistive heating, and conduction heating [6], [4]. These novel heating techniques aim to reduce energy consumption, improve cycle time, and develop customized surface coatings and material structures.

1.3.4 Resistance Heating

In resistance heating, the blank is situated between two electrodes and a current is passed between them. Thin cross-sectional areas and the native electrical resistivity of the blank causes localized Joule heating that brings the blank to austenization temperature. The experimental results used in developing and confirming the transformation kinetics model proposed in this thesis were obtained by use of a Gleeble 3500 thermo-mechanical simulation system, which operates according to similar principles.

This heating technique can be integrated into a stamping assembly by combining it with the forming die as demonstrated in Figure 5. The complete apparatus requires far less space than the roller hearth/forming die, and the transfer time between the heating and forming stages is reduced from 5 seconds for a roller hearth furnace to 0.2 seconds [17].

As previously mentioned, the electrical resistance of the blank is inversely proportional to its cross-sectional area. Accordingly, the large electrical resistance required for austenite formation limits the geometries that could be used to long narrow steel sheets. Furthermore, complex blank geometries cannot be heated using this technique, since non-uniform shapes in the blank lead to non-uniform heating given the distributing properties of electrical currents. Process control is further complicated by the temperature-dependent nature of the material’s electrical resistivity, which resulted in varying temperature along the piece and ultimately varying material properties.

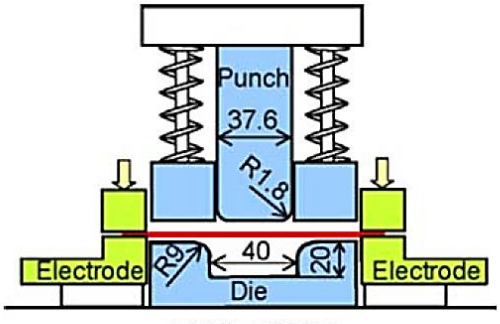

(a) Electrifying

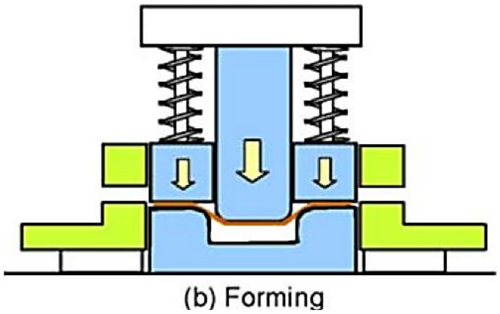

(b) Forming

Figure 5: Combined resistance heating and forming die [17]

A technique developed by Mori *et al.* (2014) was shown to produce components with tailored properties by using bypass and separated current apparatus. This is covered in more detail in Section 1.3.7.5.

1.3.5 Induction Heating

Induction heating was suggested by Kolleck *et al.* [18] for use in HFDQ. It is an established technology used for different applications, e.g. melting, tempering, and heating of materials for bulk metal forming. In this technique, alternating voltage is used to generate a strongly fluctuating magnetic field which induces eddy currents within the blank and results in Joule heating. The magnetic permeability and electrical conductivity are directly-correlated to the heat generated within the blank as well as the frequency of induced currents.

The frequency of the generator used in the apparatus affects the penetration depth of the magnetic field: low frequencies correspond to a high penetration depth, while high frequencies to a low penetration depth. This effect has use in applications like surface hardening which defines the thickness of the hardened layer. Three main variants of induction coils exist: longitudinal field, cross field, and face inductors. They each produce magnetic waves with different efficiency factors and result in various levels of temperature homogeneity. Of the three inductor coils, longitudinal field and face inductor were used for their combined ability to produce a uniform temperature distribution of ±10K that reaches above Ac3. Research by Kolleck *et al.* [18] still has to prove whether induction heating is compatible with the Al-Si coating and whether this technique can be expanded to produce tailored components.

1.3.6 Direct Contact Heating

In direct contact heating, the focus of this thesis, two hot plates are used to heat blanks to austenization temperatures through conduction. The two hot plates are typically mounted in a die and act as its striking surface and there are numerous ways to heat the plates. The first technique to use direct contact was developed by Ploshikhin *et al*. [19] and used induction heating to bring two plates above 1173 K. To overcome coating adhesion Ploshikhin *et al.* [20] later designed the process so that the die was minimally opened with the blank suspended between the die surfaces. This resulted in a portion of the heating process using radiation heat transfer to heat the blank to the austenizing temperature, allowing the Al-Si-Fe coating on the blank to mature. Figure 6 depicts the heating profile that the blank underwent, highlighting the heating techniques used throughout the process.

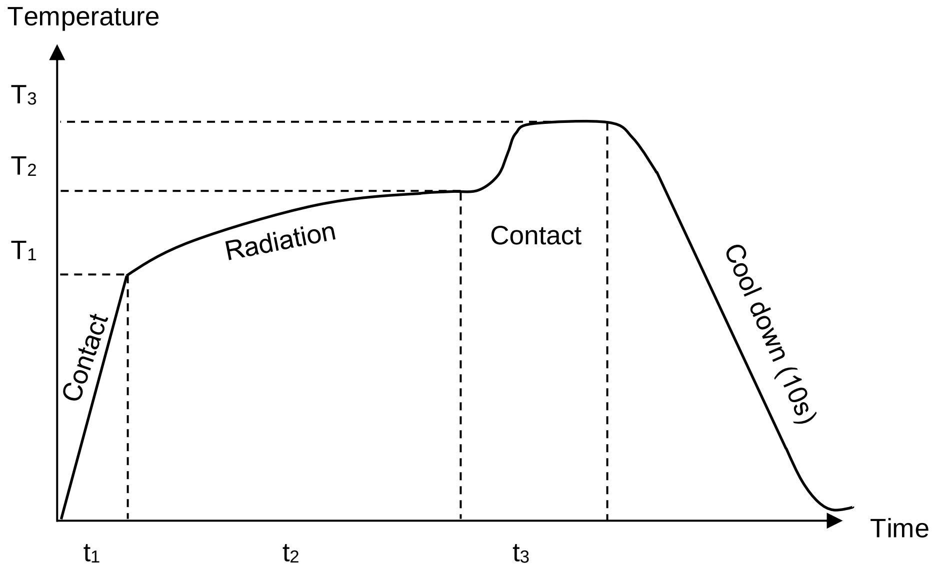

Figure 6: Temporal shape of heating profile presented by Ploshikhin *et al.* [20]

This work and its prototype [15] used resistance heaters embedded in the bottom die to heat the striking surfaces. This technique was capable of bringing the tested coupon to full austenization in 21 seconds, and transformed the Al-Si coating into a permanent Al-Si-Fe intermetallic layer with the intermetallic compounds typically found in furnace-treated samples [15]. Figure 7 shows an SEM image of a cross-section of a tested Usibor® 1500P sample in the prototype heating die. The transformation of the coating is highlighted and the intermetallic compounds found are itemized in Table 2 [15].

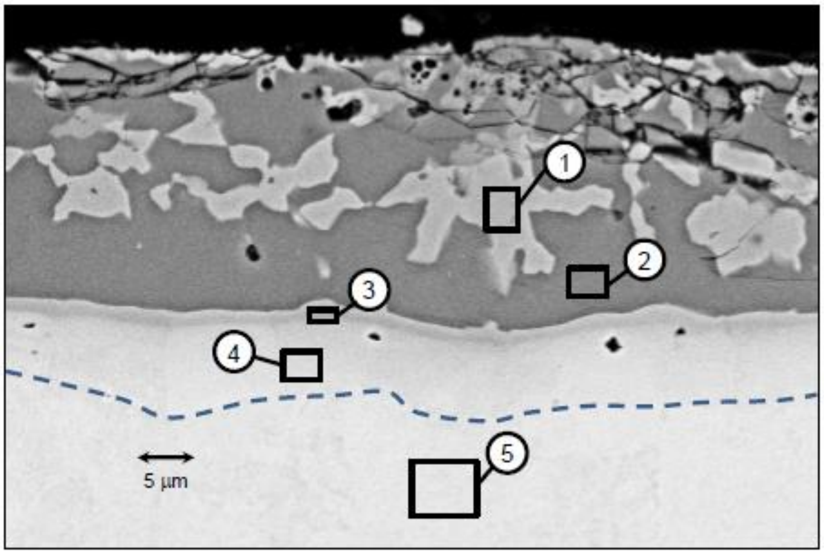

Figure 7: SEM image of the cross section of a 25-second direct contact heated Usibor® 1500P coupon, with EDS investigation regions highlighted. Dotted line denotes the separation of the coating α -Fe region from the steel substrate [15]

Table 2: Chemical composition of Al-Si-Fe intermetallic phases by EDS [15]

Num.	Phase	Chemical Composition (at.%)			
		Al	Fe	Si	Mn
1	AlFe	39.59	41.82	17.52	1.07
2	Al_5Fe_2	70.57	27.05	1.86	0.51
3	AlFe	39.67	43.47	13.88	0.96
4	α-Fe	14.77	79.09	4.44	1.20
5	Fe substrate	0.45	92.91	0.59	1.72

Drawbacks for this technique involve the fragile silicon carbide heaters used to heat the die; the heaters fractured on several occasions due to a combination of thermal expansion and electrical grounding with the die. Another drawback addressed by Rasera [15] is the adherence of the Al-Si coating to the striking surface of the die. A boron nitride spray was found to prevent sticking but it was slowly removed during subsequent testing.

1.3.7 Tailoring

During automobile collisions the safety of the passenger relies on: *(i)* the crumple zone to absorb the energy from the impact; and *(ii)* the high material strength of the safety cage (passenger compartment) to ensure that it remains intact. In rear and front collisions the crumple zones are designed in the rear and front of the cars as shown in Figure 8.

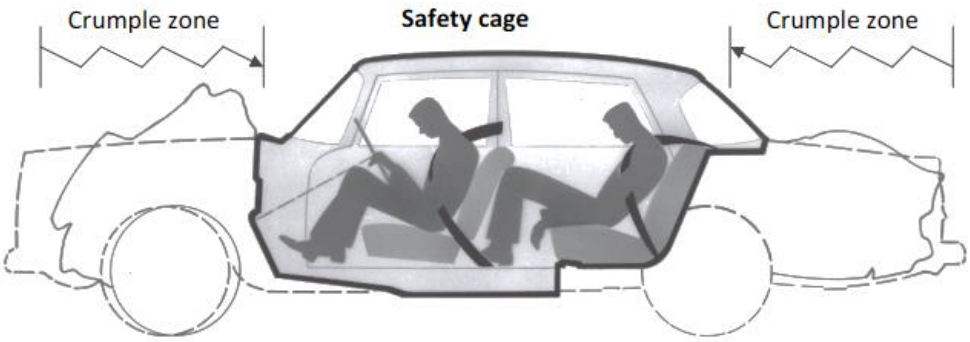

Figure 8: The major crash management zones of a vehicle [21]

These two generalized areas (crumple zone and safety cage) have distinct safety requirements and are therefore typically equipped with steels that have different material properties, for example, a dual phase steel would be used for a crumple zone due to its plasticity, and a martensitic steel with high yield strength would be used to prevent intrusion of the safety cage during a crash event [21].

In contrast, the side of automobiles do not have readily available regions to act as crumple zones and as such are the most difficult to design for to meet the Insurance Institute for Highway Safety (IHSS) standards, which were refined in 2011 to significantly strengthen pillars so as to resist intrusion and absorb crash energy [22], [23]. In order to meet this standard, automotive manufacturers have started investigating tailored B-pillars that have distributed material properties so they can act as both the crumple zone and safety cage.

Tailoring refers to a method of manipulating the crystalline structure in steel to achieve formed parts having distributed material properties. Methods to achieve these properties include: tailor welded blanks (TWB), tailor rolled blanks (TRB), tailored quenching, post tempering, and partial austenizing, which includes the tailoring technique used in this work. The following sections discuss the previously listed techniques, their advantages, and their disadvantages.

1.3.7.1 Tailor Welded Blanks (TWB)

This process uses several different alloys with various strength or thickness to produce a part by joining the materials into a single sheet. A door ring, front rail, and rear rail were successfully produced using TWB with reduced weight and retained intrusion prevention by Munera *et al.* [24]. Drawbacks of this process include heat affected zones, which can cause limited formability and shifting of the weld line between different materials during forming [25]. It is therefore crucial that the blank is properly located within the die prior to forming the component.

1.3.7.2 Tailor Rolled Blanks (TRB)

Tailored rolling produces strips of varying thickness along the length of a single blank [26]. This approach differs from TWB as the blank in TRB is composed of a single as-received material. Twelve different vehicle models were shown to use TRB parts to reduce overall weight by a survey conducted by Perez-Santiago *et al.* [27] . The varying thickness of the blank allows for the component to be designed as either intrusion-protected or energy-absorbing. This process is advantageous over TWB as it eliminates the joining process before or after forming. A disadvantage of this process lies in the potential movement of the thickness step during the forming stage of TRBs. This change could alter the contact pressure between the blank and dies and affect the cooling rate of the formed part, resulting in different microstructure and mechanical properties than intended.

1.3.7.3 Tailored Quenching (Tailored Tempering)

This technique employs different cooling rates to take advantage of the different phases produced by various low quenching rates as demonstrated by the TTT diagram in Figure 9.

Mori *et al.* [28] produced a tailored top hat component by introducing low cooling rates in the quenching tool. This was done by using a grooving tool to introduce gaps between the tool and work piece so that some regions of the blank do not contact the chilled tool. This led to a hardness of 275HV for the low quenching rate regions and a hardness of 450HV for contacted regions. This technique was capable of tailoring without requiring in-die heaters, but this technique is only readily applicable to flat surfaces.

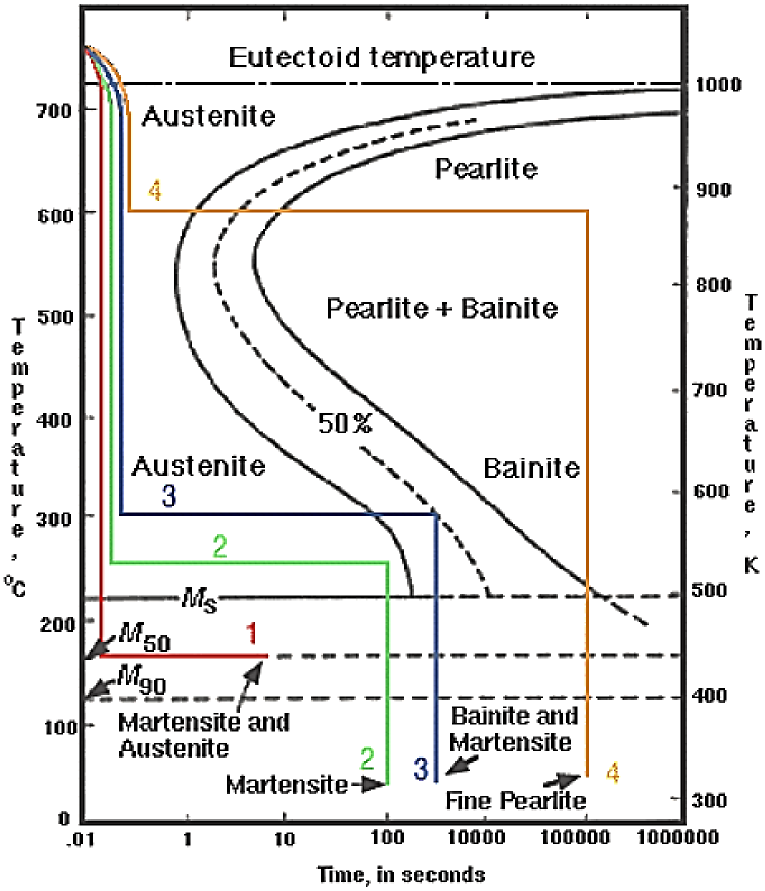

Figure 9: TTT diagram for boron alloyed steel [21]

Mori *et al.* [28] described using die materials with varying thermal conductivities to control the cooling rate of the blank and influence the final microstructure of the component. Ceramic plates with a low thermal conductivity of 2W/(m·K) were used in regions of the quenching die to achieve areas with a hardness of 250HV whilst regions in contact with the native die material, 4140 steel with a thermal conductivity of 25W/(m·K), resulted in a hardness of 475HV. It should be noted, however, that the thermal diffusivity, not thermal conductivity as stated by Mori *et al.* [28], should be the mentioned material property responsible for these results as it dictates the time rate of temperature change as heat passes through a material. This technique is advantageous in that it also does not require in-die heating, which can be costly, however the range of materials that are operational at the temperatures and forming pressures needed for this process limits the available range of thermal diffusivity that can be used with this technique.

George *et al.* [29] used in-die heating to produce partially tailored pieces. Cartridge heaters were installed in the lower half of a die segment to heat a local region up to 673 K with another die segment separated by an air gap of 1 mm to act as the cooled die region. The heated region developed a bainitic and ferritic microstructure with a hardness range of 262-304 HV and the cooling tool achieved a fully martensitic microstructure of 505 HV. The ability of this method to vary the temperature distribution is a favorable attribute of this design, however the additional machining cost to produce this die is disadvantageous as well as the difficulty in maintaining precisely controlled temperature gradients given that the die would constantly be moving towards thermal equilibrium. Several other researchers have used similarly designed tailor quenching dies, such as Erturk *et al.* [30], Banik *et al.* [31], and Svec and Merklein [32], and have had comparable results.

1.3.7.4 Post Tempering

Post tempering used for tailoring purposes amount to heat treating of local regions in as-formed hot stamped parts. A study conducted by Labudde and Bleck [33] investigated the effects of heat treatment in an atmosphere furnace for 30 minutes at set temperatures of 473 K, 573 K, 673 K, 723 K, and 873 K, followed by slow cooling to room temperature. The Vickers hardness of the specimen before post-tempering was recorded at 550HV, and after tempering the hardness reduced to 515 HV, 470 HV, 380 HV, and 270 HV, respectively. This process eliminates the need for expensive and complex in-die heating designs with cartridge heaters and coolant channels. The main drawback is that post tempering amounts to an additional step which has a relatively long processing time and is a major drawback from a production standpoint.

1.3.7.5 Partial Austenizing

This technique is accomplished by heating only one region of a blank to cause partial austenization. Wilsius *et al.* [34] used a technique where a heat shield was placed above and below a region of the blank during heating, and this resulted in the hardened region having an ultimate tensile stress (UTS) of 1600MPa with 6% elongation and the shielded region with a UTS of 700 MPa and 16% elongation.

Another technique, employed by Mori *et al.* [35] used resistance heating with a bypass strategically situated to divert the current from select areas, thereby preventing these areas from reaching austenizing temperatures. This process is shown schematically in Figure 10. Mori *et al.* [35] also investigated a separated current technique to divert the current but had less successful results than with the by-pass apparatus.

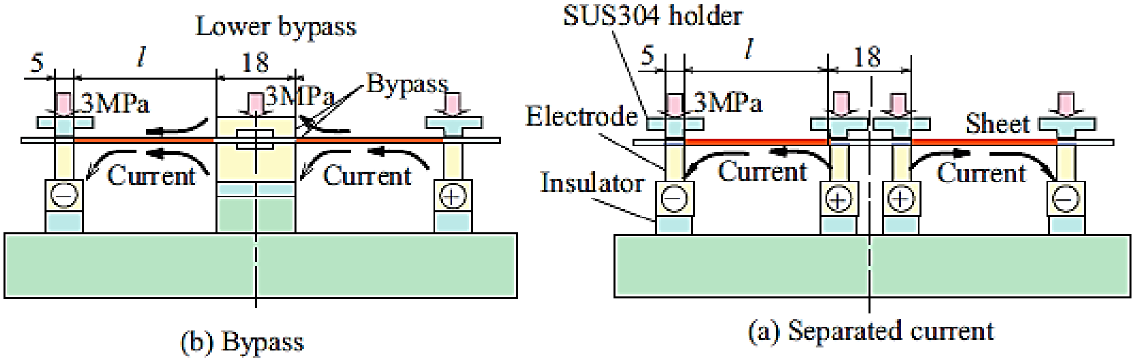

(b) Bypass

(a) Separated current

Figure 10: Resistance tailored heating by separated current and bypass [35]

This tailoring technique allows for control over the component microstructure without complex die designs; controlling multiple thermal zones may be challenging, however, and the blank must be properly aligned before heating. This technique also suffers from the shortcomings associated with resistance heating, as described in Section 1.3.4.

The tailoring technique, used during the prototype testing phase, used a striking surface that had regions of different thermal effusivities [15]. Regions of low thermal effusivity took significantly longer to heat the steel to austenization temperature in comparison to the high thermal effusivity region; this allowed for partial austenization of the blank when it was removed from heating at a strategically designed time. The striking surface was made out of an interchangeable steel plate, allowing for an easy transition to different tailoring geometries as desired, shown in Figure 11. Based on these trials the technique was adopted for this work as well.

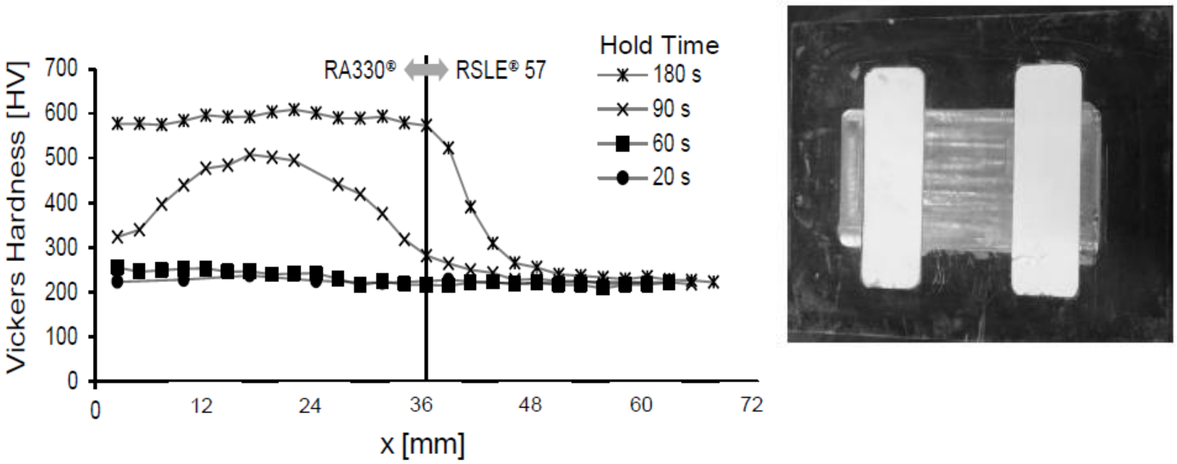

Figure 11: Micro-hardness map of tailored transition region in heat treated Usibor® 1500P sample (Left) and prototype striking surface for tailoring with ceramic inlays (white) (Right) [15]

The low effusivity material was RSLE 57, a high temperature resistant alumina silicate. The material used for high thermal effusivity was RA330, a nickel alloy steel resistant to oxidation, and carburization at high temperatures. Since the tailoring of the steel microstructure was performed on the heating side, this process only required a rapid quenching technique to produce the desired martensitic microstructure. This removes the need for expensive and complicated heating-quenching dies, or additional heat treatments necessary in post-tempering operations. It also has a reduced production time in comparison to most techniques, since drawn out cooling times are not required, or additional low temperature holding periods. Challenges encountered with this process involve achieving proper alignment needed to realize the tailored segments in the intended regions, and coating adhesion to the die surface, which was discussed in Section 1.3.6.

1.4 Thesis Objective

The goal of this work was to develop a semi-industrial sized direct contact heating die for application in HFDQ, based on the prototype by Rasera [15]. This included addressing the challenges outlined during the prototype testing phase; *(i)* the need for an automated transfer system from the direct contact heating die to quenching apparatus; *(ii)* preventing the adherence of the blank to the heating die surface; and *(iii)* the need for a thermo-metallurgical model to predict the martensite composition of the blank to facilitate optimization of the tailoring geometries in the surface of the heating die.

1.5 Thesis Outline

This work presents the design process for a semi-industrial size direct contact heating die for HFDQ. Chapter 2 details the criteria and constraints for designing the contact heating die, quenching die, and transfer mechanism. Simplifications made to the governing heat transfer equation in the initial design phase are presented and compared to subsequent multiphysics models used to predict the behavior of the contact heating die. Based on these predictive models the material selection, electrical configuration, and the final contact heating die design are also presented. The transfer mechanism and quenching die are discussed, and a heat transfer model is presented on the quenching die as it pertains to possible future use in a continuous operation setup.

Chapter 3 discusses the tailoring model developed to predict the final microstructure of the heat treated component. The kinetics of austenite phase transformation is detailed along with a literature review of models used to describe the kinetics phase transformation. Experimentation on the phase transformation of austenite in 22MnB5 steel is described, and the results are used to develop a predictive austenite kinetics model. The final model is combined with the heat transfer models presented in Chapter 2 to give the integrated thermo-metallurgical model used for tailoring.

Chapter 4 outlines the testing procedure for heat treatment of the blank. The preparation of the blank for heat treatment is discussed as well as the methods used to analyze the material properties after the heat treatment.

Chapter 5 presents the results of experimental testing and discusses the testing procedure and post-heat treatment analysis. The data collected is used to validate the multiphysics tailoring models presented in Chapter 2 and Chapter 3.

Chapter 6 presents the main conclusions of this thesis. Improvements to the design process and additional testing regimes are suggested.

Chapter 2

Experimental Equipment Design

This chapter outlines the design process for the direct contact heating apparatus. The design considerations, based on the criteria given and constraints experienced, are detailed and presented primarily in three separate sections: the direct contact heating die (often referred to as the 'heating die'); the quenching die; and the transfer mechanism. The design of the heating die is discussed in more depth compared to the other components since it is the focus of this research and has the most complex design needs. The major challenges encountered during the design and operation of the heating die were electrical failures of the heating elements and complications associated with transferring the heated blank from the heating die to the quenching die. A heat transfer model of the die, which was designed as an input for the predictive tailoring model and is covered more extensively in Section 2.5, was a key tool in selecting a configuration for the electrical system to overcome heater failures encountered. Designing, modeling, and testing of the die, was an iterative process to validate the predictive heat transfer model and optimize the final system. The heat transfer model of the die was a crucial component to the design process, the details of which are presented in Section 2.5. The quenching die also required a heat transfer model, which is also presented in Section 2.5.

2.1 Experimental Lab Constraints and Design Criteria

The direct contact heating apparatus was tested in the University of Waterloo High Pressure Laboratory. There are two hydraulic presses in the aforementioned lab that are capable of accommodating the heating die designed in the present work, as shown in Figure 12.

(a) (b)

Figure 12: 250 ton press (a) and 900 ton press (b)

The press shown in Fig. 12 (a), which was used for the prototype testing, operates at 250 tons and has a working area of 0.6m^2. The press shown in Fig 12 (b) is a 900 Ton Macrodyne high speed hydraulic press. It has an bolster area of approximately 2m^2 (1.2m x 1.8m), with an external user interface that controls the opening and closing operation of the press, monitors the temperature of up to 8 thermocouples, and controls cushion pins residing within the bolster of the press. The press is equipped with a safety light curtain that discontinues all press activity once an object is detected within a meter of the front of the press and a mobile furnace is located on the side of the press.

The criteria for the final design was identified by the research partner, F&P Manufacturing Inc., during the prototype phase. The final heated die design must be compatible with an automated industrial manufacturing line and perform on a competitive level with roller hearth furnaces, which are the current standard for HFDQ. Those needs are detailed in the following criteria:

1. The blanks must be austenitized uniformly in regions intended for martensitic microstructure; uniform austenization in a steel blank is achieved by uniformly heating the blank past the Ac3 temperature and quenching at a rate above 27K/s
2. The die needs to be able to run continuously while maintaining the required operating temperature. It has to accommodate the transfer and removal of blanks from its striking surface without requiring significant heat-up time in between loading and unloading;
3. The die should require less energy for operation compared to roller hearth furnaces;
4. The austenite-martensite process needs to have a competitive material processing time, i.e. the time required for full austenization of the blanks must be less or equal to that of roller hearth furnaces;
5. The Al-Si surface coating of the Usibor® 1500P blanks must remain intact and become fully transformed into the Al-Si-Fe coating as confirmed by optical metallography; and
6. The die needs to easily facilitate automated input and removal of blanks onto its striking surface

Prototype testing was able to demonstrate criteria points 1, 3, 4, and 5 to be satisfied, however points 2, and 6 were not within the scope of Rasera's research [15]. Listed below were the requirements necessary for satisfying points 2 and 6:

1. A transfer system, to remove the hot blank from the heating die;
2. A means to prevent sticking of the blank to the striking surface;
3. A quenching die, to simulate in-die quenching used in industry; and
4. A more flexible electrical insulator for the heating elements to prevent electrical failure

Rasera [15] also suggested modelling the behavior of the steel during heat treatment to optimize the blank heat treatment process and final product performance. These suggestions entailed:

- Examining the effects of axial conduction in shielded (tailoring) regions; and
- Developing a kinetics model to predict the blank austenization fraction.

These points are examined and discussed in Chapter 3.

2.2 Direct Contact Heating Die Design

The direct contact heating die was designed as a larger version of the lab scale prototype. The goal of this work was to improve upon the issues encountered during the prototype phase while scaling the experimental work closer to the expected size of an industrial die. Consequently, the design work and material selection made use of results from the prototype stage, which allowed for an expectation of the final design shape and performance. This section details the design process for the heating die, starting with a preliminary estimation of the heating requirements, losses, and performance of the heating die, followed by the material selection, and electrical design, and concluding with the final product and performance.

2.2.1 Heating Power, Heat Losses, and Thermal Effusivity

This section reviews design-phase calculations of three key performance metrics of the die: the heating power required to bring the die up to temperature, expected heat losses, and the heat flux between the die surface and blank. The goal of these calculations was to establish power loads and heat transfer to the blank to a first approximation and inform the die design, as such, simple physical systems were used to represent the die and blank. A full multiphysics model of the final design was developed in COMSOL [36]; details of this model are presented in Section 2.5.

2.2.1.1 Heating Power

Heat is provided to the die by heaters embedded within the monolith. This heat can be adjusted by varying the number and location of heaters; modifying the electronic configuration of the heaters, wiring them in series or parallel; and altering various characteristics of the power supply. In order to choose the heaters for the die, finding the power required to heat the die to operating temperature was necessary. Section 2.2.3 describes the process for selecting and placing heaters and the design of their electrical configuration once the necessary heating power of the heaters was established.

The power required to heat the die is calculated using an energy balance. Heat transfer in the die resembles heat transfer in the prototype [15], which is dominated by conduction to the press bolster and radiation from the striking surface to the surroundings. However, as the die is closed during heating, radiative losses during this period are not significant. Figure 13 shows a cross-section of the heated die.

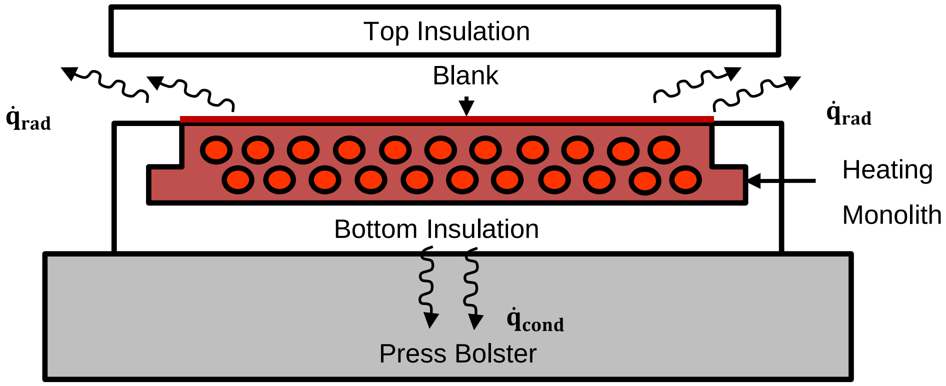

Figure 13: Diagram of primary heat losses in heating die

A control volume was taken around the heating die, shown in Figure 14, and was analyzed to determine a first estimate of the power required from the heaters to heat the die to operating temperature.

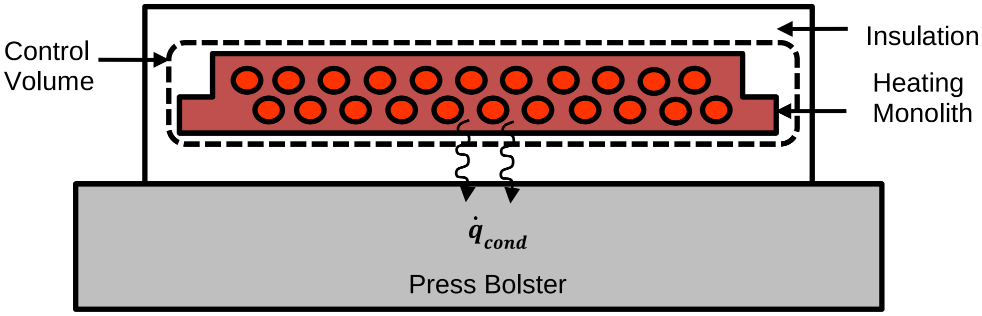

Figure 14: Control volume used in preliminary calculations

Calculating this energy balance required knowledge of the die geometry, material, and operating heating parameters, this was estimated as follows: the area of the die was estimated given that the heating die size must be approximately half of the bolster area, as stated in Section 2.1. The area used for electrical wiring was taken as a third of the total die area, and the transfer system was estimated to require about a 250 cm space between the dies which left an area of area of 0.5 m² (1 m x 0.5 m) for the monolith and surrounding insulation. The thickness of the insulation around the die was taken to be the maximum available for RSLE 57, the insulating material used in the prototype, at 50.8 mm. Given all of this, the estimated area of the monolith was 0.4 m^2. The height of the monolith was taken to be close to that of the prototype at 60 mm. The mass of the monolith was calculated to be 191 kg, using the density of RA330 (7944 kg/m^3), the material used in the prototype, and the estimated volume (0.024 m^3).

The heating requirements of the heating die relied upon the austenite formation of the blank. Since complete austenization occurred after the Usibor® 1500P blank reached Ac3, it was imperative that the monolith reach temperatures exceeding 1153 K to ensure the finished product had the desired microstructure. Experimental work using the prototype showed that a surface temperature of 1273 K was required for the blank to heat to 1153 K in 20 s; therefore the heating die was designed to reach surface temperatures above 1273 K, with an expected operating temperature inside the die between 1373 K and 1473 K.

The Biot number of the heating die was calculated using,

$$Bi = \frac{UL_c}{k} \tag{1}$$

where U is the overall heat transfer coefficient of the heat energy leaving the heating die to the press, L_c is the characteristic length, and k is the thermal conductivity of the heating die. The term U was calculated by using the conduction shape factor for a cuboid in an infinite medium and was found to be 4.82 $W/(m^2 \cdot K)$, the characteristic length was calculated as the volume of the die divided by its contact area with the press to be 60mm, and k was taken as the averaged thermal conductivity of the RA330 from room temperature to 1273 K, at 18.95 $W/(m \cdot K)$. This gave a Biot number of 0.01, which suggested a lumped capacitance approach was suitable.

Heating of the die was calculated as a lumped capacitance problem with the bolster temperature constantly at standard temperature. This temperature condition was selected to provide an upper bound on the heating power estimate. Only conductive losses were considered, as radiation during the heat up period was not significant [15]. The expression,

$$mc_p \frac{dT_{die}}{dt} = P_h - \frac{kA_{surf}(T_{die} - T_\infty)}{L} \tag{2}$$

describes the energy balance of the die where the T_{die} is the temperature of the die, m and c_p are the mass and specific heat of the monolith, respectively; T_∞ is the press surface temperature; k_1 is the thermal conductivity of the bottom insulation; A_{surf} is the area of the bottom of the die; L is the thickness of the insulation; and P_h is the power delivered by the heaters.

Taking the power P_h to be constant and $T = T_\infty$ at $t = 0$, the solution to Eq. (1) is given by

$$T_{die} = -\frac{LP_h}{k_1 A_{surf}} e^{-\frac{k_1 t A_{surf}}{mc_p L}} + \frac{LP_h}{k_1 A_{surf}} + T_\infty \tag{3}$$

The power P_h in Eq. (2) was computed to be 19.4 kW for the die to reach operating temperature in two hours using the estimates described earlier, along with the temperature-averaged specific heat of RA330 (0.5 kJ/(kg·K) at 873 K), and thermal conductivity of RLSE 57 (0.75 W/(m·K)). This calculation did not consider the removal of material from the monolith to make space for the heaters.

A more refined simulation of the die was conducted using finite element analysis (FEA) in COMSOL® (see Section 2.5 for further details), with the calculated P_h as a starting value. The COMSOL® analysis found that 19.4 kW was a suitable power output for the heaters to heat the die surface to 1273 K within 2 hours. This power output was later used in determining the heaters chosen and the die was designed around this requirement.

2.2.1.2 Heat Losses

The main heat losses by the die to the environment was by conduction to the press bolster, and radiation from the die surface when the die was opened, as previously mentioned. The heat lost by conduction is described by the last term of Eq. (1) and is plotted in Figure 15, it can be better approximated by using the temperature of the bottom of the monolith (instead of an assumed lumped monolith temperature) as well as by replacing the term T_∞ with a varying bolster temperature during heat-up. A refined analysis of the heat losses by conduction was acquired by using COMSOL® Multiphysics software (see Section 2.5 for further details) to compute the averaged temperature difference between the bottom of the monolith surface and press bolster surface in the right hand term of Eq. (1); these results are also plotted in Figure 15.

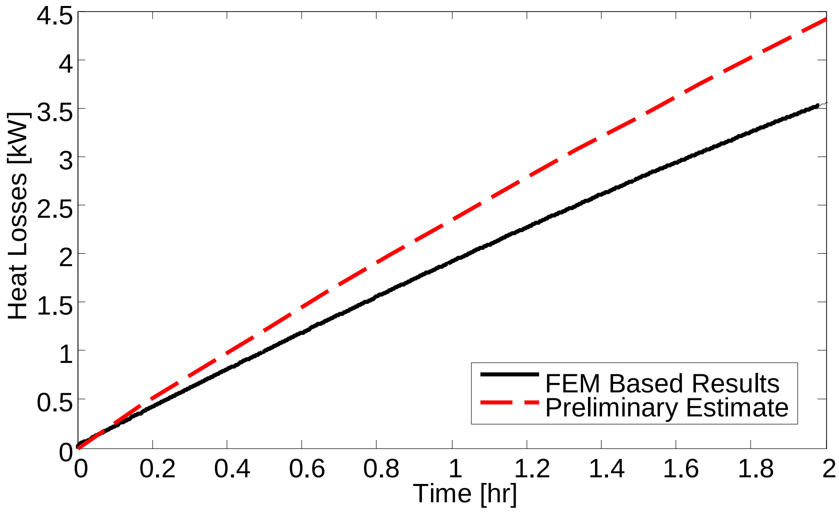

Figure 15: Heat loss by conduction to press bolster during heat up

The heating die and press were modelled to begin at room temperature with no temperature difference to drive heat losses. As the monolith temperature increased the temperature difference between the monolith bottom surface and press bolster increased, and the heat losses increased correspondingly. The heat losses during operation were therefore expected to be around 3.5 kW. An estimate of the maximum heat loss by conduction was taken to be 30% higher than the FEM results.

Radiative losses from the surface of the die to the environment were dependent on the distance between the surface of the die and the top insulation (open distance). This relationship was calculated using

$$q_{rad} = A_{surf} F_{surf-surr} \varepsilon \sigma \left(T_{surf}^4 - T_{surr}^4 \right) \tag{4}$$

where the die surface area was estimated to be A_{surf} = 0.4m^2; die surface temperature was T_{surf} = 1273 K; surrounding temperature was T_{surr} = 293 K; emissivity ε (a conservative estimate for the emissivity for oxidized nickel at a high temperature [37]), σ = 5.67x10^{-8}W/(m^2·K^4), and the view factor between the die surface and surroundings is $F_{surf\text{-}surr}$ [38].

The view factor relationship used was

$$F_{surf-surr} = -\left(\frac{2}{\pi XY}\right)\left\{ln\left[\frac{(1+X^2)(1+Y^2)}{1+X^2+Y^2}\right]^{\frac{1}{2}} + X*(1+Y^2)^{\frac{1}{2}}*atan\left(\frac{X}{(1+Y^2)^{\frac{1}{2}}}\right) + Y(1+X^2)^{\frac{1}{2}}*atan\left(\frac{Y}{(1+X^2)^{\frac{1}{2}}}\right) - X*atan(X) - Yatan(Y)\right\} \tag{5}$$

where x =0.69 m, y = 0.35 m, are the revised length and width of the heating die surface. L_{open} is the separation distance between the upper and lower surfaces of the heating die, $X = x/L_{open}$, and $Y = y/L_{open}$. This treatment assumes the die and top insulation surfaces are uniform and equal in temperature. The radiative heat losses as a function of distance between the top insulation of die surface is shown in Figure 16. Given that heat loss by radiation increased as the die opening increased, the die was programmed to open minimally during operation.

Natural convection losses from the striking surface were found using Newton's law of cooling:

$$q_{conv} = \bar{h}A_{surf}\left(T_{surf} - T_{surr}\right) \tag{6}$$

The convection coefficient was derived from [38]:

$$\overline{Nu_L} = \frac{\bar{h}L_c}{k_f} = 0.54Ra_L^{1/4} \tag{7}$$

where

$$Ra_L = \frac{g\beta\left(T_{surf} - T_{surr}\right)L_c^3}{\alpha_{td}\nu} \tag{8}$$

The term L_c is the characteristic length given by $L_c = A_{surf}/P$, $T_f = (T_{surf} + T_{surr})/2$. T_f is the film temperature, at which the air properties in Eq. (**8**) are evaluated.

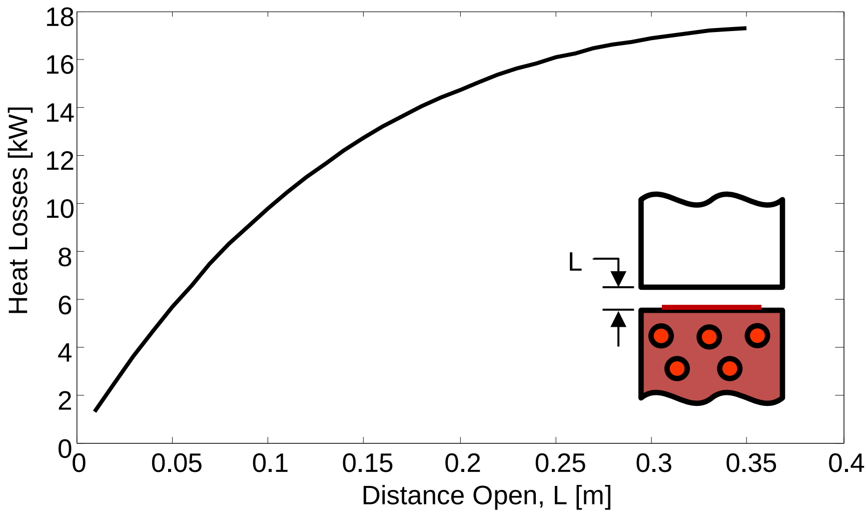

Figure 16: Predicted heat losses from striking surface as a function of die open distance, *L*

The radiative and convective heat losses were confirmed to be insignificant compared to the conduction losses during the heat-up time of the die.

2.2.1.3 Thermal Effusivity

The transfer of energy from the die to the blank by conduction depends on the thermal effusivity of the surface material, and as such, the thermal effusivity of the striking surface was investigated. Previous work with the prototype showed the thermal effusivity had a significant effect on the heat transfer between the blank and striking surface. The heat flux between the blank and striking surface was calculated using

$$\boldsymbol{q''_{\rho c_p k}(t) = -\frac{(\rho c_p k)^{\frac{1}{2}}}{\pi^{\frac{1}{2}} t^{\frac{1}{2}}}\left[T_{surf} - T(t_0)\right]} \tag{9}$$

where the term $(\rho c_p k)^{\frac{1}{2}}$ is the thermal effusivity of the material used [39], assuming a constant striking surface temperature. This calculation presumes 1D heat transfer and was more thoroughly investigated when modelling the heat transfer to the blank in the FEM model computed using COMSOL.

Materials with high thermal effusivities allow for higher rates of heat transfer and vice versa which allowed for the local manipulation of austenite formation in the blank by selective heating in the prototype [15]. A graph showing the heat flux expected from the striking surface to the blank is shown in Figure 17 for a material of high thermal effusivity (RA330) and low thermal effusivity (RSLE 57). These materials were used in the tailored striking surface of the prototype and ultimately in the tailoring plate developed through this research.

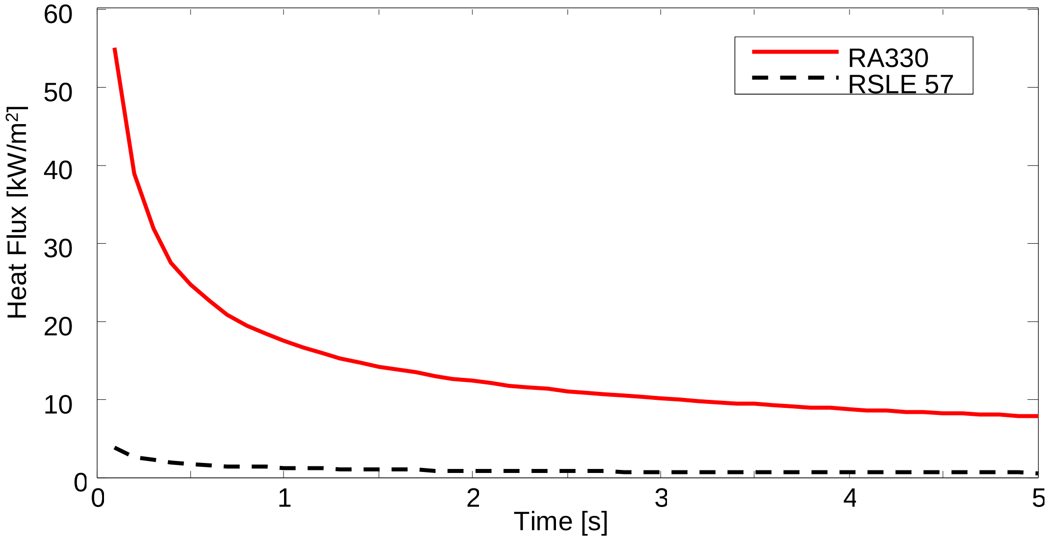

Figure 17: Prediction of striking surface to blank heat flux for RA330 alloy heating surface and RSLE 57 insulating surface

The decreasing trend seen in Figure 17 was attributed to the blank heating up after initial contact with the die surface; as the blank approached the die surface temperature, the heat flux declined with decreasing temperature difference. This trend is not as easily noticeable with the insulation material, RSLE 57; the thermal effusivity of the material was low enough that high temperature difference had comparatively low effects on the heat flux. This served as a favorable characteristic when combined with a high thermal effusivity material like RA 330 since it allowed for tailoring the blank microstructure. Using coupled materials with different thermal effusivities has limitations, however, in the form of axial conduction. A region of partial austenization developed between the high and low thermal effusivity segments, which was affected by the blank heating hold time, size ratio of the high and low thermal effusivity regions, and thermal effusivities used.

Further examination on the effect a higher thermal effusivity material had on the blank showed that the higher the heat flux, the quicker the blank was heated to Ac3; this translated to a faster, and therefore more profitable, manufacturing process.

2.2.2 Material Selection

As identified in Section 2.2.1, the material chosen for the monolith needed to withstand temperatures up to 1473 K. Referring to the prototype experiments, the material would also need to withstand compressive forces and be resilient to oxidation. The material chosen for the prototype, RA330 (35Ni-19Cr-1.25Si), proved suitable for operation under these conditions and was therefore ultimately chosen. Other suitable materials considered included Inconel 600, Inconel 601, and SS310. The Inconel materials both had superior high temperature performance compared to RA330, but cost nearly three times that of RA330. SS 310 had a more competitive price to RA330, but inferior high-temperature properties.

The monolith insulation consisted of RSLE® 57 ceramic insulation, with a thermal conductivity of 0.75 W/(m·K) at 1273 K. This material was chosen for its mechanical resilience at high temperatures and machinability.

Hot rolled steel was used for surrounding structural support of the die because of its lower cost compared to cold rolled steel. Since the hot rolled plates were at the very bottom and top of the heating die, they were insulated from the monolith and were unlikely to experience temperatures greater than 573 K.

2.2.3 Electrical Design

As detailed in Section 2.2.1 the steady state power consumption of the die was estimated to be 19.4kW, so the electrical configuration was chosen to supply at least 20 kW. The heating die prototype used silicon carbide heaters for their relatively low cost and high temperature performance. Gas fire heating and magnetic induction were considered as heating options, but they were ultimately not chosen to avoid large capital costs and complex designs [15]. In terms of other heater options, most cartridge heaters cannot reach the required die operating temperature (>1273

K), and molybdenum disilicide ($MoSi_2$) heaters required complex electrical configurations while having the additional complication of sagging at high temperatures.

The main issue surrounding the silicon carbide heaters used in the prototype concerned their fracture during operation. The thin spiral body of the heaters proved to be fragile and easily fractured due to pressure from thermal expansion of its surroundings or improper handling. In selecting the elements it was of upmost importance to use elements that could withstand transport by forklift and the stresses induced by operation. Another major criteria was using elements that minimized the space used by the die, given the space constraints discussed in Section 2.1. This lead to the decision to use multiple "U-leg" silicon carbide Starbars®, shown in Figure 18. The shape of these elements allowed an electrical configuration that was only necessary on one side of the monolith, and boasted a more durable design than previously used elements.

The electrical configuration designed using these elements is shown in Appendix A, comprising 12 U-leg heaters. Subsequent complications with the electrical system of the press led to multiple reconfigurations that finally converged onto the electrical design shown in Appendix B.

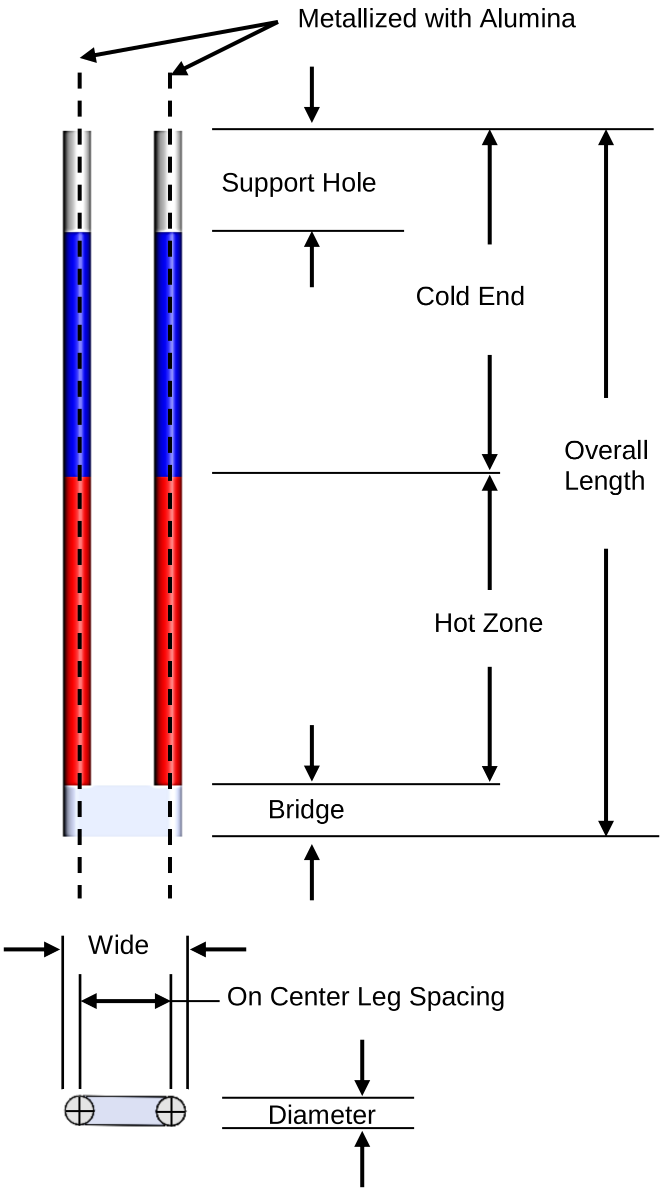

Figure 18: U-multiple leg Starbar® heater [40]

This final configuration, shown in Figure 19, used 8 U-leg heating elements and 8 straight heating elements, which, when combined, dissipated 16.5kW at a nominal current of 14A. This resulted in a warm up period of 5.5 hours, based on the FEM model. The straight heating elements complicated the operation of the die, as they had spiral bodies prone to fracture. This modification required extreme care when transporting the die, as well as alterations to the casing surrounding the elements to prevent the likelihood of them breaking during handling.

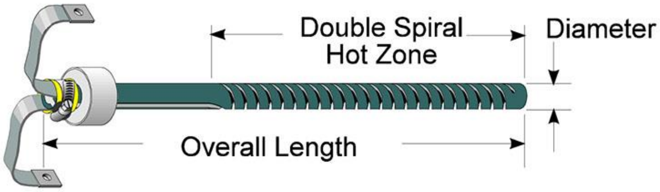

Figure 19: Straight silicon carbide elements used in final electrical configuration

One reoccurring problem encountered with the prototype involved the elements short-circuiting by making contact with the die via fracture or dislocation by thermal expansion of the monolith. The prototype used rigid ceramic RSLE rings to electrically-isolate the heaters from the monolith body, however since the monolith expands and deforms as it is heated, the ceramic rings imposed stresses on the heating elements and caused them to fracture. To prevent these problems, 10 mm of clearance was designed for the element holes in the semi-industrial sized die, and different insulators were investigated.

The configuration used to electrically-insulate the heaters is a combination of RSLE 57 rings and ASPA-1 refractory sheet. The refractory sheet is an electrically-insulating, high-temperature ceramic that is available in various thicknesses and is flexible enough to surround the elements. RSLE 57 crescents were used on either end of the heaters to provide structural support, while the insulation paper ensured any expansion by the die did not result in electrical contact. The structural support by the crescents was an additional measure used because the paper slowly dehydrated if it remained in contact with the heaters at operating temperatures. As shown in Figure 20, the element holes were lined with the refractory sheet, and the ceramic rings ensured minimal contact between the heaters and refractory sheet while allowing for movement of the heaters due to thermal expansion of the die.

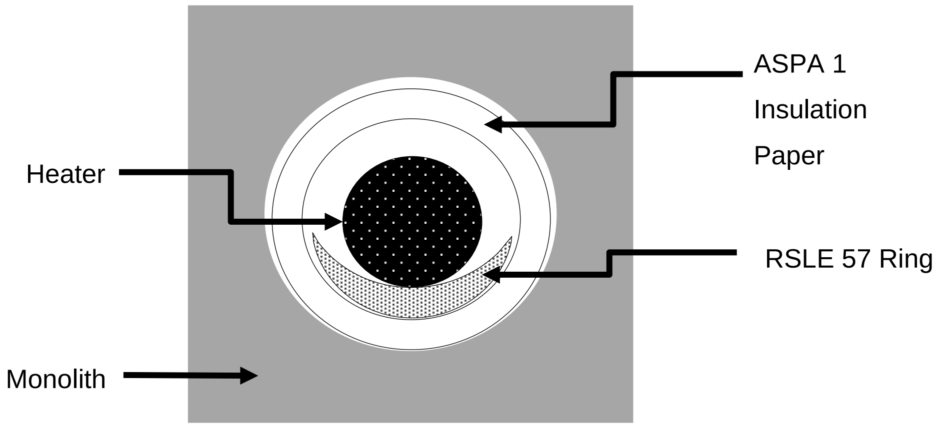

Figure 20: Insulation around heaters in monolith

2.2.4 Final Design

2.2.4.1 Monolith

The heating die was designed to use approximately half of the available press area, as the quenching die was expected to take the remaining space. The monolith was fitted with 24 holes to accommodate the initial design of 12 U-leg resistance elements, 6 holes for ejector pins, 4 holes for thermocouples, 4 holes for fastening the monolith to the baseplate of the bottom die, 2 holes for electrical grounding, and 4 holes for overhead crane transportation. The layout of the monolith resembles that of the prototype, with a bed of elements and side tabs for ease of transport and fastening. The thermocouples embedded in the die were located between element holes in the configuration shown in Figure 21. These locations were chosen to monitor the temperature of the die along its length. Four thermocouples were chosen so that, in the event a thermocouple malfunctioned, the die could still be operated with the remaining three sensors. High temperature Inconel sheathed thermocouples rated for 1473 K were used.

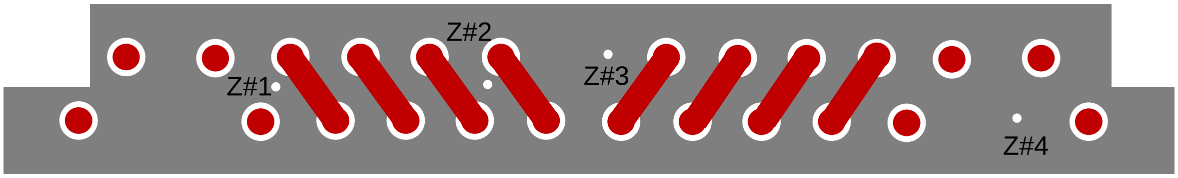

Figure 21: Die thermocouple locations

A finite element analysis was carried out to investigate thermal expansion, surface temperature uniformity, and local stresses in the die. The closer the elements were spaced together, the more uniform the surface temperature of the die would be. Spacing the elements too close would compromise the structural integrity of the die, however, because the thickness between the holes would be insufficient to bear the force of the press.

The FEM simulation verified that the minimum thickness (11 mm) between the element holes was capable of withstanding the maximum pressure used with the prototype, with a safety factor of 6. Design for a system with smoothly applied loads recommends a safety factor of between 2 and 4 [41], the overdesign for a safety factor of 6 allowed for future experimentation with higher pressures if desired while still remaining in a suitable range for the safety factor.

The ends of the die experienced the greatest heat loss so the heating elements with the higher resistance were placed on the ends to minimize these effects and optimize surface temperature uniformity. Based on the simulation, this difference in temperature required that some areas be well above 1273 K to ensure that the ‘cooler’ middle region of the die were at least at 1273 K during operation. Given that the austenite formation kinetics are dependent on the heating rate of the material, the ‘coldest’ regions of the die would be the determining factor for how long a blank needed to remain in the heating die for uniform austenitization.

The die was insulated with 50.8 mm (2”) of RSLE 57 on all sides, and the bottom. The top of the die is exposed when opened and insulated by a 50.8 mm slab of RSLE 57, fastened to the top component of the die. The portion of the elements that extended beyond the die was surrounded by ¾ inch Zircal 95 sheets with holes drilled into them so that the electrical components connecting to the heaters would not overheat. The monolith was fastened to the baseplate of the die by 150 mm M14 bolts however the holes used were made with a clearance of 4 mm to accommodate thermal expansion. Detailed CAD drawings of the monolith can be found in Appendix C.

2.2.4.2 Ejector Pins

Ejector pins were designed to lift the blank off of the die surface after heat treatment because the Al-Si coating was expected to melt, causing the blank to adhere to the striking surface. The pins also provided a simple means for the transfer mechanism to grasp the blank from the heating die, and were planned to be used to conduct a contact/radiation heating technique used by Ploshikhin [19]. The pins were made from an RA 310 rods in order to withstand the high temperatures experienced in the monolith. The pins rested on a concealed plate below the monolith which was supported by springs; the springs chosen had a compression length of 2 cm, along with a compressive force capable of supporting 6 kg, and were heat and corrosion resistant. In the open position the springs were uncompressed and the pins extended beyond the tailoring plate by 10 mm. When the die was closed the weight of the top die components compressed the springs through the pins and they became flush with the tailoring surface, shown in Figure 22.

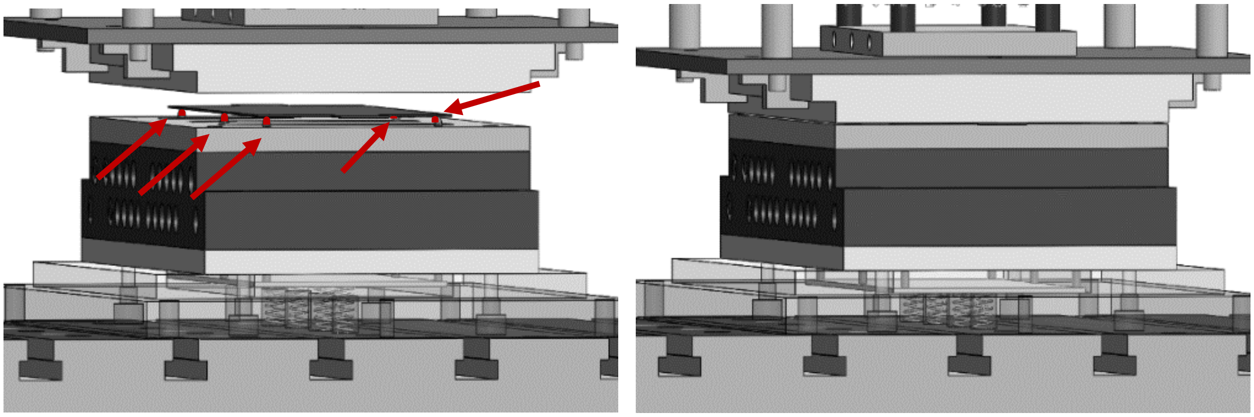

(a) Open die

(b) Closed die

Figure 22: Ejector pins (red) in die opened and closed

The first design for the ejector pins used cushion rods to push the moving plate instead of springs. The cushion rods were embedded in the press bolster and controlled by the press user interface to life or lower objects on the press surface. The use of these pins offered precise movement of the plate so that the ejector pins would lift uniformly, but programming the motion of the cushion rods into the operation cycle proved to be too complex for execution and was ultimately not used.

Initial testing found that the monolith expanded such that the alignment holes between the monolith and insulation no longer coincided. This caused the pins to warp as shown in Figure 23. The insulation holes were opened to accommodate the thermal expansion experienced by the monolith. Unfortunately, further complications were encountered with the moving plate and springs that could not be addressed in the timeframe of this work. An alternative system was designed for manual transfer of the blank and is discussed in Chapter 4. The grippers of the transfer system were altered to accommodate the malfunctioning pins, as described in Section 2.4.

Figure 23: Warped ejector pins

2.2.4.3 Nitrogen Springs

The force exerted by the press onto the die was maintained below 15 kN by use of nitrogen springs. Whilst high contact pressures encourage heat transfer between the blank and striking surface through a reduction in contact resistance [42], the force used was maintained at the lower spectrum of applied loads to reduce the adhesion of the blank to the die surface, which was shown to be most pronounced for high applied loads in the prototype phase [15]. The nitrogen springs were mounted to the top part of the die to absorb the load with a pressure gauge. It was noticed that the nitrogen spring temperature exceeded their recommended operating range (323 K) after the first test run, so a cooling block was constructed and attached to the upper die as shown in Figure 24. The cooling block was intermittently run during experiments so as not to significantly hinder the heat-up time of the die while keeping the nitrogen spring temperature below 323 K.

Figure 24: Cooling block and nitrogen springs installed in upper die

2.2.4.4 Tailoring Surface (Interchangeable Striking Surface)

The tailoring plate was designed with three shielded regions made of RSLE 57. The shielded regions are constructed by removing an entire rectangle of material in the plate and replacing it with RSLE 57. Three different widths were used: 20 mm; 50 mm; and 60 mm. These values were chosen as lower and upper limits of the thickness used in the prototype and were used to better understand the axial conduction limitations for tailoring.

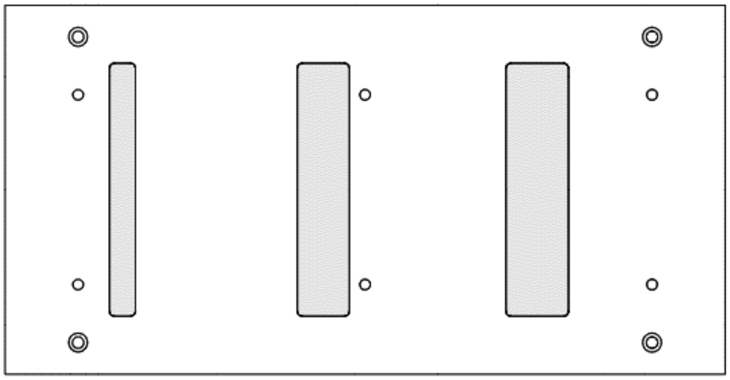

Figure 25: Tailoring plate with three shielded areas

2.3 Quenching Die Design

A flat quenching die was designed through collaboration with Mr. Mike D'Souza of F&P Manufacturing Inc., with the objective of demonstrating the feasibility of forming martensite and tailoring. The die is shown in Figure 26 and this design was chosen to minimize the complexity of the experiment well as serve as an interchangeable structural frame for a U-channel forming die for future work.

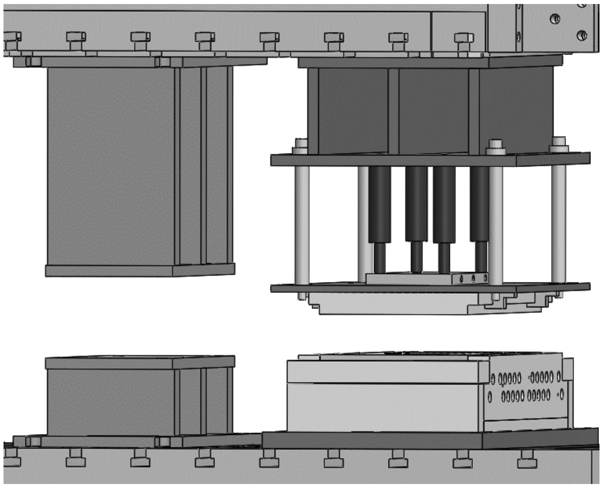

Figure 26: CAD of quenching die (left) in press with heating die (right)

The quenching die was designed with thick plates as the contact surfaces for the blanks; this ensured the blanks had a high quenching rate due to the comparably larger thermal mass of the quenching die. To quantify how many blanks could be cooled successively, an FEM model was run in COMSOL in which a blank initially at 1273 K comes into contact with the quenching die for two minutes and is then immediately replaced with a new blank at 1273 K. This simulation therefore did not account for a cooling period for the quenching die between blank quenching. The temperature histories presented are from three points along the length of the blank halfway through its thickness. Figure 27 shows that the quenching die can be used for a nonstop succession of 4 blanks before the blank cooling rate becomes too slow to produce a fully martensitic microstructure. Figure 28 shows the martensite start line (M_S), martensite finish line (M_F), bainite start line (B_S) and bainite finish line (B_F) provided by ArcelorMittal and taken from the work of Bardelcik [43]. The 30 K/s quenching rate of a Gleeble sample presented by Bardelcik [43] was superimposed on the start and finish lines to get a conservative estimate for the martensite finish temperature expected in the blanks during quenching.

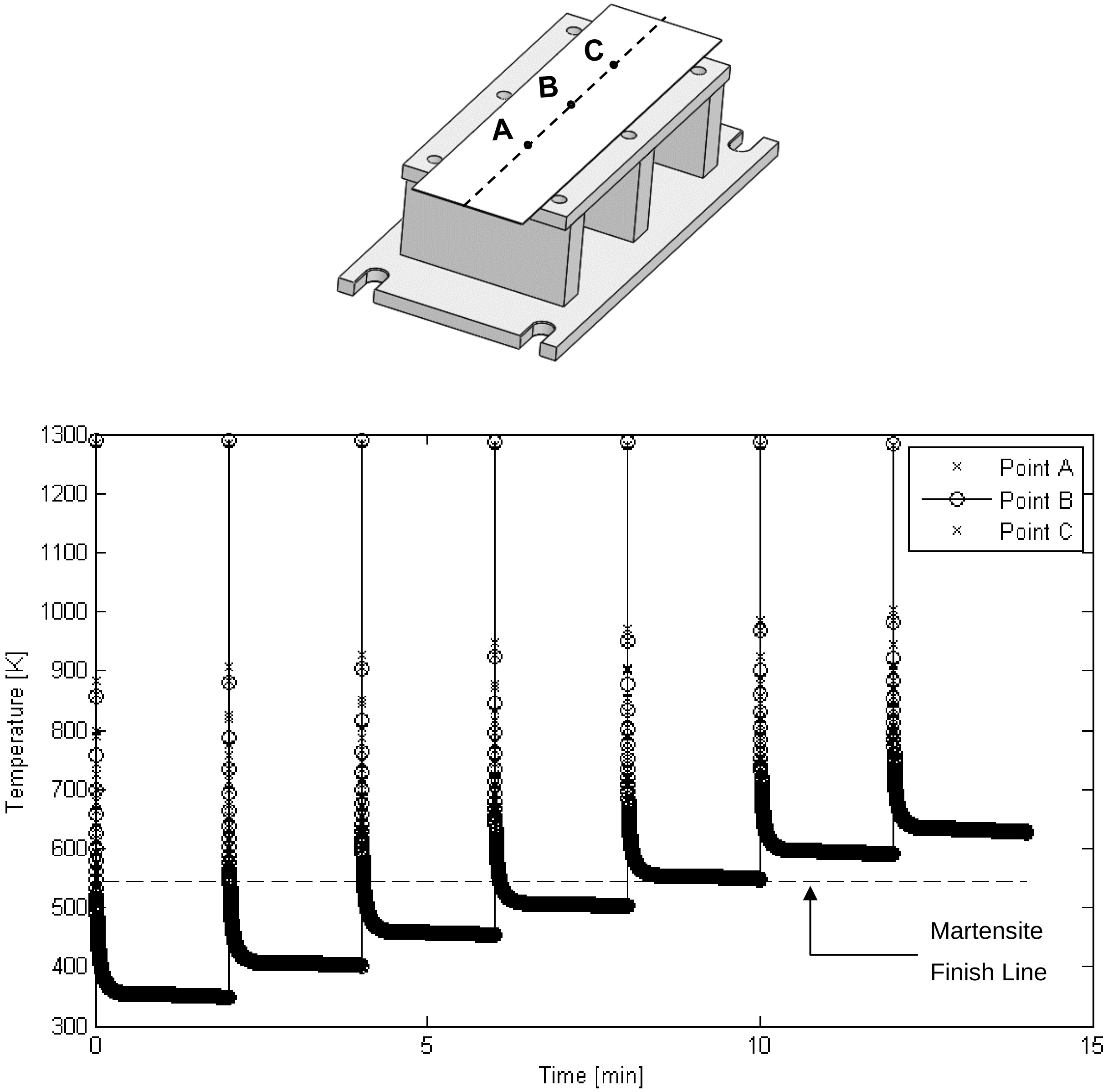

Figure 27: Subsequent blank cooling curves in quenching die

The results from the simulation, in Figure 27, indicate that the die would be sufficient in its cooling capacity for the scope of this work. The points A, B, and C in Figure 27 have temperature curves that are indiscernible, suggesting that heat transfer from the blank to the die can be modelled as one dimensional. If the quenching die was required to cool more blanks, or was installed into a setup that required a longer operation time, a cooling block could be attached to the bottom of the quenching die to ensure that a sufficiently high cooling blank was produced so as to ensure a fully-martensitic blank.

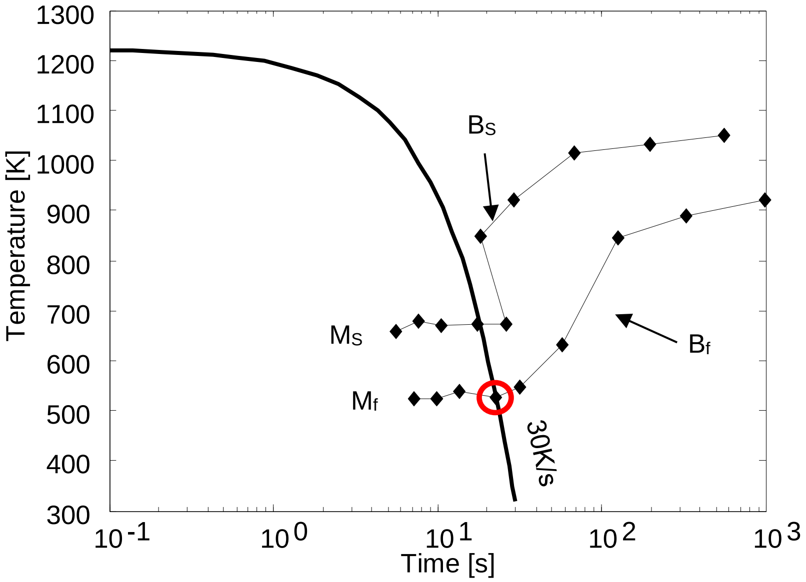

Figure 28: Continuous cooling transformation diagram for 22MnB5 [43]

The quenching die was designed to be lower than the heating die by 22 mm so that if the blank sagged due to high temperatures, the automated transfer system could still successfully mount the blank into position for quenching. The difference in height between the two dies was 12 mm, while the height difference between the ejector pins and heating die surface was 10 mm.

Spool retainers were installed on the heating die to compress the top components of the heating die and ensure the quenching die could close completely, given it was not at the same height as the heating die. Figure 29 shows the compression achieved through the spool retainers.

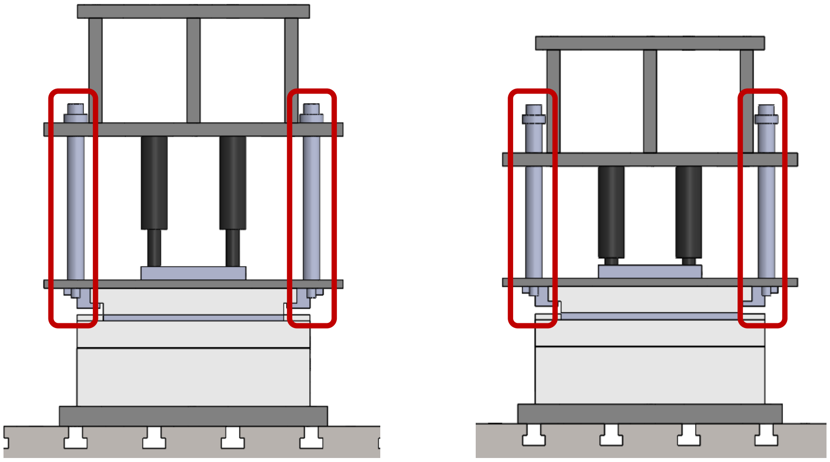

Figure 29: Compression stroke of heating die with spool retainers, circled in red

After the cooling block was installed it was discovered that it reduced the compression stroke of the heating die. This was compensated for by using blocks between the press punch and top of the quenching die.

2.4 Transfer System Design

Fourth year mechanical engineering students at the University of Waterloo, Alex Wigle, Ben Sincennes, Dalton Crosswell, and Evan Waugh, expressed interest in collaborating with Professor Kyle Daun to supervise and guide their capstone design (ME481/482) project. As per Professor Daun’s recommendation, the students were partnered with this research work and assigned to design and build the transfer mechanism.

The final design of the transfer mechanism used pneumatics to drive a pair of grippers along a track to move the blank into and out of the heated die. The system moved from left to right and the only motion in the vertical direction was by the closing of the grippers as they released or gripped the blank, a distance of 4 mm. The system can be seen on the front and back of the press in Figure 30.

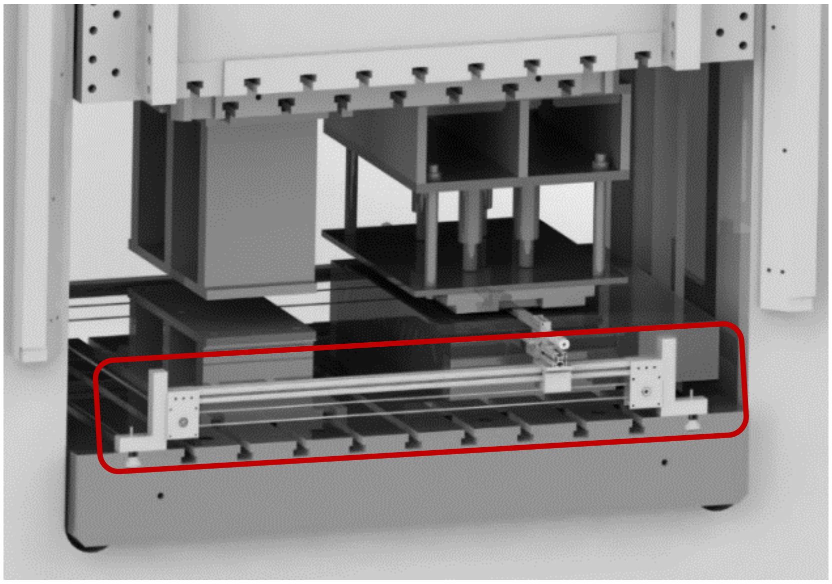

Figure 30: CAD of transfer system (circled in red), quenching die, and heating die

The transfer system was designed to load the blanks into the heating die and transfer the hot blank from the heating die to the quenching die. Due to the limited space in the press the quenching die was chosen as the loading start point for the blanks. Since the quenching die was designed to be lower than the heating die and the transfer system had limited vertical motion, a mobile platform was design to augment the difference in height. The platform could easily be moved onto and off of the quenching die manually and was key to the loading stage of the blank by the transfer system into the heating die.

A manual way of transferring the heated blank into the quenching die was developed as a contingency plan in the event the transfer system failed to operate. This was executed by a long “shovel” that pushed the blank from the heating die, over a bridge between the dies, and onto the quenching die.

The grippers were altered to have a ‘lip’ that lifts the blank and a hook that pushes the blank so that the combined forces overcome sticking and friction between the blank and die surface. Since the pins could not be modified to work during the timeframe allocated for this work, the ‘lip’ served to overcome the height difference between the blank and grippers caused by the absence of the pins. Figure 31 shows these alterations highlighted in red.

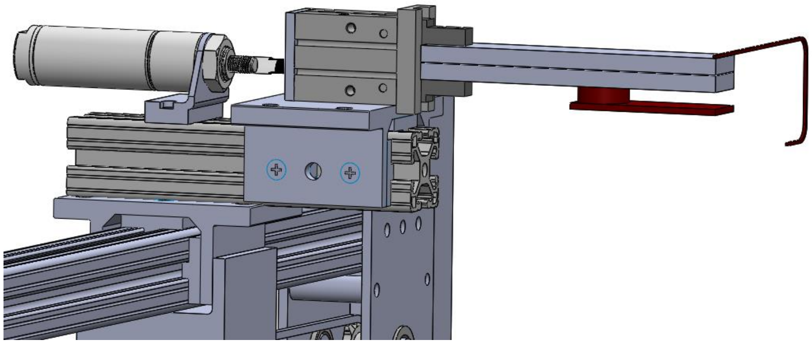

Figure 31: Transfer mechanism gripper adjustments, in red

2.5 Design of Die Heat Transfer Models

The data presented in Section 3.3.2 and Chapter 5 are based on models developed using COMSOL Multiphysics finite element analysis software. These models were used to predict design outcomes and were improved and validated by experimental results. Given the nature of this project the analysis conducted in COMSOL was chosen as time-dependent. The temperature distribution is governed by the heat equation

$$\frac{\rho c_p \partial T}{\partial t} = \nabla \cdot (k \nabla T) + Q \tag{10}$$

To model the heating die the geometries and assembly of the monolith, heating elements, insulation, press bolster, and top insulation of the top die were used to build a virtual representation that would model the thermal stresses, solid heat transfer, surface-to-surface radiation, and solid mechanics expected of the heating die. The exposed surfaces were modelled with radiation and natural convection boundary conditions and the insulation was assumed to be in thermal contact with the heating monolith. The thermal conductivity, density, specific heat capacity, and emissivity were obtained from the suppliers Rolled Alloys, Zircar, and Metal Supermarket, for RA330, RSLE 57 and the structural steel, respectively. The press bolster was modelled as stainless steel with the properties ρ=7850 kg/m^3, k= 45 W/(m·K), c_p=475 J/(kg·K), and ε=0.8 [36]. A grid refinement study showed that the temperature field became grid-independent using 104,764 elements, which was the level of refinement used for the following analysis. To reduce computing time half of the die was modelled using a symmetry boundary condition, shown in Figure 32.

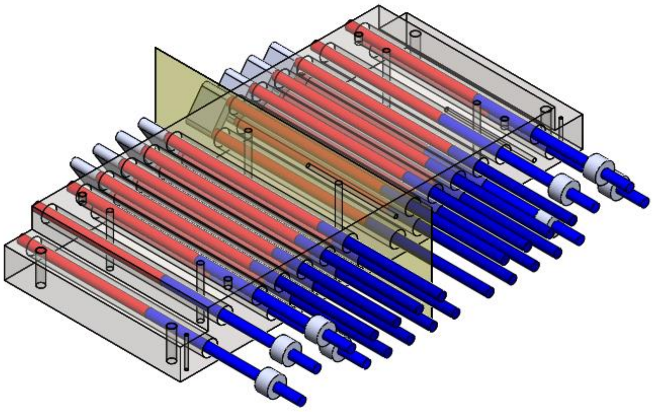

Figure 32: Heating die showing heater locations with hot zones (red) and cold zones (blue) and plane of symmetry (yellow)

A Neumann (heat flux) boundary condition was specified over the red areas depicted in Figure 32. The heat flux specified was dependent on the element used, and was calculated using the current running through the heaters, voltage, and heater electrical resistance. As discussed in Section 2.2.3, the electrical configuration consisted of two heater types: one with a nominal resistance of 6.57 ohms and the other with 4.34 ohms. An expected current of 13.75 amperes was suppled to each electrical zone with a voltage of 600 volts. The heat flux calculations used are as follows:

U-element:

$$heat\ flux\ per\ element\ =\ I^2R = (13.75A)^2(4.34\Omega) = 820.5W \tag{11}$$

Straight element:

$$heat\ flux\ per\ element, P =\ I^2R = (13.75A)^2(6.57\Omega) = 1242.1W \tag{12}$$

The resistance used in the above calculation assumed the heaters operated at the nominal operating temperature of 1344 K.

The insulation and structural steels were modelled to be in thermal contact with the die, radiation from all surfaces was included.

The results from the heating die model were saved and used as initial conditions for the blank model. In the blank model a 2 mm thick rectangle with the material properties of Usibor® 1500P was used to represent the blank and inserted into the previous model with the heating die. The temperature history of the simulation plane corresponding to the blank midplane was saved and used as an input for the tailoring model.

The quenching die model was implemented separately from the heating die model. The quenching die was built in COMSOL Multiphysics® according to the Solidworks® assembly provided by F&P. The goal of this model was to investigate how many successive blanks could be quenched by the die until it was too warm to cool a blank to martensitic composition. To simulate the subsequent quenching of blanks, the temperature profile of the die after quenching a blank was saved and used as the initial conditions for the following simulation. The quenching die was modelled to have the material properties of stainless steel (ρ= 7850 kg/m^3, c_p= 475 kJ/kg·K, k=45W/m·K, and ε=0.8) [36]. Heat transfer to the surroundings by radiation was modelled for the quenching die surfaces, except for the two surfaces that directly quenched the blank since the die was minimally open during operation.

Chapter 3
Tailoring Model

The tailoring model presented in this chapter relies on the input from two submodels. The first is the blank heating model computed in COMSOL®, discussed in Section 2.5, which provides the thickness mid-plane temperature field of the blank during heating. The second submodel predicts the austenite kinetics based on the temperature history of the material. Combined, these models were used to predict the phase composition along the blank mid-plane during simulated time of the blank heating process. The austenite kinetics are examined in the chapter and kinetics models are investigated for their ability to predict phase transformation curves derived from experimentally determined dilatometry results.

3.1 Literature Review

3.1.1 Austenite Transformation

Due to a lack of literature on austenite transformation in 22MnB5 steel, the kinetics of dual phase steels, which are similar in chemical composition and have been studied more extensively, will be discussed. Austenite formation can be described in two steps: the first is the transformation of carbon saturate pearlite phases to high-carbon austenite; and the second step is the dissolution of ferrite matrix into the austenite growth sites. Figure 33 illustrates how austenite transformation takes place via three stages within dual phase steel during inter-critical annealing in a one-dimensional scenario.

In Step 1, the austenite nucleation begins at the pearlite/ferrite boundary, or cementite particle/ferrite grain boundaries depending on the initial microstructure, which is followed by the dissolution of carbon rich pearlite and subsequent growth of austenite. In this process the amount of alloying elements present affects the rate of pearlite dissolution and the final austenite fraction. Higher carbon steels were demonstrated by Spiech *et al.* [44] to exhibit a much slower pearlite dissolution rate at the same temperature, due to the increased activation energy needed for diffusion in high carbon steels. Step 2a represents the growth of austenite into the surrounding ferrite matrix to achieve equilibrium volume fraction, and Step 2b follows with the diffusion of manganese at the outer rims of austenite islands to form enriched manganese zones. Step 3 finishes with the slow diffusion of enriched manganese rims into the austenite phase.

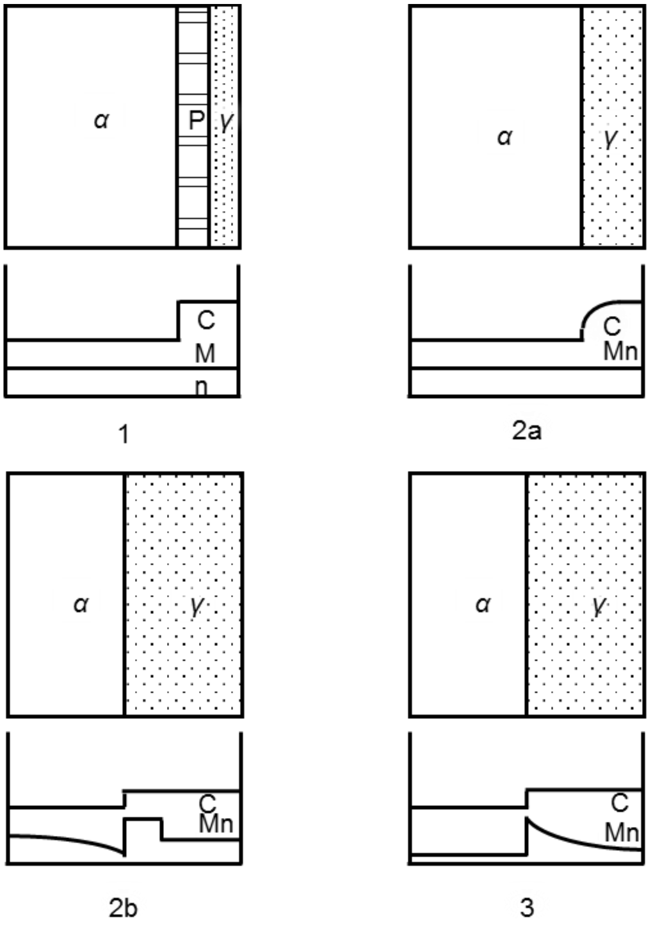

Figure 33: Austenite growth schematics: 1. Dissolution of pearlite; 2a. Austenite growth with carbon diffusion in austenite; 2b. Austenite growth with manganese diffusion in ferrite; 3. Final equilibration with manganese diffusion in austenite [44]

When the 22MnB5 steel is heated to Ac3 the austenite transformation progresses completely into the ferrite matrix to the point where there the steel is completely austenitized. While the physical process of austenite formation is mostly understood, few kinetics models of this process have been proposed in the literature.

3.1.2 Austenite Kinetics Modelling

Datta and Gokhale [45] used quantitative metallography during isothermal austenite formation from pearlite and ferrite aggregates, to show that the radial growth of the austenite particles was proportional to the square root of elapsed time at temperatures between 1073 K and 1113 K, which suggests that the formation is diffusion controlled. They found that at 1143 K the kinetics were different such that the radial growth approached a constant value at long times. Roosz *et al.* [46] also used quantitative metallography to study isothermal austenitization of eutectoid steel between 1003 K and 1018 K and determined activation energies for the nucleation and growth with respect to temperatures above Ac1.

These two approaches were later combined by Caballero *et al.* [47] to model non-isothermal austenite formation in ferrite and pearlite with a constant heating rate. The Avrami kinetics model describes the solid transformation from one phase to another at constant temperature. It was used to predict pearlite dissolution and austenite growth with independent equations that determined nucleation and austenite growth rate as a function of overheating (above Ac1). Constants of the Avrami equation derived by Roosz *et al.* [46], were used in the aforementioned model.

Nath *et al.* [48] investigated non-isothermal austenization of various plain carbon steels using differential scanning calorimetry (DSC) by for steel processing applications. The activation energy associated with the pearlite dissolution DSC peak was determined by using a modified Kissinger approach [49].

The entire austenitization of dual phase steel was modelled using an Avrami equation by Kulakov *et al.* [50]- [51]. A Gleeble thermo-mechanical simulator was used to produce dilatometry data of dual-phase steel samples that underwent non-isothermal and constant heating rates of 1 K/s, 10 K/s, and 100 K/s. These results led to the conclusion that the austenization process observed was independent of heating rate.

3.2 Testing Methodology

Phase transformation kinetics can be monitored through a variety of procedures. One possible procedure is calorimetry. During phase transformation the energy released by the system is unique and measureable [52]. These measurements are used to predict the transformation fraction of the system.

Another technique used is dilatometry, which correlates the dilation of a sample being heated with the phase transformation fraction in the material [53]. This is possible because the crystalline structures of the phases have unique molar volumes that are distinguishable through minute dimensional measurements. The measurement technique used for this work was by dilatometry, using C-gage measurements on dog-bone samples heated in the Gleeble thermomechanical simulator.

The steel samples were procured from ArcelorMittal and had an initial thickness of 2 mm and a nominal chemical composition shown in Table 1. The Usibor® 1500P steel used for testing was machined to the geometry shown in Figure 34 and stripped of the Al-Si layer (about 20 μm) by soaking the samples in a sodium hydroxide solution. The geometry shown in Figure 34 was based on the geometry used by Chester *et al.* [54].

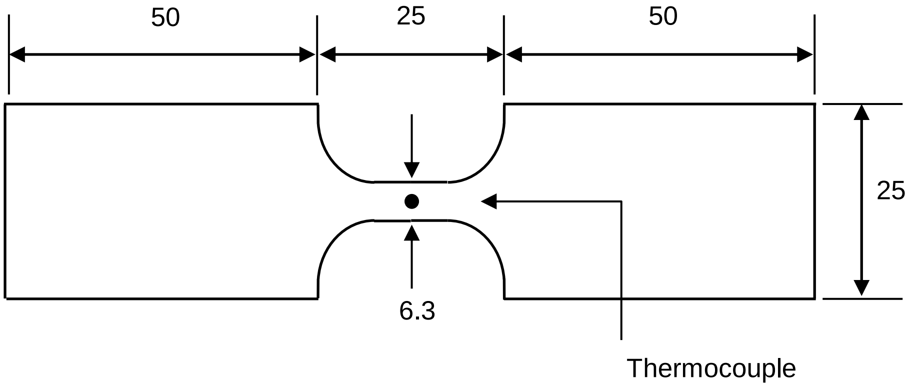

Figure 34: Sample geometry for Gleeble dilatometry tests [54]

The samples were machined such that the long axis of the sample was aligned parallel to the rolling direction of the sheet. Temperature measurements were used to monitor and control the sample temperature; these measurements were taken with a K-type thermocouple that was spot-welded to the center of the sample. The heating rate was fixed at 5 K/s between the temperatures of 298 K and 773 K, and then changed to a heating rate between the range of 1 K/s and 20 K/s from 773 K to 1373 K, after heating the sample was allowed to air cool. Dilation was measured with a c-gauge dilatometer and recorded.

3.3 Austenization Kinetics Model

The dilatometry measurements were recorded during the austenite transformation of the material. The phase fraction of austenite was then inferred using a lever-type rule similar to the one used by Huang *et al.* [55],

$$\alpha_{exp} = \left|\frac{dL_1}{dL_1 + dL_2}\right| \tag{13}$$

In this work, the term α_{exp} refers to the phase fraction of austenite determined from experimental data using Eq. (13). The quantities dL_1 and dL_2 are depicted in Figure 35; dL_1 is the difference between the expected dilation corresponding to *slope 1* and the recorded dilation at a given temperature. dL_2 is the difference between the recorded dilation and the expected dilation according to *slope 2* at a given temperature.

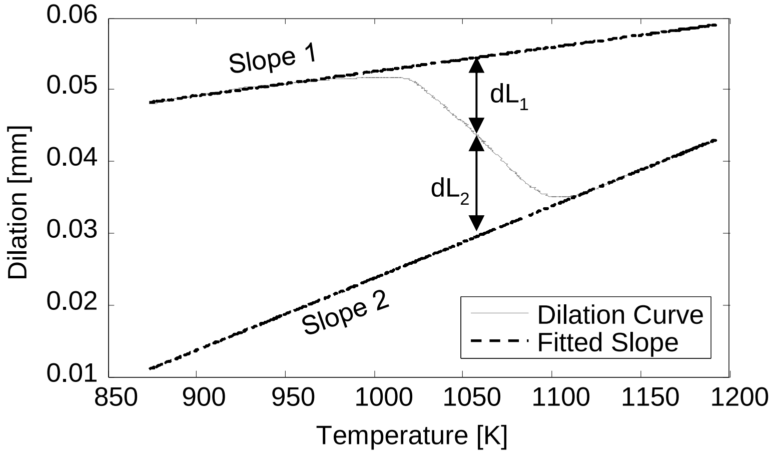

Figure 35: Lever rule approach for determining α_{exp}

The process of identifying slope 1, slope 2, Ac1, and Ac3 was automated. The first two terms were calculated using dilation measurements that corresponded to specific temperatures that are listed in Table 3, and the last two terms were calculated using the first derivative of the dilation curve. These identification points are described in Table 3 and Figure 36.

Table 3: Terms used in automated process for identifying Ac1 and Ac3 points

Feature	Identification method
Point 1	First point for slope1 (873 K)
Point 2	Second point for slope1 (973 K)
Point 3	Lower bound for Ac3 range (1073 K)
Point 4	Upper bound for Ac3 range (1193 K)
Point 5 (Ac1)	Point where first derivative crosses zero line
Point 6 (Ac3)	Point where first derivative crosses zero line
Slope 1	Polyfit between point 1 and point 2
Slope 2	Polyfit between point 6 and point 4

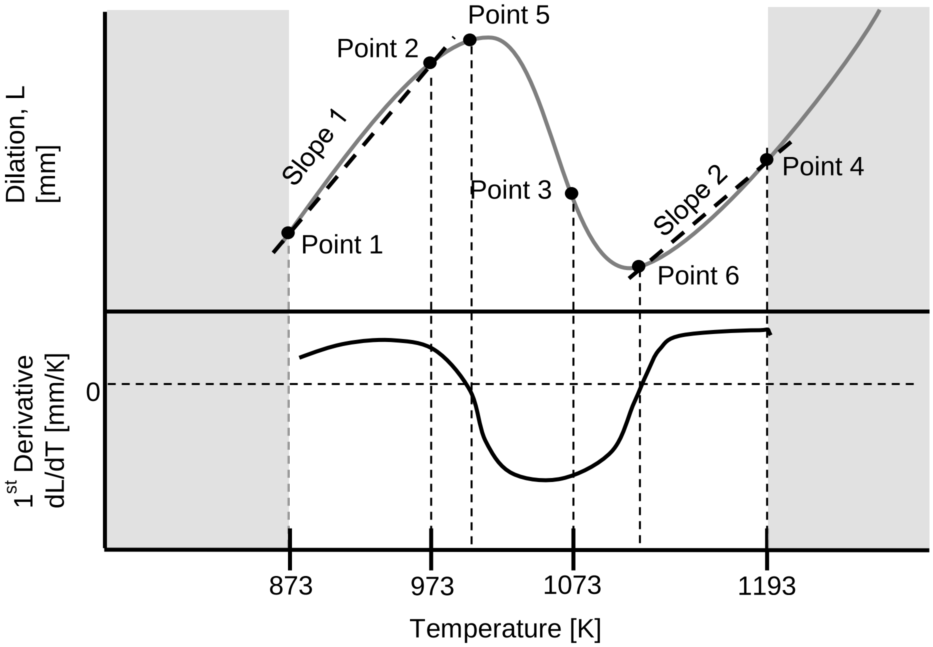

Figure 36: Schematic diagram of terms used in automatic Ac1 and Ac3 identification process

The ASTM A1033-10 standard [56] for determining Ac1 and Ac3 uses the slope of the dilation curve to identify these points, but it does not define a robust procedure for identifying the onset of austenite formation and complete transformation of the material into austenite. The Ac1 and Ac3 temperatures calculated for 26 tests with varying heating rates is presented in Figure 37. The range exhibited for the Ac1 and Ac3 temperatures had a maximum of 20 K difference with the average, demonstrating the importance of multiple test repeats during dilatometry experiments.

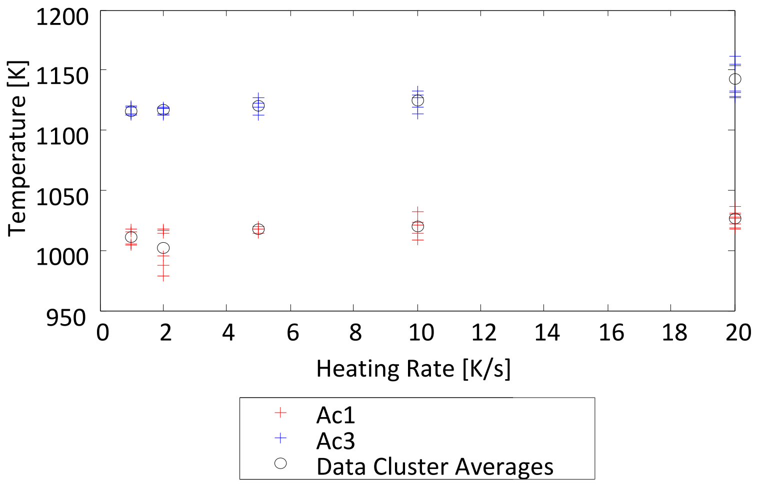

Figure 37: Ac1 and Ac3 temperatures with different heating rates

Empirical relations predicting the Ac1 and Ac3 were summarized by Pawlowski [57]. These relations are based on the chemical composition of the steel, summarized in Table 1. The Ac1 and Ac3 temperatures were calculated using these relations and are listed in Table 4.

Table 4: Predicted Ac1 and Ac3 values using various correlations

Method	Ac1 (K)	Ac3 (K)	Reference
Grange	1002	1094	[58]
K.W. Andrews	1003	1095	[59]
G.T. Eldis	989	1035	[60]
H.P. Hougardy	1009	1120	[60]
O.G. Kasatkin	1005	1115	[61]
J. Trzaska, L.A. Dobrzanski	1011	1109	[62]
Average of Thesis Findings	1012	1124	

The Ac1 and Ac3 values predicted in Figure 37 were within reasonable range of those calculated in Table 4, with values obtained using correlations presented by Hougardy [60], Kasatkin [61], and Trzaska *et al.* [62] being the closest to those found in the present study.

3.3.1 JMAK Model

The kinetics of austenite formation in steel is commonly modelled using the JMAK equation

$$\alpha = 1 - exp(-Kt^n) \tag{14}$$

This equation predicts the process of nucleation and growth of austenite under isothermal conditions. Isotropic behavior of the material is assumed and the term α represents the fraction of austenite phase in the material, *K* is a temperature dependent function, *t* is the elapsed time after overheating (above Ac1), and *n* is the Avrami exponent. Eq. (14) was used with the dilatometry data to establish the transformed phase fraction as a function of time, and therefore temperature. Eq. (15) was rearranged to the form

$$ln\left[ln\left[\frac{1}{1-\alpha_{exp}}\right]\right] = n\, ln[t] + ln[K] \tag{15}$$

and plotted, where the slope of the line and the intercept correspond to the Avrami exponent *n*, and the temperature dependent function *K*, respectively. To solve for the unknown K_0 and E_A values, several dilation curves need to be obtained at different isothermal temperatures and used with

$$K = K_0 e^{-\frac{E_A}{RT}} \tag{16}$$

$$ln[K] = ln[K_0] + \left(-\frac{E_A}{R}\right)\left[\frac{1}{T}\right] \tag{17}$$

K_0 and E_A values were obtained from research articles shown in Table 1. E_A and ln(K_0) values were chosen to be 117.07 kJ/mol and 11.8 respectively, because the corresponding *n* value was the most similar *n* value to what was calculated.

The Avrami exponent, *n*, is dependent on the phase transformation mechanisms and is an indicator of the starting grain structure [63]. It was therefore important to identify previous studies that focused on materials with similar compositions to 22MnB5 and comparable Avrami exponents to ensure that the comparisons were relevant.

The process of pearlite-to-austenite transformation is primarily driven by diffusion of carbon in the steel. The activation energy of carbon diffusion in ferritic (bcc) iron is given as 84 kJ/mol in [64]. The presence of high wt. % Mn in the steel composition contributes to an increased activation energy required for the pearlite to austenite transformation and could explain the higher activation energy seen in Table 1, at 117.07 kJ/mol.

Table 5: JMAK parameters of similar steel compositions [54]

Reference	n	$\ln(K_0)$	E_A [kJ/mol]
[65]	1.45	12.2	117.07
[66]	1.12	11.06	99.91
[67]	1.62	11.63	117.07
[68]	1.9	11.8	117.7

To model the non-isothermal conditions in the experiment, work by Chester *et al.* [54] used Scheil's additivity rule [69],

$$\sum_i \frac{\Delta t_i}{t_i} = 1 \tag{18}$$

which is an approximation that uses a large number of isothermal transformation steps. The term t_i is the time required to transform to a phase fraction, α, isothermally at the current temperature and Δt_i is the time step. This rule is used for isokinetic reactions implying that the phase fraction transformed at a given temperature depends on time and a single function of temperature.

Alternative kinetic models, detailed by Khawam *et al.* [70], were investigated, which included the Avrami-Erofe'eev (Model A4), and First Order Reaction (Model F1). Comparison of these models to experimental results showed that the F1 model, described below, was superior to the JMAK model and A4 model at predicting the austenite kinetics during non-isothermal and constant heating rate and was subsequently used for developing the tailoring model.

3.3.2 Model F1

The F1 model is mathematically equivalent to an Avrami model with the Avrami exponent, *n*, equal to 1. The equation for the F1 model with a constant heating rate β (K/s) is:

$$g(\alpha) = \frac{A}{\beta}\int_{O}^{T}\left(e^{-E_A/RT}\right)dT = -\,ln(1-\alpha) \tag{19}$$

The intermediate term g(α) is initially evaluated by replacing the α term on the right hand side of the equation with the experimentally-calculated phase fraction term, α_{exp}. The unknowns, E_A and *A*, are the activation energy and pre-exponential constant of the reaction. *R* is the universal gas constant, 8.314×10^{-3}kJ/(mol·K) and *T* is the temperature. The terms E_A and *A* are determined by using the Coats-Redfern method [70]

$$ln\left(\frac{g(\alpha)}{T^2}\right) = ln\left(\frac{AR}{\beta E_A}\left[1-\left(\frac{2RT_{exp}}{E_A}\right)\right]\right) - \frac{E_A}{RT} \tag{20}$$

where the temperature integral is approximated using a series expansion and the term T_{exp} is the mean experimental temperature.

By employing the Coats-Redfern method, a linear regression was carried out on $\ln(g(\alpha)/T^2)$ vs 1/T, where the slope represented $-E_A/R$. The activation energy was then used with the first term on the right hand side to find *A*. Limitations of the F1 model, discussed by DiCiano *et al.* [71], concern accuracy at the beginning and ending of the phase transformation process. Complexities due to pearlite dissolution at the onset of austenization and growth reduction due to austenite region impingement at the end of the process are not entirely captured by the F1 model, and subsequently the first and last 10% of the reaction, corresponding to 0.1 to 0.9 austenite phase fraction, were truncated from the regression.

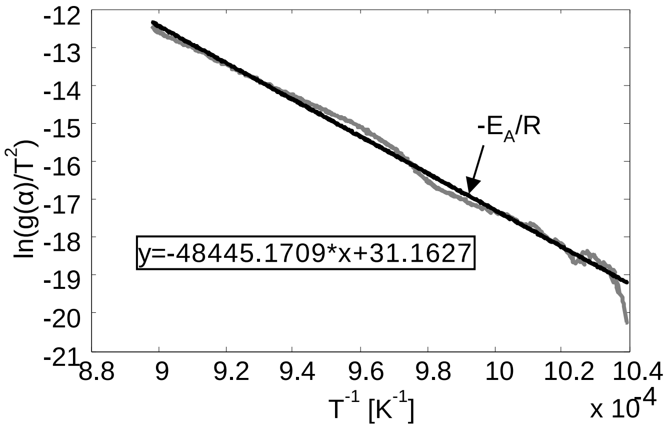

Figure 38: Coats-Redfern method for determining Ea and A for F1 model. Data truncated from fraction austenite of 0.1 to 0.9 for data fitting

The E_A and A terms inferred from the dilatometry measurements carried out at different heating rates are presented in Figure 39. No clear correlation can be seen between both terms and the heating rate, which is consistent with the finding from Kulakov *et al.* [51].

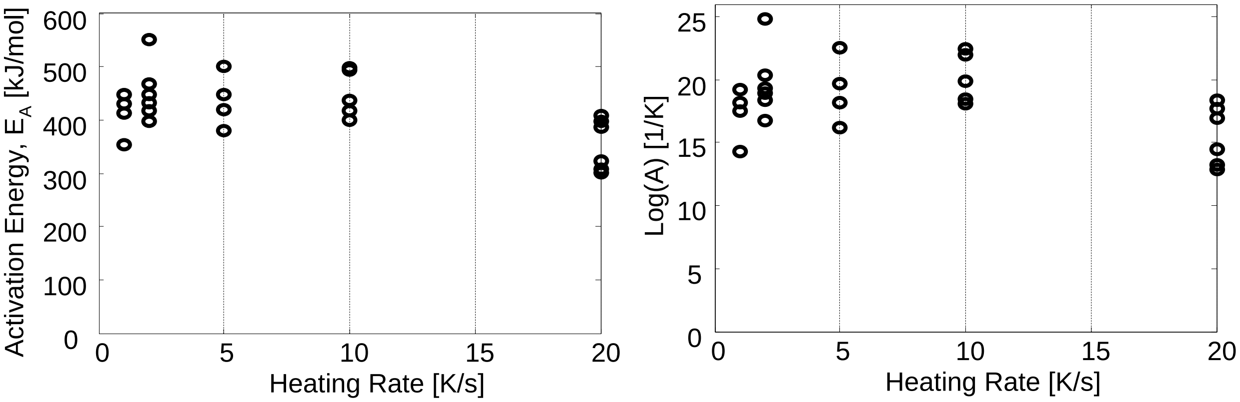

(a) (b)

Figure 39: Calculated Ea (a), and A (b) terms with different constant heating rates

A correlation was presented by DiCiano *et al.* [71] to show that the activation energy and pre-exponential factor have a strong correlation, which may be due in part to the Coats-Redfern fitting method.

The mean values for E_A and *log(A)* were 401.7kJ/mol and 18.4 respectively, and the F1 model was run with these values and compared to experimental results in Figure 40.

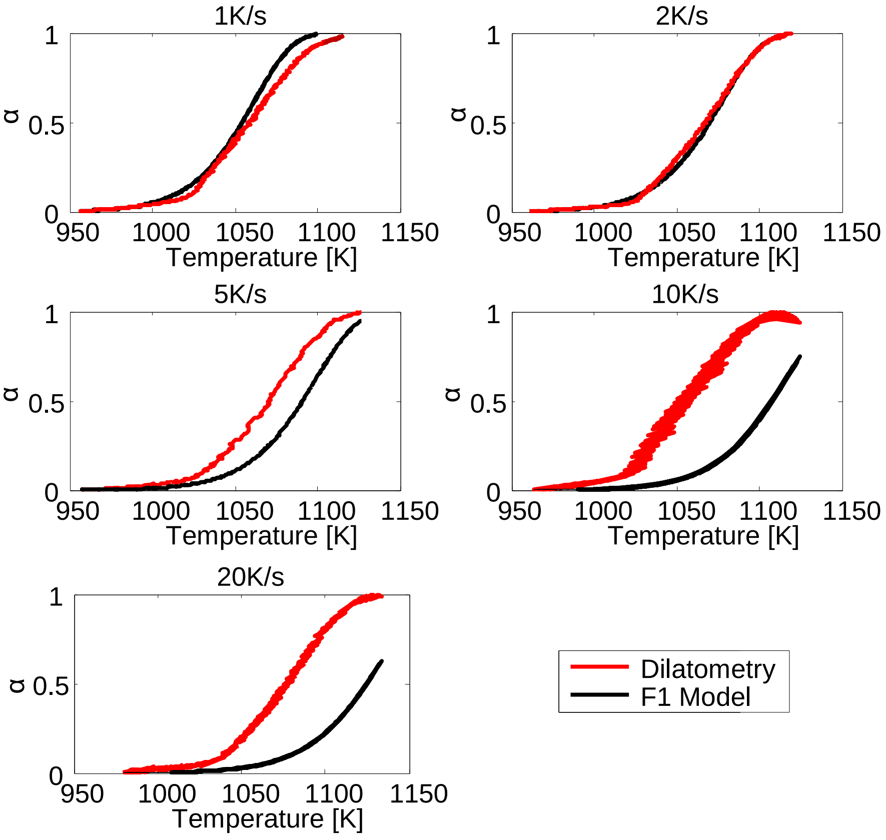

Figure 40: F1 Model predictions vs experimental results for different constant heating rates

The heating rates 10 K/s and 20 K/s can be seen to decrease with higher constant heating rates. This discrepancy can be attributed to the simplifications that are inherent in the F1 model [71], including the combination of the nucleation and growth processes into one activation energy, which are independently represented in work by Roosz *et al.* [46].

The integral expressed in Eq. (19) was modified to account for non-constant heating rates to better model the heating conditions expected in direct contact heating. Vyazovkin recommends [72]

$$g(\alpha) = A\int_0^t exp\left(-\frac{E_A}{RT(t)}\right)dt \tag{21}$$

This change allowed the model to be directly applied to heating rate schedules as dictated by HFDQ heating procedures. The start time was taken as the time at which the material reached the averaged Ac1 temperature for the 1 K/s heating rate.

The modified F1 model was used in the tailoring model with inputs from the heating histories dictated by the blank heating model presented in Section 2.5. Figure 41 shows the model prediction of the microstructure of a blank at the 1 mm thick plane at a hold time of 2 minutes.

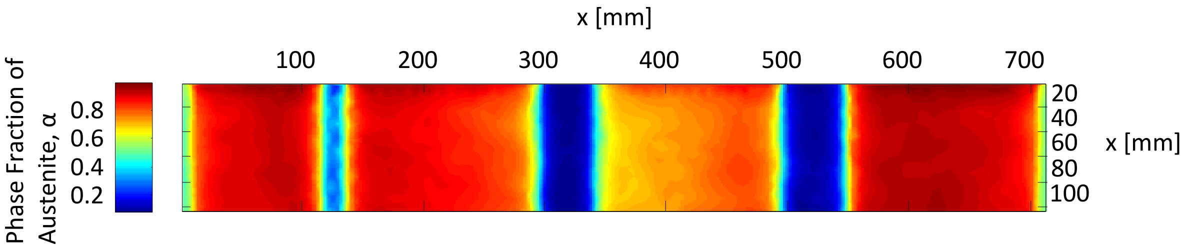

Figure 41: Tailoring Model Prediction of Phase Composition at 1 mm Thick Plane

This model prediction is later compared to experimental results in Chapter 5 to validate the 10 K/s adjusted F1 model as a predictive austenite phase fraction model for direct contact heating. The experimental procedure used to produce the experimental results is detailed in the following chapter.

Chapter 4

Testing Methodology

This chapter covers the experimental testing methodology used to heat the 22MnB5 steel blanks with the experimental apparatus discussed in Chapter 2. The preparations that were performed on the blank before heat treatment, the testing procedure followed during heat treatment, and the analytical techniques conducted on the steel after heat treatment are detailed in this chapter.

4.1 Blank Preparation

The blanks used in this research were 2 mm thick, 203 mm × 711 mm (8″ × 28″) Usibor® 1500P steel sheets. The blank has 38 mm (1.5″) of extra material on each end that serve as tabs for transporting the blank to and from the heating die.

4.1.1 Coating Considerations

Experiments were conducted on blanks without the Al-Fe-Si coating. Initial attempts of removing the coating used NaOH pellets dissolved in water, but this approach proved to be impractical due to the large size of the blanks, and subsequently the large quantity of NaOH solution required. As an alternative, the coating was successfully removed using sandblasting which avoided the formation of an oxide layer, which develops after treatment with NaOH.

Experimentation on blanks with the Al-Fe-Si coating could not be conducted as there was insufficient time to re-design and fix the ejector pins, which were necessary in preventing the coating from adhering to the die surface.

4.1.2 Blank Instrumentation

Measuring the temperature readings of the blank during heat treating required thermocouples that were able to withstand:

1. Temperatures above 1273 K
2. Rough treatment through transferring the blank
3. Contact pressure between the blank surface and die striking surface

In order to prevent the thermocouple from being crushed between the blank and the die, a groove was machined into the blank so that the thermocouple lay flush with the blank surface. Thermocouple “voids” created in the material of interest cause disturbances in the temperature field, which can lead to increased measurement error [73]. To minimize this error the smallest possible thermocouple was chosen. A thermocouple was constructed using two K type perfluoroalkoxy (PFA) insulated single strand wires spot welded to the location of interest; these wires were chosen over a pre-manufactured thermocouple because previous attempts at isolating the wires in sheathed thermocouples proved to be unreliable for diameters below 1 mm. The length of the wires within the blank grooves were exposed to high temperatures (>1173 K) which exceeds the melting temperature of the coating on the wires. This, in turn, could lead to electrical contact between the two thermocouple wires and would constitute alternative junctions, leading to large measurement errors. Measures taken to prevent the coating from melting involved threading the wires through high temperature resistant ceramic tubes and fiber glass sheaths. The measurements from the thermocouples were fed to a data acquisition (DAQ) system connected to a laptop.

4.2 Testing Procedure

The press used for this work was equipped with a user control interface that controlled the vertical motion of the press, and a power supply for the die elements. Thermocouples embedded in the die were connected to the user interface of the press for monitoring, and each thermocouple corresponded to a designated heating region, or “zone” of the heated die. A temperature set-point was allocated to each zone/thermocouple so that the thermocouple reading acted as an input to a PID controller to maintain the specified set-point temperatures.

A cycle was programmed into the press with an opening position, closing position, and idle period so that the heat treatment process was almost completely automated. The procedure was designed in accordance with the standard operation procedure of the press, available in Appendix D.

The testing procedure could be performed manually or automatically. For the manual procedure three personnel were required. The first person was responsible for operating the press and transfer system, the second person was responsible for removing the mobile platform after the transfer system acquired the blank, and the third person was responsible for using the “shovel” to push the heated blank from the heating die to the quenching die. As the third person moved the blank into the quenching die, if resistance was encountered while pushing the blank, the first person was responsible for using tongs (while wearing protective equipment) to jostle the blank to stop it from adhering to the surface. Throughout each step the first person manually operated the opening and closing of the die so that the mobile platform and “shovel” were not crushed during operation.

The automatic procedure required two personnel. The first person was responsible for initiating and monitoring the operation of the press and transfer system, and the second person was responsible for moving the mobile platform after the blank was loaded into the heating die.

The process of quenching in industrial applications typically uses a set of dies to cool and/ or form the blanks at a rate of 27 K/s or greater [4]. This work used a quenching die designed by F&P Manufacturing Inc., as described in Section 3.2.

The original testing matrix dictated that the blanks were to be heat-treated for hold times of 45 seconds, 75 seconds, 120 seconds, and 150 seconds, using the tailored striking surface, and each holding time to be repeated 3 times to produce a total of 12 heat treated blanks. Due to a heater failure on one side of the die, only two tests were conducted at 120s hold time where half of the blanks had usable data.

4.3 Heat Treated Sample Analysis Procedure

In order to evaluate the effect of tailoring during heating, samples were taken from each heat treated blank in locations depicted in Figure 42. The shaded region covering half of the blank represents the area of the blanks that could not be analyzed due to heater failure.

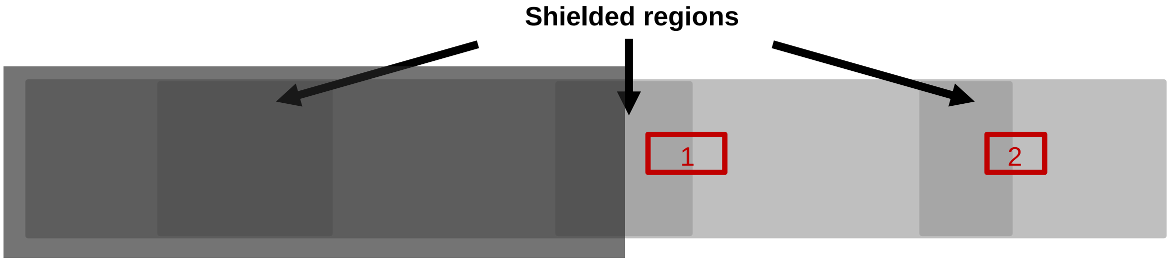

Figure 42: Layout of sample locations from a heat treated blank

Samples 1 and 2 were used for micro-hardness mapping. After each sample was cut to a usable size, they were mounted in a fast drying resin. The samples were then polished using sandpaper starting at 220 grit and ending at 1200 grit. Further polishing was done with a 3 μm diamond suspension which was progressed to a 1 μm colloidal silica suspension.

A Vickers hardness tester was used to produce a micro-hardness map for each sample according to ASTM E384. The tester used a diamond indenter with a load of 1000 grams-force which left a square indent on the sample that was measured with an optical microscope, shown in Figure 43. The lengths measured were then used to calculate the Vickers hardness of the local region by

$$HV = \frac{1854.4F}{d^2} \tag{22}$$

where *F* is the applied force of the indenter in grams-force and d is the average diagonal of the square in microns (μm) [74].

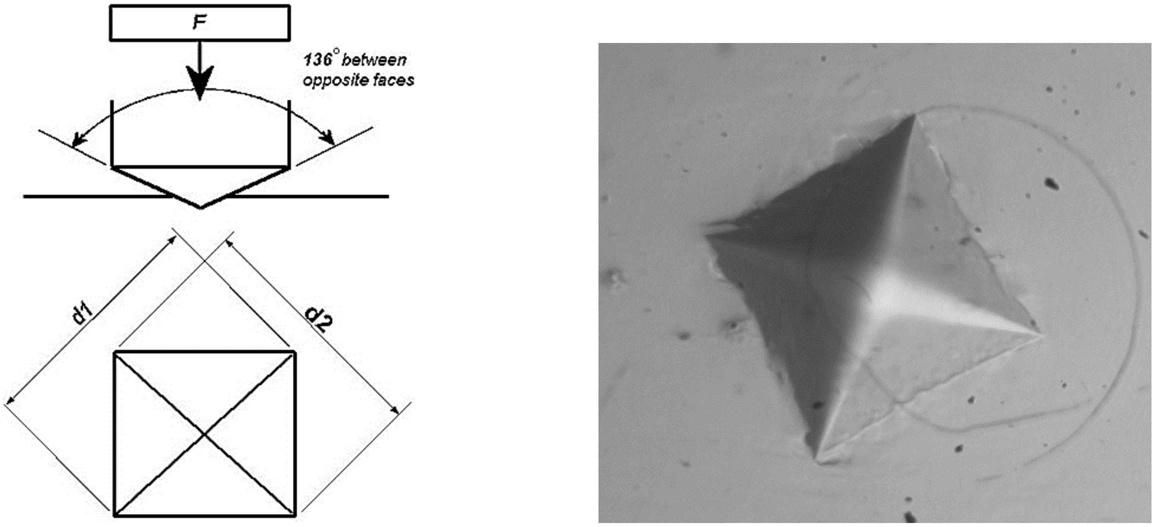

Figure 43: Indenter schematic (left) [75], indentation in optical micrograph (right)

The micro-hardness mapping used a spacing of 0.635 mm with 40 hardness measurements per sample, covering a distance of 25.4 mm. A Vickers hardness greater than 466 was taken to indicate a 97% martensitic structure [43], and therefore a close enough approximation to a fully martensitic microstructure.

Samples were not taken from blanks heated with a non-tailoring (i.e. homogenous) striking surface for two reasons. First, thermocouple measurements taken for blanks tested with a uniform striking surface (non-tailoring) showed that the blanks uniformly exceeded their Ac3 temperatures, meaning that the as-formed microstructure is likely to be entirely martensite. Second, regions existed in the tailoring surface that had identical thermal effusivities to that of the uniform surface, so samples taken from that region (Sample 4 from Figure 42) were assumed to be representative of what would be obtained using a homogenous striking surface.

The experimental preparation and procedures outlined in this chapter were carried out to measure the heating rate of the blanks and die, and to quantify the phase fraction of austenite present in tailored samples. In the following chapter, these results are compared to the heat transfer model and tailoring model that were discussed in Chapter 2 and Chapter 3 for verification of the models.

Chapter 5

Results, Validation, and Discussion

The heating die design discussed in Chapter 2 and the testing methodology presented in Chapter 4 were used to produce experimental results that are summarized in this chapter. The models presented in Chapter 2 and Chapter 3 were revised and validated through comparison with the experimental results. The heat transfer model was found to predict the die heating with a maximum error of 2% and the blank heat transfer model was found to overestimate the thermal diffusivity of the die. The tailoring model predicted the austenite transformation with a maximum error of 13% which was noted to occur at the low-high thermal effusivity boundary.

5.1 Die Heating and Thermal Model Validation

When the heated die was first activated, the set-point temperatures were adjusted in 150 K increments to investigate the temperature distribution throughout the die at any instant. As expected, the spiral heaters heated the ends of the die faster than the u-shaped heaters in the middle of the die, due to their higher power output. It was found that the middle of the die required take 30-45 minutes to equilibrate with the ends of the die if the corresponding zone set-point temperature were not increased. If the set point temperatures were ramped to the final objective temperature of 1373 K, the middle of the die would lag by about 150 K throughout the heat-up period. The heating die required about 6.5 hours to reach operating temperature. This was longer than the desired time because of the change in electrical configuration that reduced the power output of the die by approximately 25%.

Comparing the die heating model to the experimental results suggested that the initial heat flux did not represent the actual heat flux supplied by the heater elements. Taking the nominal resistance of the heaters to be the same throughout the heating up time of the die did not prove to be suitable, through a comparison of thermocouple measurements with the simulated temperature readings of the same location, shown in **Error! Reference source not found.**. his required inputting a temperature-dependent heat flux into the model based on the manufacturer-specified temperature-dependent heater resistance [76], as plotted in Figure 44.

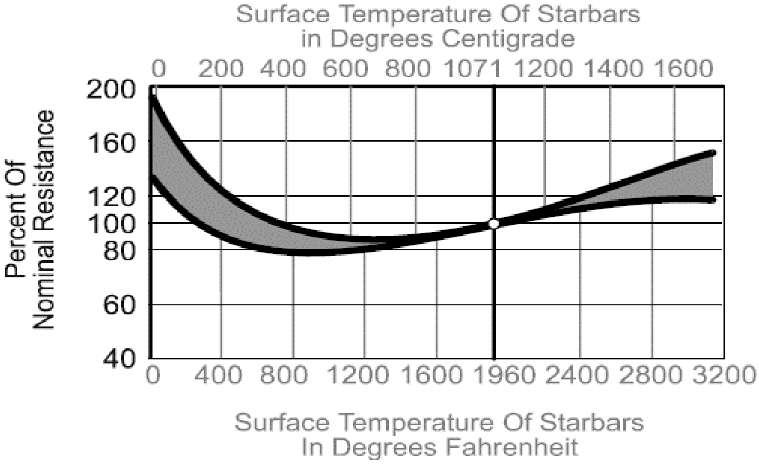

Figure 44: Heater resistance as a function of temperature [76]

The relationship between each element heat flux and the resistance of the elements is given by

$$I = \frac{V}{4 \cdot R_u(T_u) + 4 \cdot R_s(T_s)} \tag{23}$$

$$P_u = \left(\frac{V}{4 \cdot R_u(T_u) + 4 \cdot R_s(T_s)}\right) \cdot R_u(T_u) \tag{24}$$

$$P_s = \left(\frac{V}{4 \cdot R_u(T_u) + 4 \cdot R_s(T_s)}\right) \cdot R_s(T_s) \tag{25}$$

where I is the circuit current, P_u is the heat flux of a U-shaped heater element, and P_s is the heat flux of a straight spiral heater element. The relationship between power and temperature is nonlinear, as the power of each element depends on the circuit current, which in turn depends resistance of every element. These relationships assume that the temperature of a single type of heater is approximately the same since they receive the same current input during operation and experience similar heat loss conditions.

Equations (24) and (25) show that the power of each element depends on the temperature of all of the elements in series, and the element temperature could not be directly measured given the high temperatures and electrically-active nature of the heater elements. This led to an investigation focused on inferring the heater heat fluxes by other means. In order to understand and subsequently predict the relationship between the heater temperatures and heat flux, the relationship described by Eq. (23) was plotted as a 3D representation of the circuit current as a function of the temperature of the two heater types, as shown in Figure 45. This plot indicates that the maximum possible current in the circuit is 11.3 A when the temperature of the heaters are both approximately 933 K with a significant drop when the heaters exceed this temperature. This phenomenon is explained by referring to Figure 44, where the heaters are shown to increase in resistance after reaching approximately 933 K, given that the current is inversely related to the resistance.

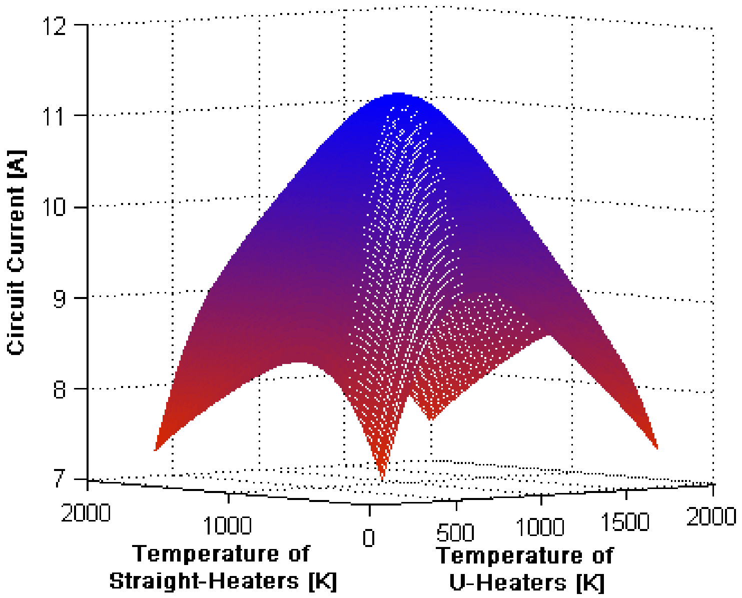

Figure 45: Circuit current as a function of u-shaped and straight heaters temperatures

Further examination of the effect the heater temperatures have on the heat flux of each heater type reveals a similar trend seen in Figure 45; the heat fluxes both peak when both heater types are at 933 K, and significantly drop after this temperature, as shown in Figure 46. Despite the fact that the resistance increased at temperatures above 933 K, the heat flux for both heater types decreased. This was due to the dominant nature of the current in the relationship shown in Eq. (11).

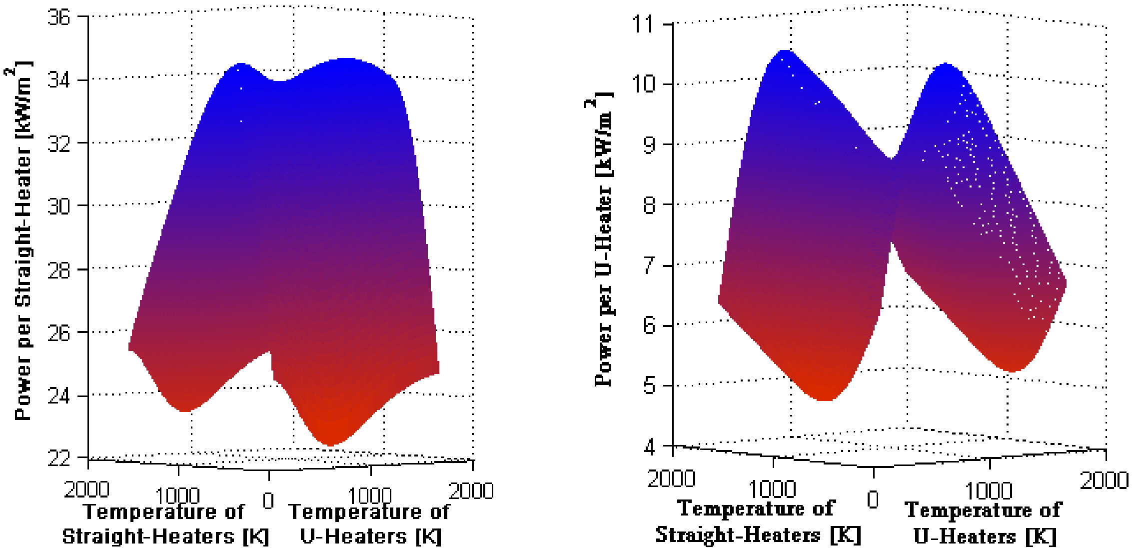

(a) (b)

Figure 46: Temperature dependent heat flux for (a) straight heaters (b) u-shaped heaters

The trends shown in Figure 46 were used to predict the temperature-dependent heat flux boundary conditions in the COMSOL model.

These predictions are supported by observation of the heaters during experimentation. The straight heaters began to visibly incandesce much faster than the U-shaped heaters and thermocouple readings showed that regions heated by the U-shaped heaters typically lagged by about 150K. Current readings from the prototype testing [15], were also used to predict the behavior of the heaters. Since only one type of heater was used in the prototype it was assumed that the heaters were all roughly the same temperature, which allowed the resistance of the heaters to be inferred from the circuit current. The resistance history of the heaters is shown in Figure 47, where the nominal resistance percentage was calculated based on the reported nominal resistance given by the manufacturer [77].

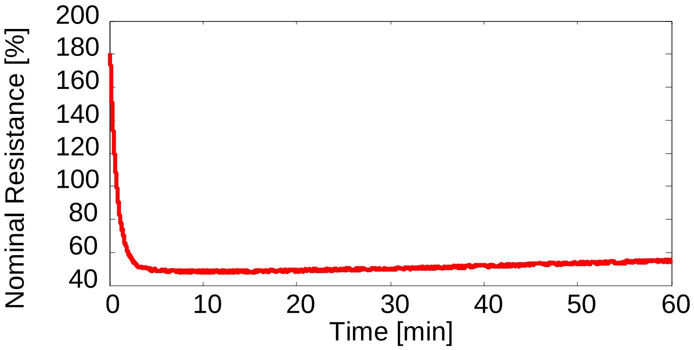

Figure 47: Nominal resistance of heaters used in prototype during heat-up

A comparison of Figure 47 and Figure 44 strongly suggested that the temperature of the heaters used in the prototype quickly reached 973 K and then slowly increased in temperature over one hour of operation. It should be noted that the minimum resistance plotted in Figure 47 is lower than what is shown in Figure 44, suggesting that the heater behavior may not follow the manufacturer's data after repeated use in the monolith.

Given the temperature lag of the U-shaped heaters, and quick heat-up to 973 K seen in previous experiments with the prototype [15], the initial conditions for the heater holes were set at 973 K and 823 K for the straight and U-shaped heaters respectively. The temperature-dependent heat fluxes used in the model were taken from the range of possible heat fluxes shown in Figure 46, and are shown in Figure 48.

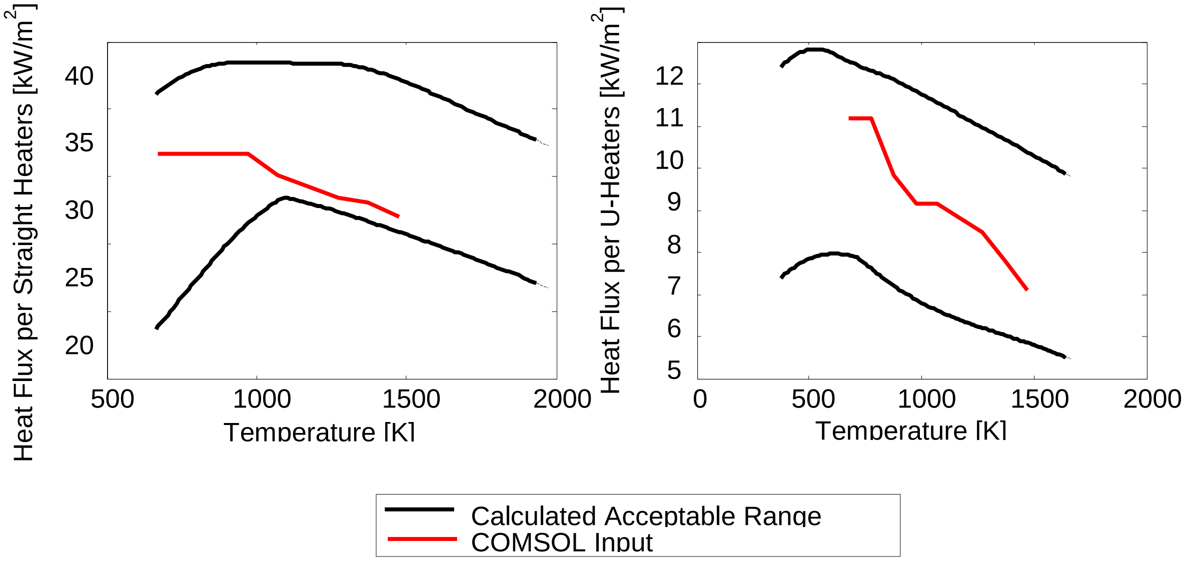

Figure 48: Heater hole heat flux inputs for COMSOL model

The results of the model using the heat flux inputs in Figure 48, is shown in Figure 49 for the zone 2 and 3 thermocouple locations, the model closely agrees with the thermocouple readings with a maximum deviation of 22 K (2%).

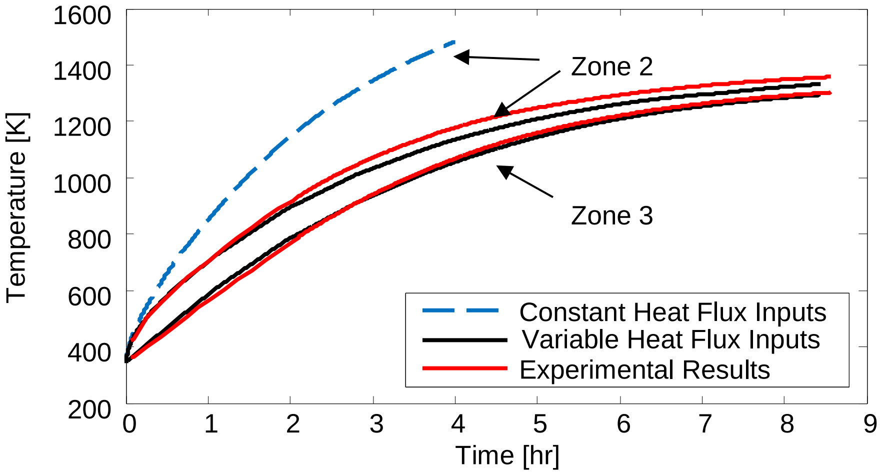

Figure 49: Simulation and experimental results using variable and constant heat flux

The limitations of this procedure lie in the need for manual adjustment of the expected heat flux of the heaters. If all of the heaters had the same resistance (as was the case for the prototype), then Eq. (23) would be simplified to Eq. (26) and the circuit current would be sufficient to know the heat flux of the heater elements, as shown in Eq. (27).

$$I = \frac{V}{8 \cdot R(T)} \tag{26}$$

$$P = \left(\frac{V}{8 \cdot R(T)}\right) \cdot R(T) \tag{27}$$

An infrared camera was used to capture the surface temperature of the die. This was compared to the surface temperature of the die predicted by the COMSOL model and is shown in Figure 50.

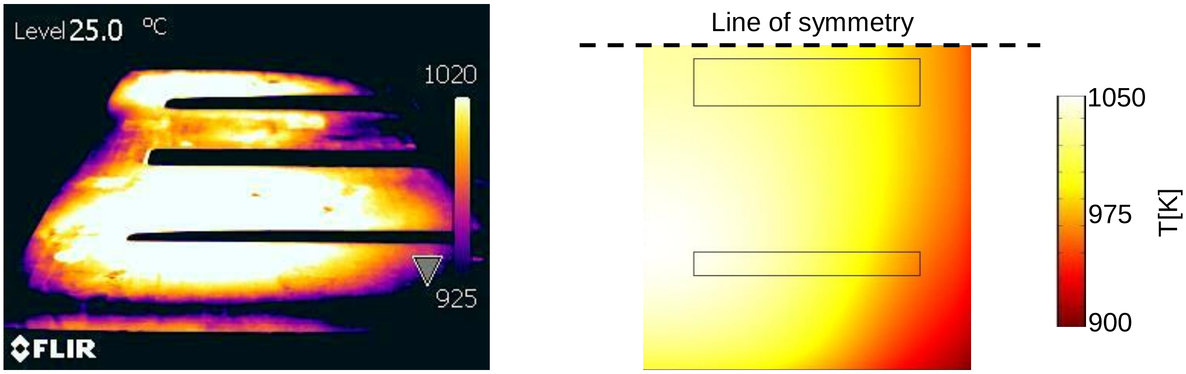

(a) (b)

Figure 50: (a) IR image of heating die surface at operating temperature (b) Surface temperature of half of heating die predicted by heat transfer model with ceramic inlays location outlined

The model prediction of the surface temperature and the IR image of the heating die both show the left side of the die to be the highest in temperature as well as having the most uniform temperature region. Given the asymmetry of die surface, the placement of the blanks during testing was shifted 30 mm to the left to take advantage of the more uniform surface temperature in this region. The coolest regions seen on the right side of the die correspond to the 'cold zones' of the heaters, and the two high temperature regions on the left are the result of the spiral bodied heaters which have a higher power output than the heaters located in the middle of the heating die. It should be noted that the ceramic inlays appear to be black rectangles in the IR image because the emissivity setting used in the camera was for the RA330 steel and the perceived temperature of the inlays was outside of the specified temperature range. In reality the ceramics were at the same temperature as the steel surface at the time the picture was taken.

5.2 Blank Heating and Model Validation

The temperature history of the blank was measured with a non-tailored surface. The location of the thermocouples is shown in Figure 51, and was chosen to get temperature data along the length of the blank given that the surface temperature of the die was not uniform.

Figure 51: Thermocouple Locations on Blank

The infrared camera found the die surface to be between 1323-1373 K. The blank reached the Ac3 temperature within 60 seconds, as shown in Figure 52. The lower temperature measurement corresponds to the middle of the blank where the die had lower surface temperatures. These results suggest that the die surface temperature needs to be above 1373 K for the blank to reach Ac3 within one minute.

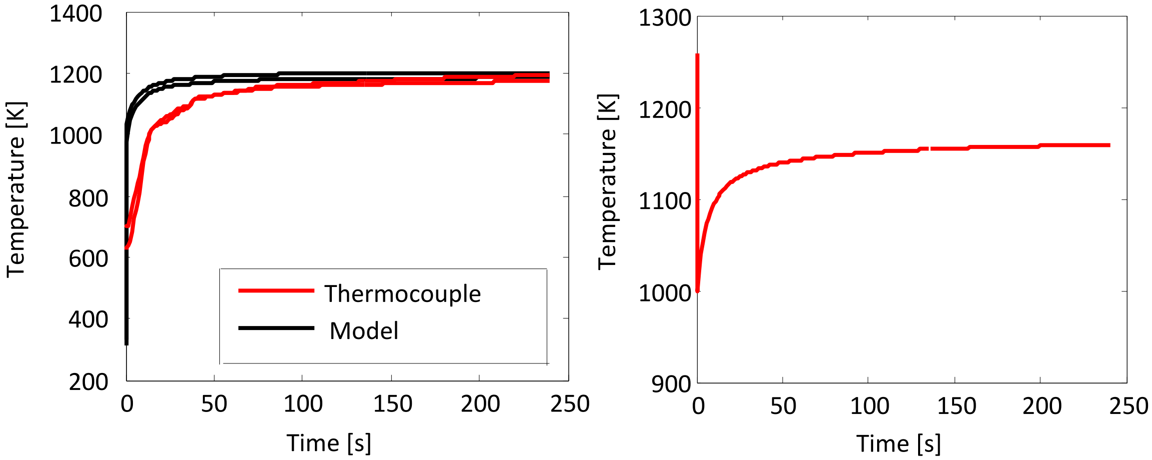

(a) (b)

Figure 52: (a) Thermocouple readings of blank during heating compared to blank model heating results; (b)Model predicted die surface temperature during blank heating

The modelled blank temperatures, also depicted in Figure 52, have a higher heating rate than the corresponding experimental results. The experimental blank heating results were analyzed to determine the heat transfer coefficient by examining a plot of $-\ln(\theta/\theta_i)\ vs\ t$ where θ is the temperature difference of the blank and die surface, θ_i is the initial temperature difference between the blank and die surface, and *t* is the time. The plot results showed a non-linear relationship. Previously, it was assumed that the die surface temperature had little variation during heat treatment of the blank, due to its comparatively larger thermal mass, however, this was shown by the model to not be the case as the temperature is seen to drop quickly and then stabilize to a lower temperature as shown in Figure 52(b). Therefore, the discrepancy between the blank model results and experimental data is likely due to the model predicting an accelerated recovery of the die surface temperature. This suggests that the thermal diffusivity of RA330 assumed in the model overestimated the true value.

5.3 Tailoring Results and Model Verification

As discussed in Section 3.3.2, the accuracy of the F1 model decreases with higher heating rates when using the averaged activation energy and pre-exponential constant of all of the heating rates. While the activation energy of the material is assumed to be constant, some variation seen in Figure 39 can be attributed to nucleation and growth processes. While these phenomena may depend on heating rate, they are excluded from the F1 model for simplicity.

To improve the accuracy of the kinetics model for the application of direct contact heating, the model used the average *Ea* and *A* for the 10 K/s dilatometry results. This was used as a close approximation to the average heating rate of the blank during the Ac1-Ac3 range which was found to be 12.5 K/s from analysis of the experimental results of the blank heating history, shown in Figure 52. A comparison of the performance of the model using averaged *A* and E_A values from 10K/s tests vs the averaged *A* and *Ea* values from all of the heating rates is shown in Figure 53 with the micro-hardness of coupons heated at 10K/s within the Gleeble and quenched at various intermediate temperatures.

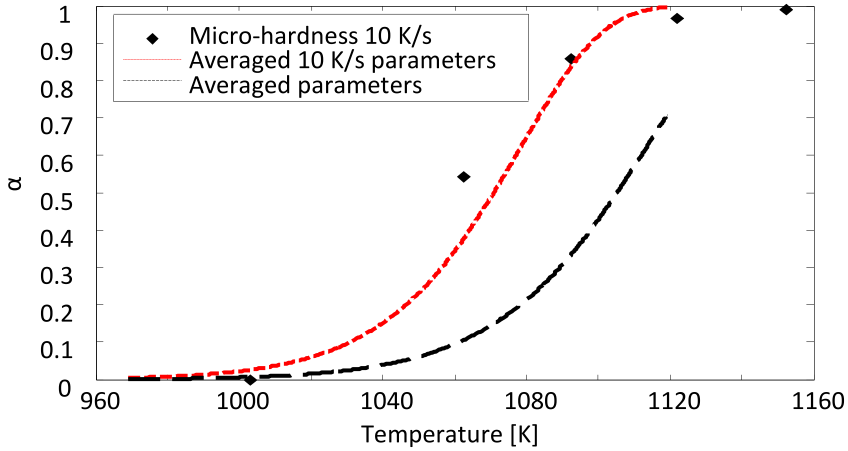

Figure 53: Micro-hardness values in sample exposed to 10K/s, kinetics model results with averaged parameters, and kinetics model results with averaged 10K/s parameters

5.3.1 Micro-hardness Results

Micro-hardness results for the 50 mm tailored strip and 20 mm tailored strip were plotted alongside the phase fraction of austenite predicted by the model for those locations in Figure 54. Figure 53 (a) shows the transition region for the 20 mm tailored strip, while (b) shows the transition region for the 50 mm tailored strip.

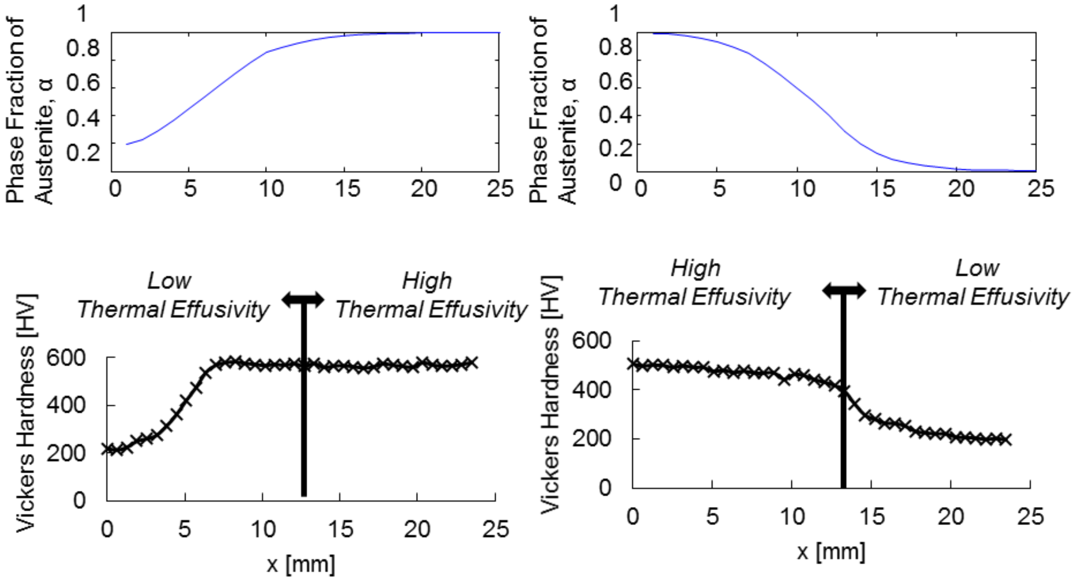

(a)

(b)

Figure 54: Vickers hardness compared to model α fraction results at 120s heating hold time

The model follows the trend seen in the micro-hardness results, but does not start at 0% phase fraction at the middle of the tailored region as the micro-hardness suggests it should in Figure 53 (a). Inspection of the die surface showed that the ceramic inlays sit slightly 0.5 mm lower than the striking surface of the RA330®. This gap was likely to have formed by a combination of factors: *(i)* differing thermal expansion of the RA330® and RSLE57® striking surface; and *(ii)* wearing away of the ceramic insert surface during operation. The air gap between the ceramic and blank surface insulated the blank and result in lower heating rates at the interface than expected. This would explain the as-received micro-hardness in the middle of the tailored region when 20% martensite was predicted by the tailoring model. The transition region of the micro-hardness results for both the 20 mm and 50 mm strips, is not as pronounced as the micro-hardness results. This could be due to an overestimation of the thermal diffusivity of the RA330, as discussed in Section 5.2 to likely be a possible reason why the measured blank temperature differs from the model results. An overestimate of thermal diffusion in the blank would produce smoother temperature transitions at the low-high thermal effusivity boundary. This would directly result in a similarly smooth transition between the low-high Vickers hardness regions. Overall, the maximum error of the tailoring model was 13%, which occurred at the low-high thermal effusivity boundary.

5.3.2 Optical Micrograph Results

Three locations along the length of the transition region of the 50 mm tailored strip were analyzed using an optical microscope. The sample locations correspond to lowest, highest, and middle range micro-hardness results, as shown in Figure 54. The micrographs, shown in Figure 55, further confirmed that regions with a hardness of approximately 500HV had a martensitic microstructure, and that the regions with a hardness of 200HV corresponded to microstructures such as ferrite-pearlite. The images shown were obtained using standard metallographic sample preparation techniques and a Nital etch.

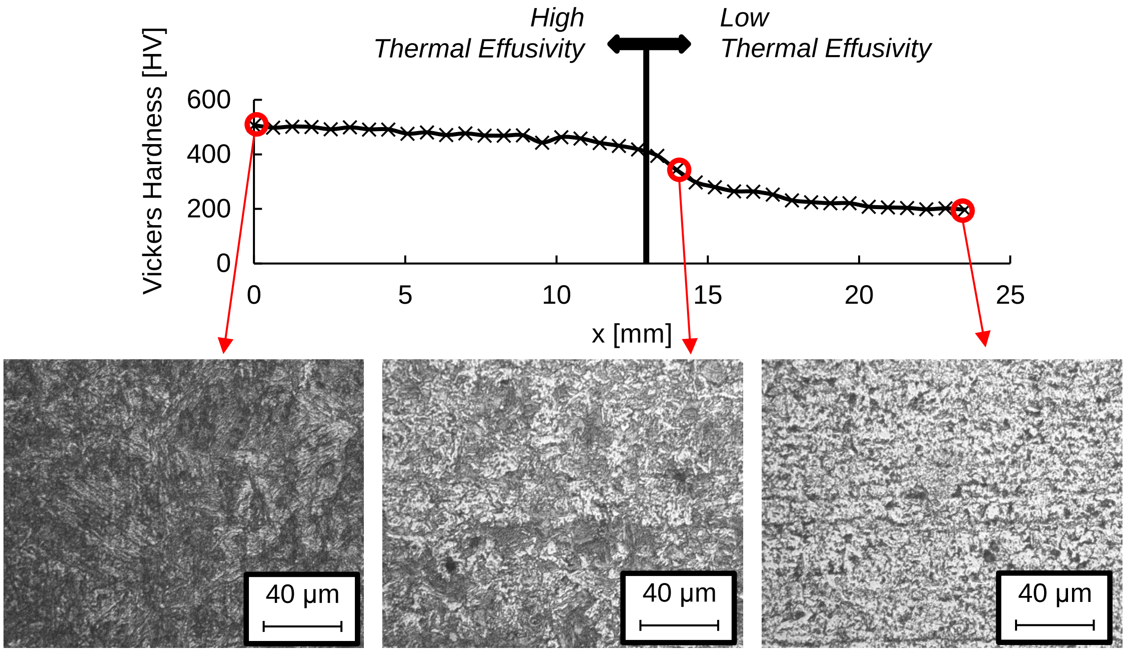

Figure 55: Optical micrographs of regions with low, middle, and high Vickers hardness

The microstructure of the transition region can be seen to have regions of martensite mixed with the as received microstructure, which is consistent with the micro-hardness measured for that location.

Chapter 6

Conclusion and Future Work

This final chapter summarized the major conclusions of this work from the results presented in Chapter 5, and presents several recommendations for future work.

6.1 Conclusions

A half-scale industrial heating die was designed and constructed of a high nickel alloy, RA330, embedded with silicon carbide heaters, and surrounded by RSLE 57® ceramic insulation. The power output of the die was 16.5kW, and required 6.5 hours to reach an operating temperature of 1273 K. The heating die was used alongside a flat quenching die, which were mounted within a 900 ton press. Usibor® 1500P 2 mm sheets, were used in the experiments. The Al-Si coating of the Usibor® 1500P blanks was removed by sandblasting to prevent adhesion of the melted coating to the die surface. The striking surface of the die was made of RA330 with ceramic inserts so that surface had regions of low and high thermal effusivity in order to produce tailored blanks, with regions of as-received composition, and fully transformed martensite. Three tailoring regions were designed into the striking surface, with widths of 20 mm, 50 mm, and 60 mm. These were chosen to investigate the impact of axial conduction on the blank region in contact with the boundaries of low and high thermal effusivities.

Dilatometry measurements performed in a Gleeble® were used to develop a kinetics model to predict the austenite phase fraction of the material as it was heat treated. Heating rates of 1 K/s, 2K/s, 5K/s, 10K/s, and 20K/s were tested in repeats of three or more. A first order reaction model was selected as the most appropriate model and values for the activation energy and pre-exponential factor were found for the average of each heating rate. It was found that using an overall averaged value for the activation energy and pre-exponential factor in the model resulted in reduced accuracy of the model, when compared to micro-hardness results carried out at high heating rates. This could be attributed to the simplicity of the model, as it does not account for nucleation and growth as separate terms. To improve accuracy, the model parameters used were the averaged values for the heating rate of 10 K/s as the average heating rate of the blank during heating in the Ac1-Ac3 range was found to be 12.5 K/s.

A tailoring model was developed by combining a heat transfer model of the blank and the F1 model. The tailoring model results were compared to micro-hardness results from heat treated blanks, which showed that the thermal diffusivity of the blank was overestimated in the model, resulting in a smoother transition between low to high austenite regions than reported from experimental results. The transition zone from martensite to softer phases was found to be about 6 mm for the tailored region at a width of 20 mm, and approximately 10 mm for the tailored region width of 50 mm. Optical microscopy confirmed the microstructure in regions corresponding to Vickers hardness of 500HV to be martensite.

6.2 Future Work

The results of this research have shown the potential of direct contact heating in HFDQ. Nevertheless, there are still design aspects and further testing necessary to bring this research to the point of implementation in an industrial facility. Concerns involving the stability of the die surface temperature after numerous tests needs to be fully investigated, and the quenching die should be configured to allow more than four blanks to be quenched consecutively before it is heated above the martensite finish temperature. Adaptations of the die to bring it to industrial standard would see the top of the die also have a bed of elements so that heating is provided from both striking surfaces, and that cooling channels or a cooling block be added to the quenching die so that it could operate continuously. The service life of the heaters would need to be determined, or different heaters would need to be used. If the silicon carbide heaters are used for further development, an electrical configuration that allows for only u-shaped elements to be used would be necessary as this would reduce the likelihood of fracture during operation. The heaters chosen would also need to have a hot zone that runs the entire width of the die so that cold corners, as seen in Figure 50 do not occur. Using one kind of heater would also likely be sufficient to ensure that the surface temperature of the die remains uniform.

The next step for this project would require investigating the formability of tailored components. This would involve adapting the flat quenching die to accommodate a U-channel form. If extra material on the ends of the blanks are still used as tabs, the geometry of said tabs would need to altered so that the temperature gradient between the heated parts of the blank and the tabs do not encourage warping of the blank before forming. The elimination of the tabs could also be realized if the pins and moving plate work. The adhesion of the Al-Si coating could also be avoided by using the pins to implement the strategy used by Ploshikhin *et al.* but the heat treatment time would increase by several minutes. The use of a thin insulation sheet secured to the bottom striking surface also has promise to prevent the blank from sticking to the die, since the blank does not adhere as much to the ceramic upper striking surface.

Bibliography

[1] G. o. Canada, "Innovation, Science and Economic Development Canada: Canadian Automotive Industry," 2014.

[2] U. S. E. P. Agency, "Federal Register Rules and Regulations," Department of Transportation, 2012.

[3] R. Wohlecker, "Determination of Weight Elasticity of Fuel Economy for," International Iron and Steel Institute, Middeltown, Ohio, 2007.

[4] H. Karbasian and A. Tekkaya, "A Review on Hot Stamping," *Journal of Materials Processing Technology,* vol. 210, no. 15, pp. 2103-2118, 2010.

[5] W. Joost, "Reducing Vehicle Weight and Improving US Energy Efficiency Using Intergrated Computational Materials Engineering," *Jom,* vol. 64, no. 9, pp. 1032-1038, 2012.

[6] A. Hund, "Continuous Improvement of Hot Forming Technology," in *3rd International Conference on Sheet Metal Forming of High Performance Steel,* Kassel, Germany, 2011.

[7] P. Akerstrom, "Modelling and simulation of hot stamping, PhD," University of Lulea, 2006.

[8] M. Merklein and J. Lechler, "Investigation of the Thermo-Mechanical Properties of Hot Stamping Steels," *Journal of Materials Processing Technology,* vol. 177, pp. 452-455, 2006.

[9] ArcelorMittal, "Steels for Hot Stamping-Usibor," 2016.

[10] A. Ingebrand, I. Valls-Angles and T. Laumann, "Integrated and Competitive Tooling Solutions for the Production of Tailored Components and Cutting of UHSS," in *3rd Hot Sheet Metal Forming of High-Performance Steel*.

[11] B. Behrens, F. Bach, M. Diekamp, S. Hubner, F. Nurnberger, J. Schrodter, L. Wolf and J. Moritz, "Process Time Reduction of Hot Stamping by Means of Early Extraction from

the Press," in *4th International Conference Hot Steel Metal Forming of High-Performance Steel*, Lulea, Sweden, 2013.

[12] R. Hund, "Continuous Improvement of Hot Forming Technology," in *3rd International Conference on Hot Sheet Metal Forming of High-Performance Steel* , Auerbach, 2011.

[13] M. Naderi, A. Saeed-Akbari and W. Bleck, "The Effects of Non-Isothermal Deformation on Martensitic Transformation in 22MnB5," *Material Science and Engineering*, vol. 487, no. 1, pp. 445-455, 2008.

[14] J. Rasera, K. Daun, C. Shi and M. D'Souza, "Direct Contact Heating for Hot Forming Die Quenching," *Applied Thermal Engineering*, vol. 98, no. 1, pp. 1165-1173, 2016.

[15] J. Rasera, "Development of a novel technology for rapid austenizing Usibor 1500P Steel," 2015.

[16] H. Lehmann, "Developments in the Field of Schwarz Heat Treatment Furnaces for Press Hardening Industry," in *3rd International Conference on Hot Sheet Metal Forming of High Preformance Steel*, Kassel, Germany, 2011.

[17] K. Mori, S. Maki and Y. Tanaka, "Warm and Hot Stamping of Ultra High Tensile Strength Steel Sheets," *CIRP Annals - Manufacturing Technology*, vol. 54, no. 1, pp. 209-212, 2005.

[18] R. Kolleck, R. Veit, M. Merklein, J. Lechler and M. Geiger, "Investigation on Induction Heating for Hot Stamping of Boron Alloyed Steels," *CIRP Annals - Manufacturing Technology*, vol. 58, no. 1, pp. 275-278, 2009.

[19] V. Ploshikhin, A. Prihodovsky, J. Kaiser, R. Bisping, H. Linder, C. Lengsdorf and K. Roll, "New Heating Technology for Furnace-Free Press Hardening Process," in *Tools and Technologies for Processing Ultra High Strength Materials*, Graz, 2011.

[20] V. Ploshikhin, A. Prihodovsky, J. Kaiser and L. Skutella, "New Heating Technology for Heat Treatment and Hot Forming (Coference Presentation)," in *Tools and Technologies for Processing Ultra-High Strength Materials*, Graz, Austria, 2013.

[21] C. Tamarelli, "The Evolving Use of Advanced High-Strength Steels for Automotive Applications," AutoSteel, Michigan, 2011.

[22] R. Arbelaez, "Side Impact Challenges for Steel Vehicle Structures," Insurace Institute for Highway Safety.

[23] R. Perez-Santiago, E. Billur, A. Ademaj, C. Sarmiento, R. Berlanga and T. Altan, "Hot Stamping a B-Pillar with Tailored Properties: Experiments and Preliminary Simulation Results," in *International Hot Stamping Conferences*, Lulea, Sweden, 2013.

[24] D. Munera, A. Pic, D. Abou-Khalil and F. Shmit, "Innovative Press Hardened Steel Based Laser Welded Blanks Solutions for Weight Savings and Crash Safety Improvements," *SAE International Jounral of Materials and Manufacturing,* vol. 1, no. 1, pp. 472-479, 2008.

[25] R. Padmanabhan, M. Oliveira and L. F. Menezes, "Deep Drawing of Aluminium-Steel Tailor Welded Blanks," *Materials & Design,* vol. 29, no. 1, pp. 154-160, 2008.

[26] P. Weissler, "Focus B-pillar 'Tailor Rolled' to 8 Different Thicknesses," SAE International, 2010.

[27] R. Perez-Santiagom, E. Billur, A. Ademaj, C. Sarmiento, R. Berlanga and T. Altan, "Hot Stamping a B-Pillar with Tailored Properties: Experiments and Preliminary Simulation Results," in *4th International Conference of Hot Sheet Metal Forming of High-Performance Steel*, Lulea, Sweden, 2013.

[28] K. Mori and Y. Okuda, "Tailor die quenching in hot stamping for producing ultra-high strength steel," *CIRP Annals - Manufacturing Technology,* vol. 59, no. 1, pp. 291-294, 2010.

[29] R. George, A. Bardelcik and M. Worswick, ""Development of a hot forming die to produce parts with tailored mechanical properties - Numerical Study," in *2nd International Conference of Hot Sheet Metal Forming of High Performance Steel*, Lulea, Sweden, 2009.

[30] S. Erturk, M. Sester, M. Selig, P. Feuser and K. Roll, "A thermo-mechanical-metallurgical FE approach for simulation of tailored tempering," in *3rd international conference of hot sheet metal forming of high performance steel*, Kassel, Germany, 2011.

[31] J. Banik, F. Lenze, S. Sikora and R. Laurenz, "Tailored Properties - A Pivotal Question for Hot Forming," in *3rd International Conference on Hot Sheet Metal Forming of High Performance Steel*, Kassel, Germany, 2011.

[32] T. Svec and M. Merklein, "“Tailored Tempering - Heat Transfer and Resulting Properties in Dependency of Tool Temperatures," in *3rd International Conference of Hot Sheet Metal Forming of High-Performance Steel*, Kassel, Germany, 2011.

[33] T. Labudde and W. Bleck, "Formability Characterisation of Press Hardened Steels," in *2nd International Conference of Hot sheet Metal Forming of High-Performance Steel*, Lulea, Sweden, 2009.

[34] J. Wilsius, B. Tavernier and D. Abou-Khalil, "Experimental and Numerical Investigation of Various Hot Stamped B-Pillar Concepts Based on Usibor (R) 1500P," in *3rd International Conference of Hot Sheet Metal Forming of High-Performance Steel*, Kassel, Germany, 2011.

[35] K. Mori, T. Maeno and K. Monogkolkaji, "Tailored Die Quenching of Steel Parts Having Strength Distribution Using Bypass resistance Heating in Hot Stamping," *Journal of Materials Processing Technology*, vol. 213, no. 1, pp. 508-514, 2013.

[36] I. COMSOL, *COMSOL Multiphysics Modeling Software Version 4.4.0.248*, Massachussetts.

[37] J. Howell, R. Siegel and M. Menguc, Thermal Radiation Heat Transfer, Boca Raton: CRC Press, 2011.

[38] T. Bergman, A. Lavine, F. Incropera and D. Dewitt, Fundamental of Heat and Mass Transfer, Hoboken: John Wiley & Sons, 2011.

[39] M. Kaviany, Principles of Heat Transfer, New York: John Wiley & Sons, 2002.

[40] "Starbar Silicon Carbide SiC Heating Elements," I Squared R Elements Co., [Online]. Available: http://heatingelements.isquaredrelement.com/category/starbar-silicon-carbide-sic-heating-elements. [Accessed 13 October 2014].

[41] D. G. Ullman, The Mechanical Design Process, New York: McGraw-Hill, 2010.

[42] A. Blaise, B. Bourouga, B. Abdulhay and C. Dessain, "Thermal Contact Resistance Estimation and Metallurgical Transformation Identification During the Hot Stamping," *Applied Thermal Engineering,* p. 8, 2013.

[43] A. Bardelcik, "High Strain Rate Behaviour Of Hot Formed Steel with Tailored Properties," University of Waterloo, Waterloo, 2012.

[44] G. R. Speich, V. Demarest and R. Miller, "Formation of Austenite During Intercritical Annealing of Dual-Phase Steels," *Metallurgical Transactions A,* vol. 12, no. A, pp. 1419-1428, 1981.

[45] D. Gokhale and A. Datta, "Austenization Kinetic of Pearlite and Ferrite Aggregates in a Low Carbon Steel Containing 0.15 Wt Pct C," *Metallurgical Transactions,* vol. 12, no. 3, pp. 443-450, 1981.

[46] A. Roosz, Z. Gacsi and E. Fuchs, "Isothermal Formation of Austenite in Eutectoid Plain Carbon Steel," *Acta Metallurgica,* vol. 31, no. 4, pp. 509-517, 1983.

[47] F. Caballero, C. Capdevilla and C. GarciaDeAndres, "Modelling of Kinetics and Dilatometric Behaviour of Austenite Formation in a low-carbon steel with a Ferrite plus Pearlite Initial Microstructure," *Journal of Materials Science,* vol. 37, no. 16, pp. 3533-3540, 2002.

[48] S. Nath, S. Ray, V. Mathur and M. Kapoor, "Non-isothermal Austenisation Kinetics and Theoretical Determination of Intercritical Annealing Time for Dual-Phase Steels," *ISIJ International,* vol. 34, no. 1, pp. 191-197, 1994.

[49] H. Kissinger, "Reaction Kinetics in Differential Thermal Analysis," *Analytical Chemistry,* vol. 29, no. 11, pp. 1702-1706, 1957.

[50] M. Kulakov, W. Poole and M. Militzer, "The Effect of the Initial Microstructure on Recrystallization and Austenite Formation in a DP600 Steel," *Metallurgical and Materials Transactions A,* vol. 44, no. 8, pp. 3564-3576, 2013.

[51] M. Kulakov, W. Poole and M. Militzer, "A Microstructure Evolution Model for Intercritical Annealing of a Low-carbon Dual-phase Steel," *ISIJ International,* vol. 54, no. 11, pp. 2627-2636, 2014.

[52] D. Leggett, "Explorations in Thermodynamics: Calorimetry, Enthapy and Heats of Reaction," Collin County Community College.

[53] P. Rivera-Diaz-del-Castillo, "In situ study of austenite formation by dilatometry in alow carbon microalloyed steel," *Scripta Materialia*, vol. 58, no. 10, pp. 926-929, 2008.

[54] N. Chester, J. Leung, M. Wells and K. Daun, "Experimental Measurements of the Austenization Process During Reheating of 22MnB5 Steel Blanks," in *Conference on Hot Sheet Metal Forming of High-Performance Steel*, Toronto, 2015.

[55] J. Huang, W. Poole and M. Militzer, "Austenite Formation During Intercritical Annealing," *Metallurgical and Materials Transactions A,* vol. 35, no. 11, pp. 3363-3375, 2004.

[56] "ASTM Standard A1033-10," ASTM International, West Conshohocken , 2015.

[57] B. Pawlowski, "Critical Points of Hypoeutectoid Steel- Prediction of Pearlite Dissolution Finich Temperature Ac1f," *Journal of Achievements in Materials and Manufacturing Engineering,* vol. 49, no. 2, pp. 331-337, 2011.

[58] A. Gorni, "Steel forming and heat treatment handbook," [Online]. Available: www.gorni.eng.br/e/Gorni_SFHTHandbook.pdf.

[59] K. Andrews, "Empirical formulae for the calculation for some transformation temperatures," *Journal of the Iron and Steel Insititute,* vol. 203, pp. 721-727, 1965.

[60] H. Hougardy, "Werkstoffkunde Stahl Band 1: Grundlagen," *Verlag Stahleisen G.m.b.H. Düsseldorf,* vol. 229, 1984.

[61] O. Kasatkin and B. Vinokur, "Calculation Models for Determining the Critical Points of Steel," *Metallovedenie i Termicheskaya Obrabotka Metallov,* vol. 1, pp. 20-22, 1984.

[62] J. Trzaska and L. Dobrzaski, "Modelling of CCT Diagrams for Engineering and Constructional Steels," *Journal of Materials Processing Technology,* Vols. 192-193, pp. 504-510, 2007.

[63] E. Jagle, Microstructure Development During Phase Transformations: Simualtions and Experiments, Stuttgart: Max-Planck Institut of Intelligent Systems, 2011.

[64] D. Porter, Phase Transformations in Metals and Alloys, Boca Raton: Taylor & Francis Group, LLC, 2009.

[65] J. Elmer, T. Palmer, W. Zhang, B. Wood and T. DebRoy, "Kinetic Modeling of Phase Tansformations Occuring in the HAZ of C-Mn Steel Welds Based on Direct Observations," *Acta Materialia,* vol. 51, no. 12, pp. 3333-3349, 2002.

[66] A. Kumar, S. Mishra, T. Debroy and J. Elmer, "Optimization of the Johnson-Mehl-Avarami Equation Parameters for alpha-ferrite to gamma-austenite Transformation in Steel Welds Using a Genetic Algorithm," *Metallurgical and Materials Transactions A,* vol. 36, no. 1, pp. 15-22, 2005.

[67] W. Zhang, J. W. Elmer and T. DebRoy, "Kinetics of Ferrite to Austenite Transformation During Welding of 1005 Steel," *Scripta Materialia,* vol. 46, no. 10, pp. 753-757, 2002.

[68] W. Zhang, J. W. Elmer and T. DebRoay, "Modeling and Real Time Mapping of Phases During GTA Welding of 1005 Steel," *Materials Science and Engineering,* vol. 333, no. 1-2, pp. 320-335, 2002.

[69] E. Scheil, *Archiv. fur Eisenhuttenwesen,* vol. 12, pp. 565-567, 1935.

[70] A. Khawam and D. Flanagan, "Solid-State Kinetic Models: Basics and Mathematical Fundamentals," *The Journal of Physical Chemistry B,* vol. 110, no. 35, pp. 17315-17328, 2006.

[71] M. DiCiano, N. Field, M. Wells and K. Daun, "Development of an Austenization Kinetics Model for 22MnB5 Steel," in review.

[72] S. Vyazovkin, "Evaluation of Activation Energy of Thermally Stimulated Solid-State Reactions under Arbitrary Variation of Temperature," *Journal of Computational Chemistry ,* vol. 18, pp. 393-402, 1997.

[73] M. H. Attia and L. Kops, "Distortion in Thermal Field Around Inserted Thermocouples in Experimental Interfaical Studies," *Journal of Engineering for Industry,* vol. 108, no. 4, pp. 241-246, 1986.

[74] G. VanderVoort and G. Lucas, "Microindentation Hardness Testing," September 1998. [Online]. Available: http://www.metallography.com/amp/micro.htm. [Accessed 6 July 2016].

[75] ASTM Standard E8/E8M 2013a, Standard Test Methods for Tension Testing of Metallic Materials, West Coshohocken: ASTM International, 2013.

[76] "Type SER and TSR, Silicon Carbide Spiral Heating Elements," I Squared R Element Company, [Online]. Available: http://heatingelements.isquaredrelement.com/viewitems/starbar-silicon-carbide-sic-heating-elements/er-and-tsr-silicon-carbide-spiral-heating-elements.

[77] I. Inc., "Type SE and TSE, Silicon Carbide Spiral Heating Elements," [Online]. Available: http://heatingelements.isquaredrelement.com/viewitems/starbar-silicon-carbide-sic-heating-elements/se-and-tse-silicon-carbide-spiral-heating-elements.

[78] A. Kirsch, *Electrical Schematic Design 1*, IsquaredRElements, 2014.

[79] E. Budziarek, *Electrical Schematics*, Waterloo, 2015.

Appendix A

Original Electrical Configuration Schematic

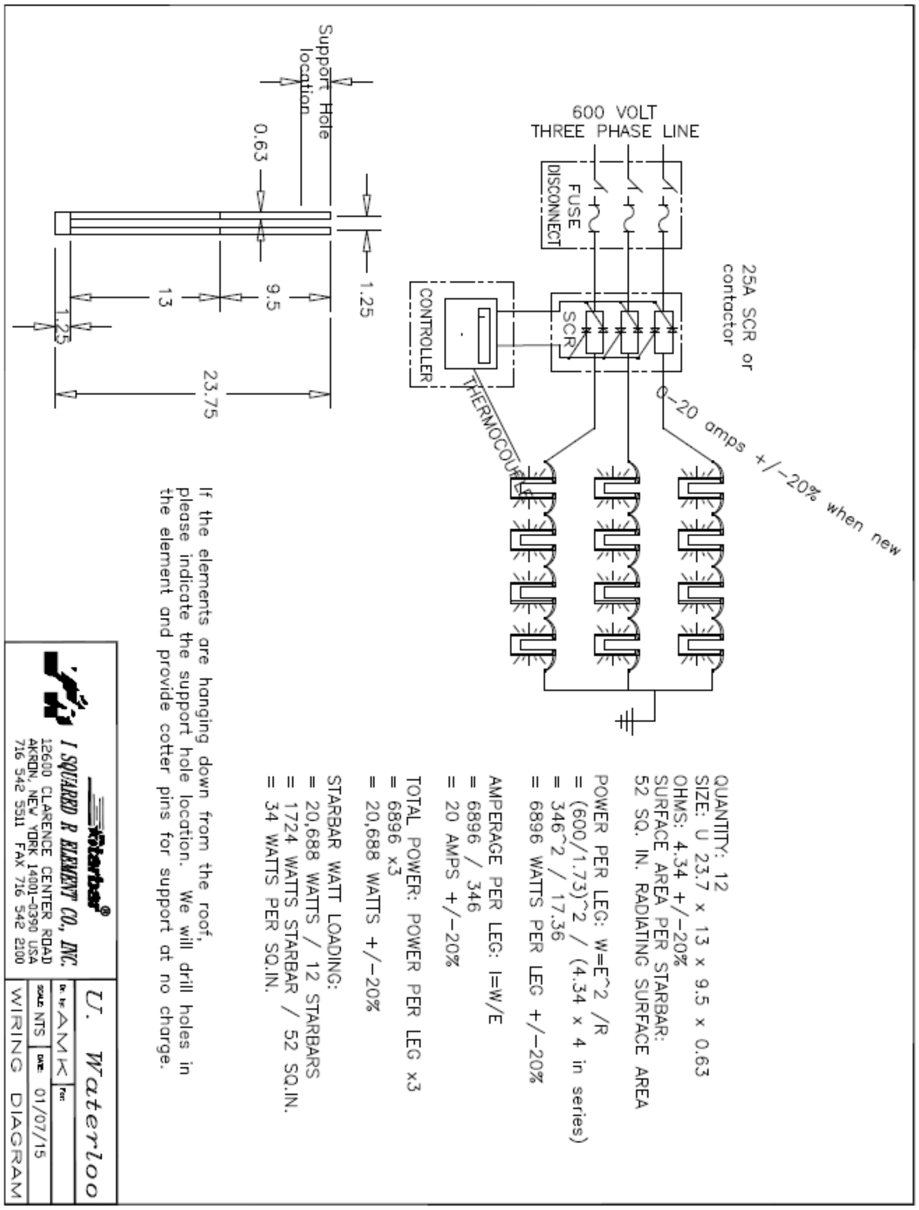

Electrical schematic of original design for heating die, using only U-shaped heaters [78]

Appendix B

Final Electrical Configuration Schematic

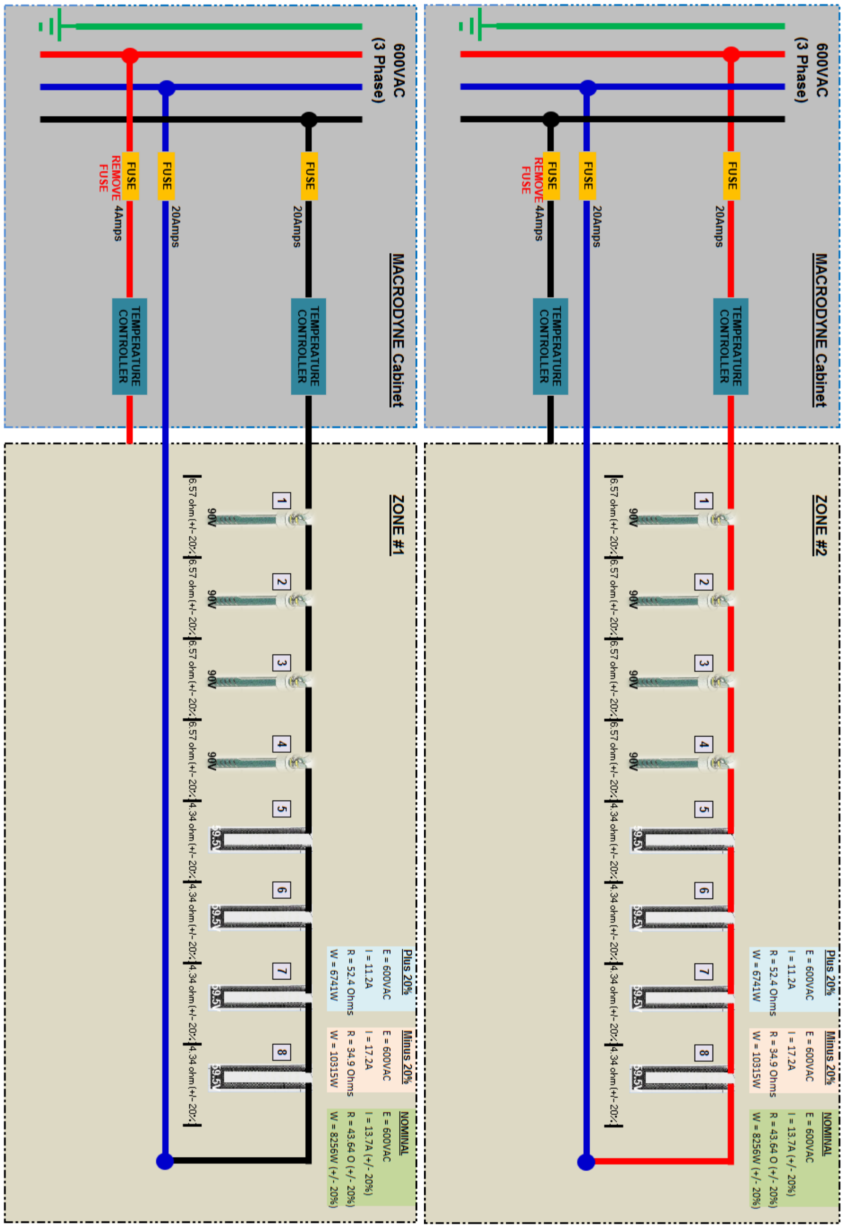

Final electrical schematic of heating die for Zone 1 and Zone 2 [79]

Appendix C

Heating Die CAD Drawings

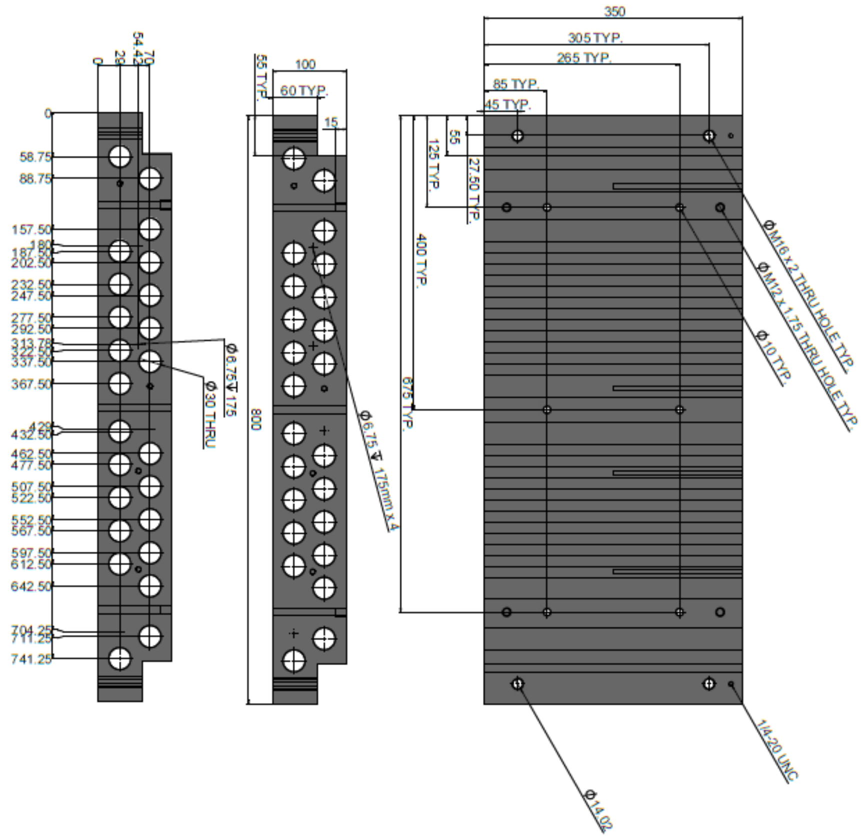

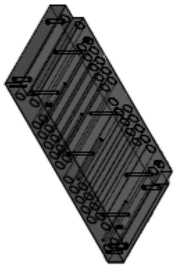

Appendix D

Safety Operating Procedure for 900 Ton Press

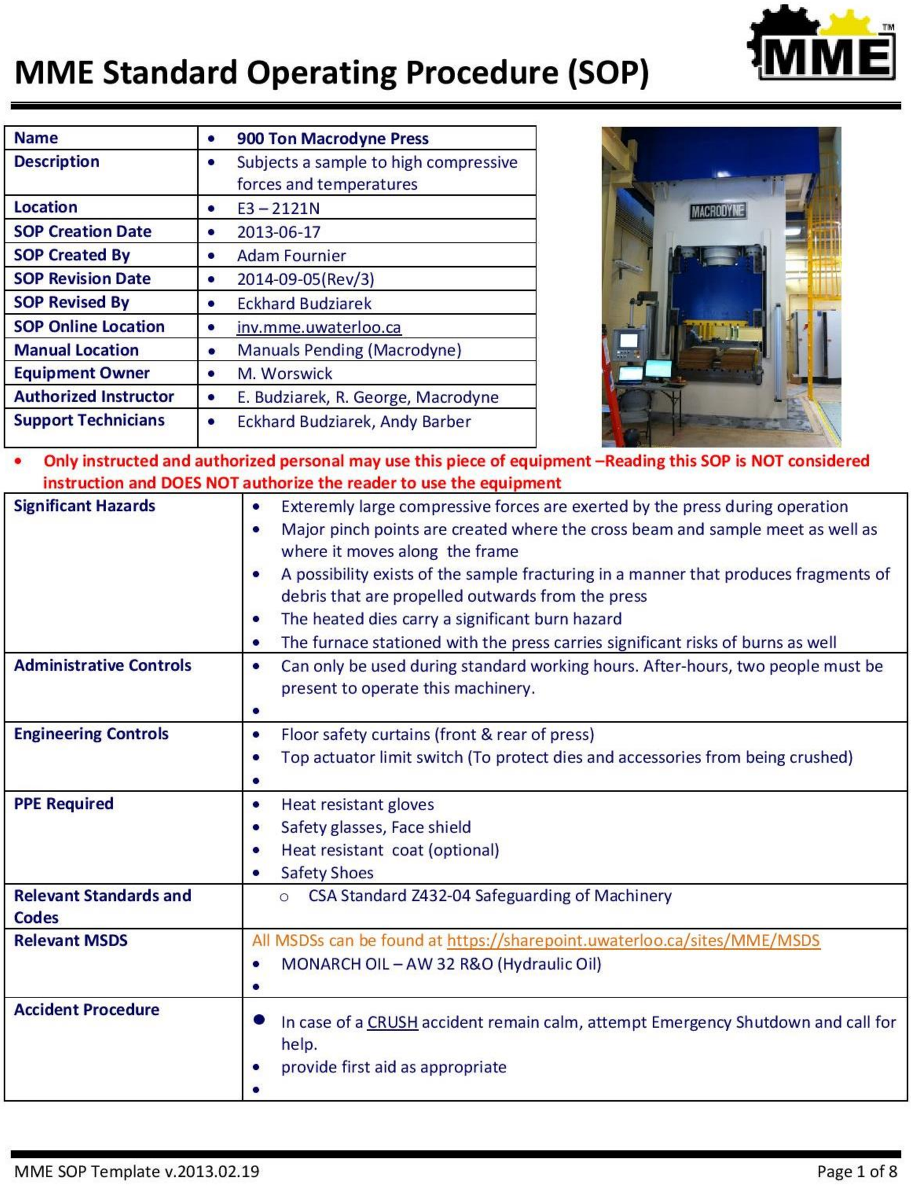

MME Standard Operating Procedure (SOP)

Name	• **900 Ton Macrodyne Press**
Description	• Subjects a sample to high compressive forces and temperatures
Location	• E3 – 2121N
SOP Creation Date	• 2013-06-17
SOP Created By	• Adam Fournier
SOP Revision Date	• 2014-09-05(Rev/3)
SOP Revised By	• Eckhard Budziarek
SOP Online Location	• inv.mme.uwaterloo.ca
Manual Location	• Manuals Pending (Macrodyne)
Equipment Owner	• M. Worswick
Authorized Instructor	• E. Budziarek, R. George, Macrodyne
Support Technicians	• Eckhard Budziarek, Andy Barber

- **Only instructed and authorized personal may use this piece of equipment –Reading this SOP is NOT considered instruction and DOES NOT authorize the reader to use the equipment**

Significant Hazards	• Exteremly large compressive forces are exerted by the press during operation • Major pinch points are created where the cross beam and sample meet as well as where it moves along the frame • A possibility exists of the sample fracturing in a manner that produces fragments of debris that are propelled outwards from the press • The heated dies carry a significant burn hazard • The furnace stationed with the press carries significant risks of burns as well
Administrative Controls	• Can only be used during standard working hours. After-hours, two people must be present to operate this machinery. •
Engineering Controls	• Floor safety curtains (front & rear of press) • Top actuator limit switch (To protect dies and accessories from being crushed) •
PPE Required	• Heat resistant gloves • Safety glasses, Face shield • Heat resistant coat (optional) • Safety Shoes
Relevant Standards and Codes	○ CSA Standard Z432-04 Safeguarding of Machinery
Relevant MSDS	All MSDSs can be found at https://sharepoint.uwaterloo.ca/sites/MME/MSDS • MONARCH OIL – AW 32 R&O (Hydraulic Oil) •
Accident Procedure	● In case of a CRUSH accident remain calm, attempt Emergency Shutdown and call for help. • provide first aid as appropriate •

MME SOP Template v.2013.02.19 Page 1 of 8

Emergency Shutdown Procedure	- The hydraulic 'Emergency Shutdown Procedure' is to engage the E-STOP switch on the press control panel located on the front of the press. - The electrical 'Emergency Shutdown Procedure' is to engage the E-STOP switch on the press control panel located on the front of the press. This will remove all electrical power from the die heaters and the furnace - There is an additional E-STOP switch located on the press control cabinet

Labelled Pictures of Specified Machine and Important Safety Features

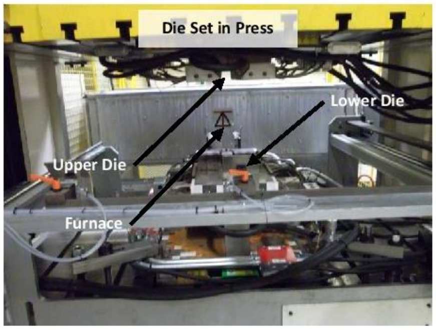

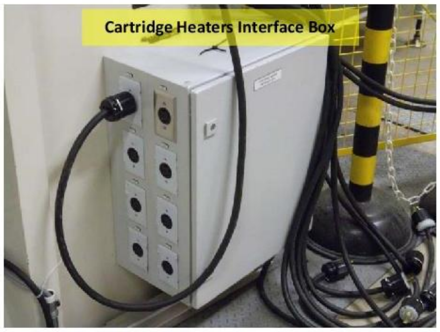

Labelled Pictures of Specified Machine and Important Safety Features

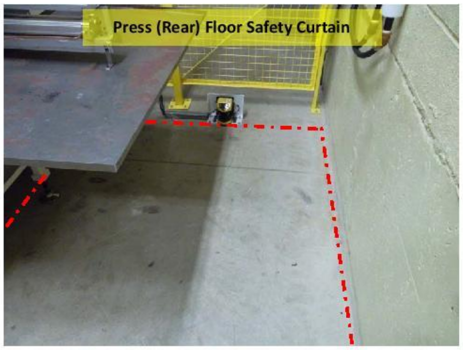

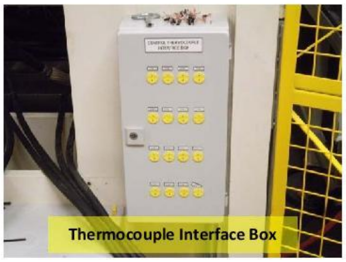

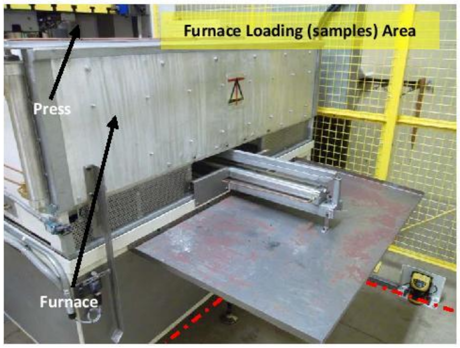

Labelled Pictures of Specified Machine and Important Safety Features

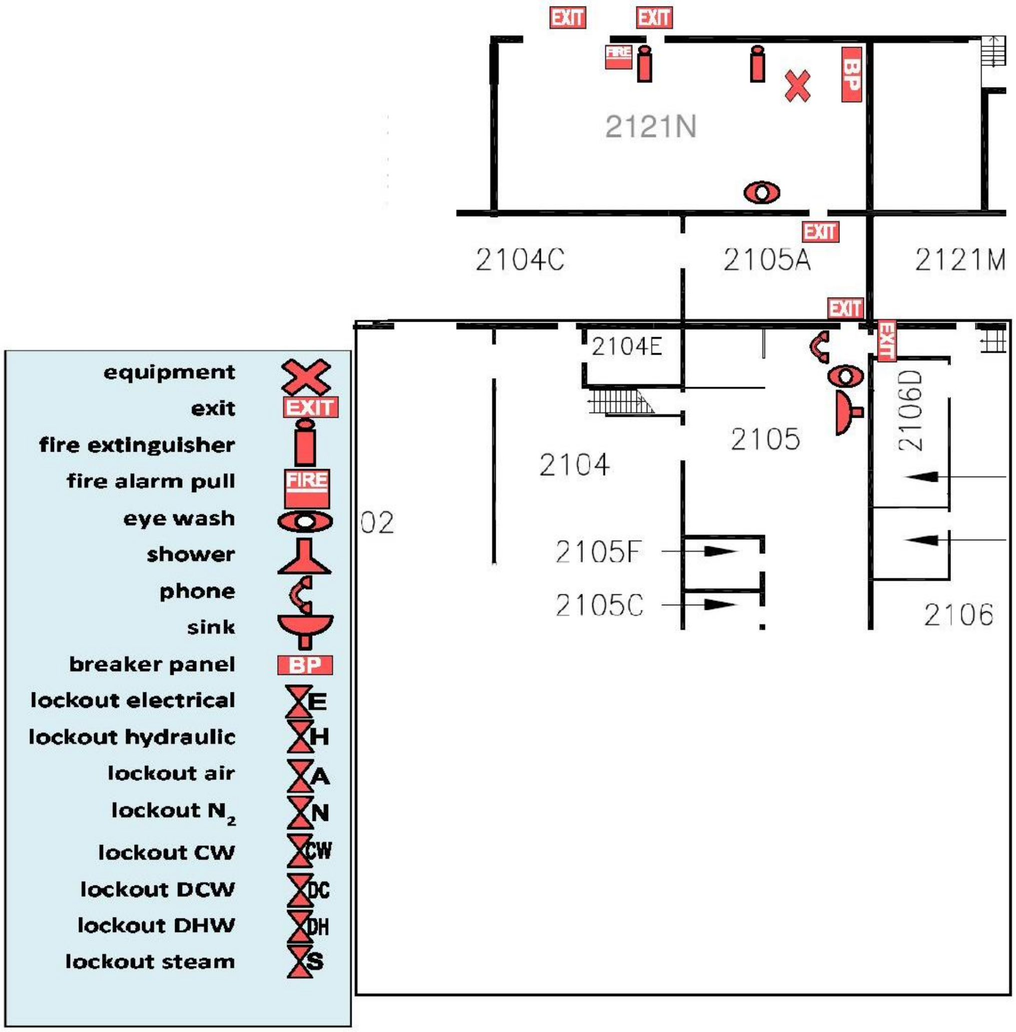

Pre-start Checklist

- None

Start-up Procedure

- Visual check of hydraulic fittings & hoses for leaks
- Check for Oil pooling on the press and floor
- Check that Floor Safety Curtain is working

Operating Procedure

- Equipment - See Manuals (Macrodyne & Delltech Furnace)
- Projects – See responsible faculty

Shutdown Procedure

- Hydraulic motor shut-down: On the control panel main screen, go to "Motor Control" then turn both the Recirculation Pump and the Main Pump to "off".
- Die heaters and furnace electrical shut-down: On the control panel main screen, go to "Platten Temperature Parameters" and switch both the Die Heating and Oven Heat to "off".

Clean-up

- Clean-up any spills / Sweep floor around work area if required
- Dispose of any unwanted materials (project material, scrap etc.)
- Return any tools or tooling no longer required

Lockout

See Health & Safety Ontario - Safeguarding/Lockout for guidance

- Electrical lockout can be perfomed by shutting off the main electrical disconnect on the front of the press control cabinet, and attaching your lock. This will prevent the hydraulic pumps from turning on, but will not guarantee that all hydraulic pressure is relieved from the system.
- Hydraulic lockout can only be performed by Macrodyne personnel.

Maintenance and Repair

- Repairs (Macrodyne & Worswick group)
- Maintenance (Macrodyne & Worswick group)
-
-